A FUNDAMENTAL MULTISCALE STUDY ON MECHANICAL, MICROSTRUCTURAL, AND TOPOGRAPHICAL CHARACTERISTICS OF MACHINING-INDUCED SURFACE INTEGRITY IN Ti-6Al-4V TITANIUM ALLOY

by

Nithin Srinivas Rangasamy

A thesis submitted to the faculty of
The University of Utah
in partial fulfillment of the requirements for the degree of

Master of Science

Department of Mechanical Engineering

The University of Utah

December 2017

The University of Utah Graduate School

STATEMENT OF THESIS APPROVAL

The thesis of **Nithin Srinivas Rangasamy**

has been approved by the following supervisory committee members:

Alagar K. Balaji	, Chair	**08/19/2016** Date Approved
Sivaraman Guruswamy	, Member	**08/19/2016** Date Approved
Ashley Spear	, Member	**08/19/2016** Date Approved

and by **Timothy A. Ameel** , Chair/Dean of

the Department/College/School of **Mechanical Engineering**

and by David B. Kieda, Dean of The Graduate School.

ABSTRACT

A fundamental understanding of machining-induced microstructural alterations and their correlation with topographical (surface roughness) and mechanical (microhardness and residual stresses) characteristics of surface integrity will aid in improved process planning for obtaining a desired surface quality. The final machined surface quality will govern the component's performance by influencing fatigue life, creep resistance, stress corrosion, and so forth. The selection of cutting conditions, cutting fluids, and cutting tools will eventually dictate the type of surface that is being produced in machining. The selection of these conditions is possible only by investigating and understanding their effects on the eventual state of the machined surface from both metallurgical and mechanical stand points. Hence, a multiscale surface integrity approach (macro, micro and submicro scale) has been adopted in this thesis to study the effects of cutting conditions, cutting tools, and varying cutting fluid applications on the final surface state.

The major aim of this thesis is to establish a fundamental understanding among topographical, mechanical, and microstructural characteristics of machining-induced surface integrity in Ti-6Al-4V titanium alloy. Additionally, this thesis also investigates the performance of Targeted Minimum Quantity Fluid (TMQF) application which strategically targets the cutting fluid (300ml/h) on the rake and flank face of the cutting tool while machining. Two inherently different cutting fluids (vegetable oil and synthetic fluid) were tested with TMQF application. The results obtained from TMQF machining are subsequently compared to those from dry and conventional flood machining (6 l/min) for further evaluation. Two different cutting tools (an uncoated tungsten carbide tool and a PVD-coated tungsten carbide cutting tool) were used to evaluate their interaction with cutting fluid application as well as their effects on the final machined surface state.

The microstructural characterization of the machined surfaces showed the presence of higher concentration of low angle grain boundaries (less than 5°) at the near machined surface for all cutting tool and cutting fluid applications under investigation. However, machining under the dry condition yielded a higher concentration of low angle grain boundaries at a larger depth (~100μm) from the machined surface compared to the other three cutting fluid applications. The presence of low angle grain boundaries is an implication of severe plastic deformation. Furthermore, machining under the dry condition produced a tensile residual stress profile and a lower hardness profile unlike those obtained with the other three cutting fluid conditions. These results clearly indicate the correlation between microstructural and mechanical characteristics of machining-induced surface integrity.

Flood machining with an uncoated tool and a PVD-coated tool produced contrasting residual stress profiles that signify the effect of the interactions between the cutting tool material and the cutting fluid application on the final surface state. Also, significantly different residual stress profiles were obtained for TMQF machining and flood machining which underline the importance of selecting the right cutting fluid application. The results from this thesis have the potential to close the knowledge gap between microstructural and mechanical characteristics of machining-induced surface integrity. Additionally, this thesis can aid in choosing the right combination of cutting fluid application and cutting tool for finish machining operation of Ti-6Al-4V titanium alloy to obtain a desired final superior surface integrity.

TABLE OF CONTENTS

LIST OF TABLES

Tables

ACKNOWLEDGEMENTS

First and foremost, I would like to thank my advisor and mentor, Dr. A.K. Balaji, for his guidance, encouragement, and support throughout this work. I would also like to thank Dr. S. Guruswamy, Dr. Ashley Spear, and Dr. Prasad Rao for their helpful suggestions and support.

I would like to thank Dr. Ravi Chandran for allowing me to use his laboratory equipment. Special thanks are due to Dr. Sekhar Rakurty, Mr. Trevor Shoemaker, and Mr. Patricio Varela for their invaluable support during my research work. They were always available to guide me through various pitfalls during this work. I would like to thank Dr. Javed Akram and Mr. Pankaj Kumar for helping me in preparing samples for microstructural analysis. I would also like to thank Dr. Paulo Perez, surface scientist at Nanofab, University of Utah. Without his guidance, I surely would not have succeeded in performing EBSD analysis. I would also like to thank Mr. Jeff Kessler and Mr. Tom Slowik for allowing me to use their laboratories and equipment. Thanks to Mr. Paul Hamric at the machine shop for guiding me through various issues that I faced while using the CNC machine. Finally, I would like to thank Vishay Measurements Group Inc., Pace Technologies, Sparks Tech Inc., DGI Supply, and Cimcool limited for providing me the resources to do this research in a timely manner.

CHAPTER 1

INTRODUCTION

Manufacturing processes help in converting a raw material into a final desired product by changing its geometry, property, and appearance. The final desired part can be obtained using different types of processing operations such as casting, forming, extruding, machining, molding, welding, additive manufacturing, grinding, and so on [1]. Generally, the final mechanical part is obtained by performing more than one of the above mentioned operations. The final operation performed on the part is known as the finishing operation or finishing process. Consequently, the finishing operation has an effect on the final surface state of the part. The term "surface state" has different meanings depending on the context. Here, the term surface state represents the *topography*, *chemistry at the interface with the atmosphere*, *metallurgy*, and *mechanical properties* [2] of the final processed part's surface. Traditionally, the choice of manufacturing process to obtain a final mechanical part depends on cost, time, and resources. However, over recent times, the state of the final surface generated has become an important factor in selecting the type of manufacturing process used to produce the final mechanical part. This is due to the fact that the final surface state of the part has a direct influence on the performance of the part during its service. This thesis focuses on one such finishing operation – machining and its effect on the final surface state.

1.1 Machining, Surface Integrity, and Microstructural Characterization

The methods used to change the geometry of a raw material can be broadly classified into three types namely: 1. Process that involves addition of material (+). 2. Process that involves moving

material from one region to another (0). 3. Process that involves removing material (-) [1]. Machining, which belongs to the third type, may be defined as the process in which excessive material is removed using a harder cutting tool, through a mechanical process of extensive plastic deformation [3]. Machining is the backbone for many manufacturing systems as it may be used as a primary manufacturing process or an important process in preparing the tooling for other processes like forming or molding. The ability of machining to produce extremely precise parts as well as its flexibility are the primary reasons for its domination over other manufacturing processes. The machining process can be classified into traditional machining processes and nontraditional machining processes. Turning, facing, boring, milling, drilling, grinding, reaming, broaching, burnishing, and honing are some of the traditional manufacturing processes, whereas electrical discharge machining (EDM), electrochemical machining (ECM), waterjet machining, laser machining, and plasma machining are some of the nontraditional machining processes.

Machining is also primarily used as a finishing operation for various components. The final machining operation used to produce a component changes the final surface state of the product. The attributes and state of the manufactured surface that influence its performance (fatigue, corrosion, and wear) are termed “Surface Integrity” [2]. Surface finish, defect-free surface, thermal damage, metallurgical changes, chemical changes, and changes in mechanical properties are some of the characteristics of surface integrity. These characteristics can be broadly divided into four categories: topographical, mechanical, microstructural, and chemical characteristics of the machined surface. Topography and chemical characteristics can be described as a surface/external feature whereas the microstructural and mechanical characteristics can be described as subsurface/internal features as shown in Figure 1.

Topographical characteristics of the surface includes surface roughness, waviness, and any microcracks present on the final machined surface. Microhardness, residual stresses, and microstructural characteristics represent the mechanical and microstructural characteristics of surface integrity. These features influence the functional performance of the machined part.

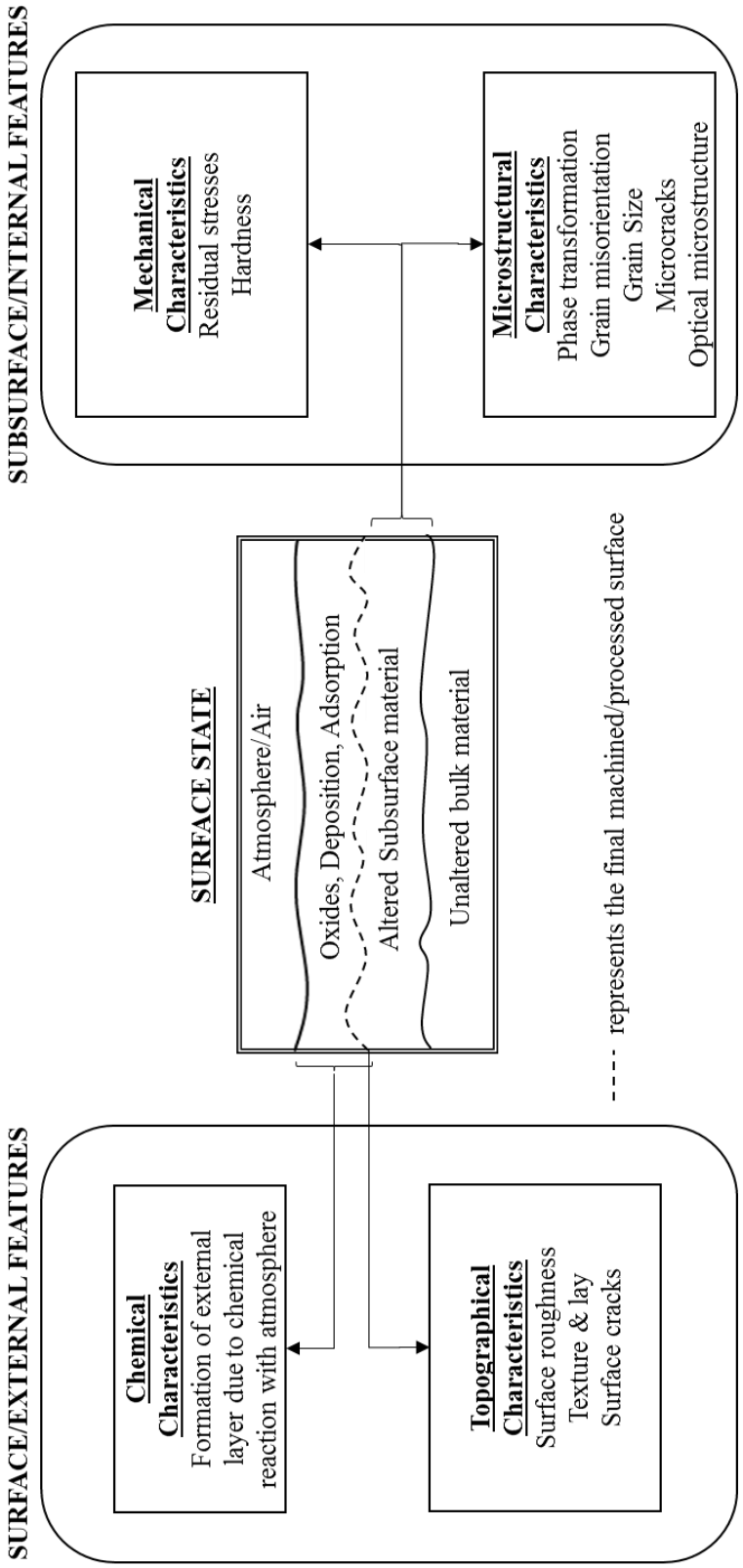

Figure 1 Features of Surface Integrity on a Typical Machined Component

Fatigue, wear, creep, and stress corrosion are some of the important functional performance parameters which are influenced by the surface integrity of the component in service. Both subsurface/internal and surface/external features of surface integrity influence the functional performance of a machined component as shown in Table 1.

Chemical characteristics of the surface are mostly dependent on the chemistry and elements present in the material and not on the manufacturing process. Hence, this aspect of surface integrity is not addressed in this thesis. Of all the topographical characteristics, surface roughness is one of the most important aspects for finishing operations and the most commonly measured variable in industry to evaluate the finishing process.

Residual stresses and microhardness of the machined subsurface constitute the mechanical characteristics of surface integrity. Residual stresses that arise due to the final machining operation have a direct effect on the performance of the part. Tensile residual stresses are considered to be undesirable as they reduce the fatigue life of the part considerably whereas compressive residual stresses tend to increase the fatigue life [1]. In machining, the material around the cutting edge is plastically deformed and dragged in the cutting direction. Hence, the hardness profile beneath the machined surface also provides valuable information regarding the final surface state of the machined component.

Microstructural characteristics of surface integrity also play a vital role in performance of the machined component. A deeper understanding of microstructural changes due to machining and their relationship with other surface integrity parameters are yet to be fully studied. Machining operations generate high strain-rates and high temperatures that are ideal conditions for microstructural changes such as phase transformation, white layer formation, changes in misorientation angle, microstructural texture formation, and so on. It is essential to establish a fundamental relationship between the microstructural changes and other surface integrity parameters to better understand the effect of the machining variables such as cutting fluid application, cutting tool, cutting conditions (feed rate, cutting speed, and depth of cut) et cetera.

Table 1. Functional Performance and Surface Integrity Features [2]

Functional Performance Influenced	External Features	Internal features
Creep	✓	✓
Wear	✓	✓
Lubrication	✓	-
Fatigue	✓	✓
Stress Corrosion	✓	✓

In this thesis, a comprehensive microstructural characterization will be carried out along with the measurement of surface roughness, residual stresses, and microhardness on the machined workpiece.

A multiscale surface integrity approach is undertaken in this thesis as shown in Figure 2. A macro, micro and submicro scale study of the surface state will help in estimating a fundamental relationship between various surface integrity parameters**.** ***No such multiscale surface integrity study has been carried out in the literature***. The multiscale approach on surface integrity will assist in studying the interactions and correlation between the various characteristics of surface integrity, thereby aiding in optimization of independent machining parameters such as cutting fluid application, cutting tool selection, cutting conditions and so on.

1.2 Cutting Fluids and Their Application

Sustainable and environmentally benign machining has received a lot of attention in recent times due to several reasons such as human health, environmental impact and diminishing world resources [4]–[7]. The most prominent environmental issue in machining is the use of cutting fluids. Apart from focusing on reducing the energy consumption in machining, there has been little research focused on optimizing the type and amount of cutting fluid used in machining. Depending on the workpiece and the manufacturing location, the costs related to the use of cutting fluid range from 7 - 17% of the total costs of the manufactured work piece [8].

Cutting fluids are most often applied in the form of a flood (on the order of 6 liters per minute or higher) directed at the cutting zone through external nozzles. They can also be internally supplied through the tool-tip at high pressure, which necessitates the use of more complex and expensive tooling infrastructures. The use of dry machining or minimum quantity lubrication (MQL) machining has bought a different perspective on the application of cutting fluid in machining. Minimum quantity lubrication (MQL) machining is a technique in which minute quantities of lubricants are atomized and delivered to the cutting zone in a compressed air jet.

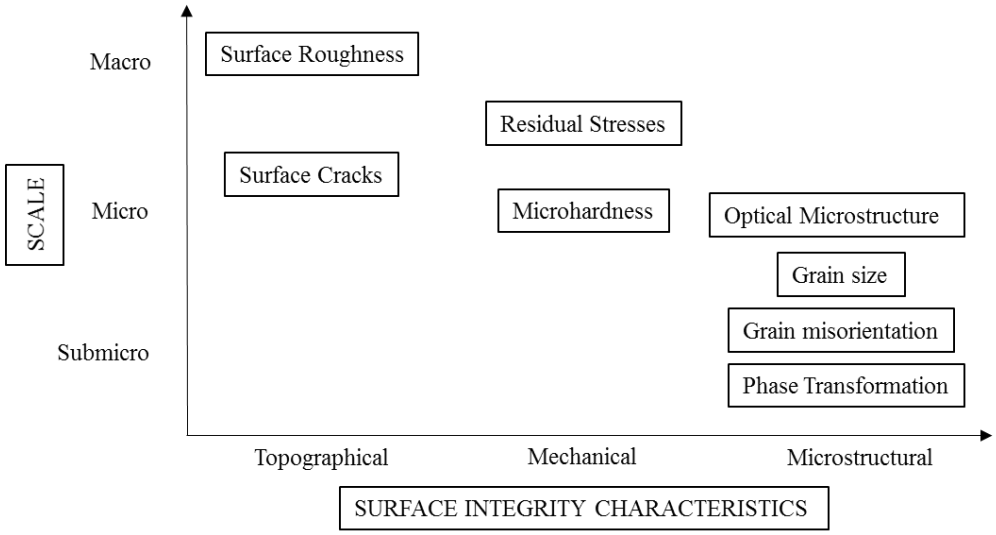

Figure 2 Multiscale Surface Integrity Approach

A major innovation in controlled and variable cutting fluid application, named the Targeted Minimum Quantity Lubrication (TMQL) system, was developed at the Sustainable Manufacturing Lab - University of Utah [9] wherein a significantly reduced volume of cutting fluid was delivered at targeted locations on the cutting tool rake face and flank face separately. In this thesis, three types of cutting fluid application, namely dry machining, flood machining, and TMQF machining will be evaluated.

The principal functions of the metalworking fluids in machining are to aid the cutting process and to provide a good surface finish and workpiece quality while extending the life of cutting tools [10]. The four common types of cutting fluid used in machining are straight oils, soluble oils, semisynthetic fluids, and synthetic fluids. Straight oils are primarily recommended for MQL. The selection of cutting fluid for machining process depends on the type of workpiece, cutting conditions, and cutting tool used. In this research, a synthetic fluid and a straight oil will be used to evaluate the TMQF system.

The effect of cutting fluids and their application has a significant influence on the final surface state. The effects of cutting fluid application on surface integrity of machined surfaces have not been well addressed in the literature. Furthermore, qualitative as well as quantitative characterization of the effects of such cutting fluid applications are also lacking. In this thesis, the effects of varying cutting fluids (controlled fluid volumes, fluid type, and fluid application target) on resulting machined surface integrity will be evaluated.

1.3 Cutting Tools

In machining, the cutting tool is the one that removes the material from the workpiece by means of shear deformation. The three basic properties that are essential for cutting tools are: 1. Hardness to withstand the wearing action. 2. Sufficient toughness to combat any interruption or vibration during the machining process. 3. Strength at high temperature to overcome the heat produced during machining [11]. The tool material plays a very important role in the life of the cutting tool

and also in the production of the machined surface. Hence, proper selection of the tool is of prime importance in machining. Cutting tools are selected based upon industrial requirements and the type of work material to be machined. Cutting tools are grouped depending on the tool geometry or depending on the type of coatings applied on the cutting tool substrate. A comprehensive study of the effect of interaction of cutting tool coating and cutting fluid application on surface integrity is an important part of this study. A coated and an uncoated cutting tool will be used in this thesis to evaluate its interactions with cutting fluid applications and also its effect on the final surface state. The tools used in this thesis will be chosen based on the industry standards for finishing operation and also for the type of workpiece material used.

1.4 Thesis Motivation and Outline

To carry out a multiscale surface integrity study, this thesis will focus on machining (facing) of a Ti-6Al-4V titanium alloy with single-point tungsten carbide turning tools. The cutting conditions such as feed rate and cutting speed will be chosen to represent a finishing process and it will be held constant for all experiments. The cutting fluid application and cutting tools are the only variables in this thesis. Once the machining experiments are completed, the surface integrity study will be carried out by measuring residual stresses, microhardness, surface topography/roughness, and microstructural alterations on the machined samples.

The main focus of this thesis is to study the effect of cutting fluid application and cutting tool on the final surface state of the machined titanium alloy. The primary motivations of the thesis are:

- The lack of in-depth research on the effect of cutting fluid application (in particular TMQF) on the final surface integrity (in a multiscale level) of machined sample.
- The lack of fundamental understanding between the machining-induced microstructural alterations and mechanical state of the machined surface.

The Ti-6Al-4V titanium alloy was one of the ideal materials to carry out this research due to several reasons such as:

- Machining of titanium alloys is a major industrial challenge due to its low thermal conductivity, low elastic modulus, and high chemical reactivity [12].
- Surface integrity is an essential aspect of Ti-6Al-4V titanium alloy as it is extensively used in critical parts of automobiles and airplanes.
- The alloy has two phases (α – HCP and β- BCC) which helps in evaluating the microstructure for phase transformation along the machined surface.
- Flood application is the recommend cutting fluid application strategy for titanium alloys. However, given the intense energy and environmental implications of such usage, evaluating the performance of TMQF machining of titanium alloy is appropriate.

The thesis is divided into five chapters. An in-depth analysis of the history of surface integrity and machining will be presented in Chapter 2. Titanium alloys and their machinability will also be discussed in detail in Chapter 2. Finally, Chapter 2 concludes with the history and importance of microstructural characterization in machined surfaces and its effect on the performance of the machined component. The detailed experimental plan will be presented in Chapter 3. The procedure to measure the surface and subsurface characteristics of the surface integrity will also be discussed in detail. Chapter 4 presents the results from the experiments outlined in Chapter 3. The discussion of the results and the discoveries will also be presented in Chapter 4. Chapter 5 will provide the conclusion of the thesis and the recommendations for future work.

Figure 3 shows a detailed thesis outline. All three characteristics of surface integrity (topographical, mechanical, and microstructural) will be tackled in this thesis. The inputs that will affect the final machined surface state will also be discussed. All the sections in this thesis and their corresponding subject area are also mentioned in Figure 3 (green colored text).

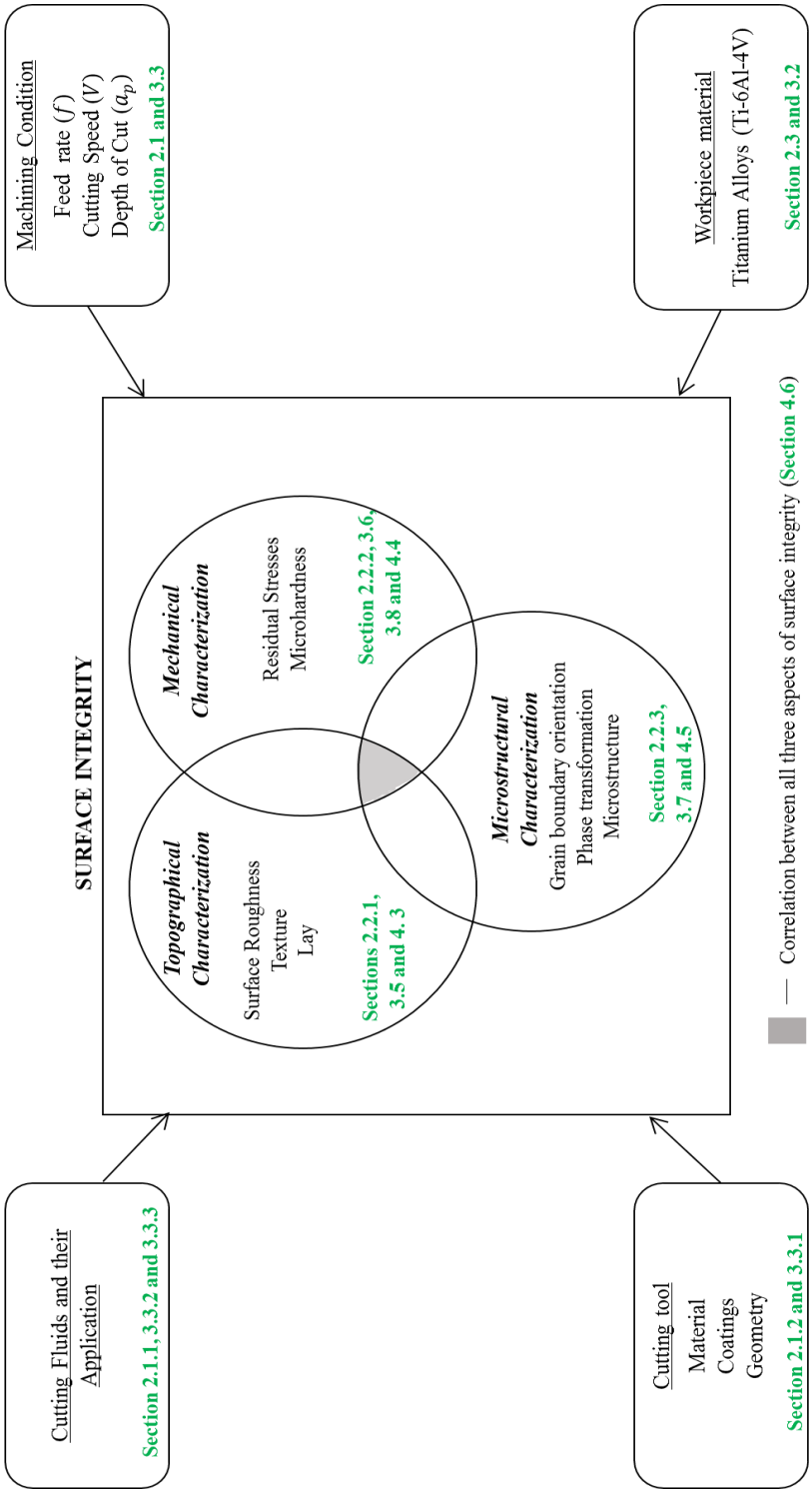

Figure 3 A Complete Thesis Outline Focusing on Machining (Facing) Induced Surface Integrity

CHAPTER 2

BACKGROUND

This chapter provides a detailed background/literature review of the topics relevant to this thesis, which includes but is not limited to machining, surface integrity, titanium alloys, and the importance of microstructural characterization of the final machined surface/subsurface.

2.1 Machining

Machining or metal cutting is one of the most commonly used manufacturing methods for removal of unwanted materials to produce the final machined part. Machining processes can be broadly classified as nontraditional and traditional machining processes. Nontraditional machining processes generally refer to a group of processes that uses electrical, thermal, chemical, and mechanical energy (or combinations of these energies) to remove material [13]. Abrasive water jet machining, electric discharge machining, ultrasonic machining, electrochemical machining, laser beam machining, ion beam machining, et cetera, are some of the common nontraditional machining processes [14]. Traditional machining processes can be further divided into cutting processes and abrasive processes. Facing, turning, shaping, drilling, boring, and milling are examples of traditional machining processes that involve metal cutting whereas grinding, polishing, honing, and buffing are examples of a traditional abrasive machining processes. The present study is focused on one of the traditional metal cutting processes.

Traditional machining (cutting) processes use a relatively sharp cutting tool to remove unwanted material from the surface of the workpiece in the form of chips. The cutting tool and the work-piece should have a relative motion in order to generate a new surface. Cutting speed and

feed rate are the two cutting conditions that represent the relative motion between the tool and the workpiece. The feed rate (f), the cutting speed (V), the depth of cut (a_p), the cutting fluid application, the cutting tool, and the workpiece are the key variables/parameters in any machining operation. The performance of the machining process depends on these parameters. The present study focuses on a facing operation which is shown in Figure 4.

In the facing operation, the cutting speed represents the speed at which the workpiece rotates and is usually represented in terms of meters per minute (m/min) or surface feet per minute (SFM). The feed rate (f) represents the distance that the cutting tool travels per revolution of the workpiece and it is represented in terms of millimeters per revolution (mm/rev). The depth of cut (a_p) represents the penetration of the workpiece below the original work surface before the start of the cutting process [15] and it is represented in terms of millimeters (mm). The feed rate (f), the cutting speed (V), and the depth of cut (a_p) used in this study can be found in Chapter 3. The cutting fluids and cutting tools are the other major input variables in machining that will be discussed in the following sections.

2.1.1 Cutting Fluids

Cutting fluids have been used in machining for a long time to increase productivity (high speed machining), prolong cutting tool life, prevent corrosion, and so on. Cutting fluids are primarily used in machining for lubricating, cooling, and removing the chips from the cutting zone [16]. Initially, water was predominately used as cutting fluid (before 1900) [17]. There was a rapid growth in cutting fluids during the industrial revolution (1900s) with the discovery of petroleum products that resulted in the introduction of compounded cutting oils and soluble oils as cutting fluids [17]. In order to reduce the manufacturing cost and environmental effects, there is a constant need for producing cutting fluids with better lubricating and cooling capacity with lowered volumes of usage. More than two billion liters of cutting fluid are currently consumed annually in the world [16].

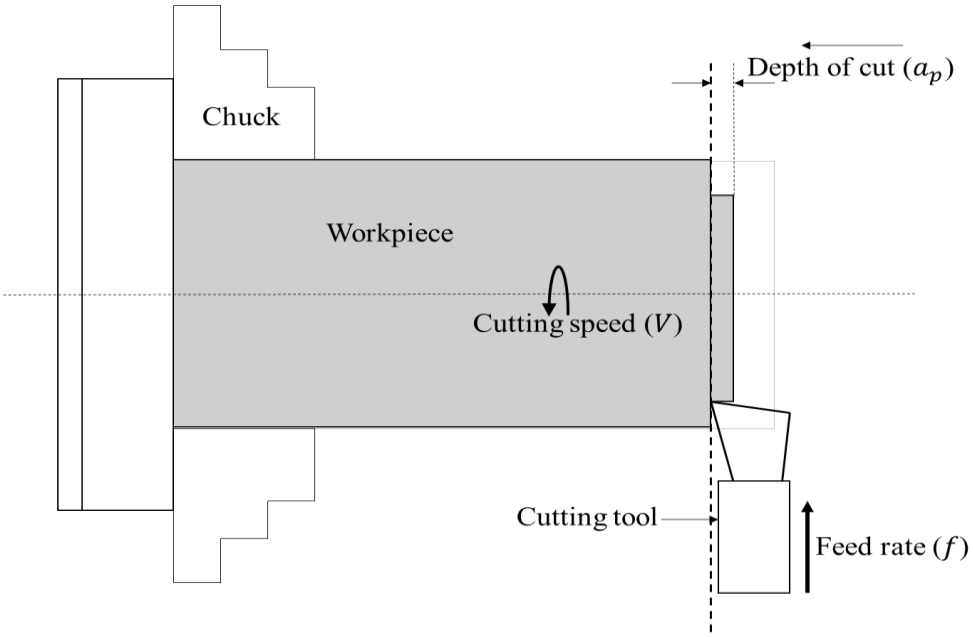

Figure 4 Schematic Representation of Facing Operation

The metal cutting process requires enormous amount of energy to plough through the workpiece using a cutting tool. This energy is converted into thermal energy in the form of high temperature. As a result, high temperature is generated in the cutting zone during the machining process. The life of cutting tools is drastically reduced due to the exposure to high temperature. It is essential to reduce the high temperature generated during metal cutting in order to improve cutting tool life. Another factor that accelerates tool wear is the friction between the cutting tool and workpiece. Hence a cutting fluid with excellent lubrication and cooling capacity is recommended while machining.

A great deal of chemistry is involved in producing a cutting fluid as it should have functional properties such as lubrication, microbial control, emulsification, corrosion inhibition and so on. [10]. Based on the chemistry, the liquid-based cutting fluids are broadly classified into 4 types.

1. Straight Oils: Straight oils consist of undiluted petroleum- or vegetable-based oils or undiluted petroleum oil, usually containing extreme-pressure (EP) or other performance enhancing additives that are used without dilution with water. The additives improve the viscosity of the straight oil, which in turn improves the lubrication effects of the straight oil. Vegetable oil and petroleum mineral oil are the most commonly used straight oil for metal working applications. Straight oils have relatively high lubrication capacity and low cooling capacity and hence are used for low speed cutting operations (such as broaching, gear hobbing, etc.). Vegetable oil is recommended for MQL application in machining [18] where minimal or low volume are used.
2. Soluble Oils: A fluid containing an emulsifier that allows it to dilute with water is called a soluble oil. Soluble oil is the most commonly used cutting fluid due to its ability to blend the lubricating effect of straight oils with the cooling effect of water. They consist of refined mineral oil, along with EP or other performance enhancing additives, dispersed in water with the aid of emulsifying agents. The soluble oil is usually supplied in concentrate form (30-

85% oil) and is diluted in water to form a solution that contains between 3-20% concentrate by volume. Soluble oils are used for light, medium, and heavy duty application.

3. Semisynthetic Fluids: The fluids containing under 30% of mineral oil are termed as semisynthetic fluids. Semisynthetics are readily soluble in water and have better solubility than soluble oils [10]. Semisynthetic fluids get their lubricating property from the mineral oil component and their cooling property from water. They also have a high tendency to foam in soft water and are unstable in hard water.
4. Synthetic Fluids: Synthetic fluids do not contain any mineral oils and offer relative high cooling effect but very little lubrication. Because they form true solutions with water, they are difficult to separate out for the purpose of disposal. The particle size of synthetic fluid is typically 3μm in diameter [19]. Emulsifiable synthetics contain some insoluble esters that improve the lubricating properties of the fluids.

Currently, some research is being conducted towards the development of nano-fluids for machining application [20]. Most often the cutting fluid used in machining is misapplied or overused and its effectiveness and potential to increase productivity is lost. Ideally, the selection of proper fluid and the method of application should be one of the critical design criteria in machining processes. It is essential to use the proper cutting fluid application to get its full benefits. The different cutting fluid application methods are discussed below.

1. Dry Machining: When a machining operation is carried out without the presence of any type of cutting fluid, then the machining operation is called dry machining. Dry machining has been gaining popularity in the last few decades due to the advancement in cutting tool materials and coatings. The increase in concerns regarding environmental pollution and worker health and safety has also led to interest in dry machining [21]. Dry machining also reduces the overall cost of machining. However, super alloys such as Ti-6Al-4V titanium alloy and inconel alloys are difficult to machine without using cutting fluid [22]. Moreover, the high temperature generated during the machining process may lead to an increase in

thermal residual stresses and hence may affect the component's functional performance [23]. Dry machining is also refereed as green machining due to associated environmental benefits.

2. Flood Machining: When machining is carried out under the influence of a jet of cutting fluid with flow rate equal to or above 6 liters/min, the machining operation is called flood machining. Since an enormous amount of cutting fluid is used in this machining, serious environmental and health issues are associated with it. However, this type of machining helps in dramatically reducing the temperature in the cutting zone and it also improves the surface finish and removes chips efficiently [1]. In flood machining, the production cost is relatively high due to the usage of enormous amount of cutting fluids. Recycling and disposing the cutting fluids also adds to the manufacturing cost.
3. MQL Machining: In minimal quantity lubrication machining, the cutting fluid is sprayed on the rake face in the form of very fine mist. Generally, cutting fluid with excellent lubrication property is used for MQL machining. The maximum flow rate of cutting fluid applied in MQL machining is 300 ml/h MQL machining is considered an alternative for dry and flood machining because of its ability to reduce temperature at the cutting zone by employing a minimal quantity of cutting fluid. However, there have been many contradicting studies in the literature on the effects of MQL machining on the final machined surface state. The negative effects of the MQL machining are primarily due to its inefficiency in reducing/optimizing the temperature in the cutting zone.
4. TMQF machining: In order to address the disadvantages of the MQL system, a novel multiple cutting fluid dispensing system called the targeted minimum quantity fluid system was developed at the Sustainable Manufacturing Laboratory, University of Utah [24]. For the traditional flood cutting fluid application and MQL application, the fluid is directly applied only on the rake face. In TMQF application, the cutting fluid is strategically targeted on the rake and the flank face of the tool to optimize the temperature generated in the cutting zone. A previous study shows a positive impact of TMQF machining on the final surface state [9].

2.1.2 Cutting Tools

The next most important variable/parameter in the machining process is the selection of the cutting tool. A cutting insert and a tool holder are the two components of the cutting tool. Sandvik Cormorant, Kyocera, Kennametal, and Iscar are the leading cutting tool manufacturers. The tool holder is selected based on the type of machining operation. The three important parameters in selecting a cutting tool insert are: substrate material, geometry, and coating.

To remove the material from the workpiece, the cutting tool material should be able to withstand the rigorous cutting action. The three basic problems that a cutting insert material (substrate) should overcome are. 1. The shock generated in the cutting action. 2. The wear that takes place at the cutting edge due to high temperature and friction. 3. The high temperature generated at the cutting zone [11]. The cutting tool insert substrate material is selected primarily based on the type of workpiece. The choice of the material plays an important role in the life of the cutting tool and also in the quality of the machined surface. Tungsten carbide, high-speed steel, or ceramic are some of the commonly used substrate materials for cutting inserts. Tungsten carbide inserts are more than three times stronger than high-speed steel and are predominantly used for hard-to-machine materials. Cutting tools are available in different shapes and the shape is selected depending on the type of machining operation performed and also the type of tool holder. Square, round, rhombic, triangle, diamond, and hexagon are some of the cutting insert shapes that are available in the market. The selection of the geometry of cutting tool also involves selecting the type of cutting edge. The cutting edge can be either chamfered, double chamfered, honed, or sharp [25]. A quick review of literature shows that the coatings on the hard insert substrate has increased tool life several fold [26-28]. 70% of the carbide tools used in industry are coated [29]. The coatings on the cutting insert act as a barrier for diffusion and thereby prevent diffusion wear. Moreover, the coating material is typically harder than the substrate and provides an excellent abrasion resistance during the machining process. The coating material helps in reducing cutting forces and cutting temperature due to their thermal properties [11]. Titanium Carbide (TiC), Titanium Nitride (TiN),

Titanium Aluminum Nitride (TiAlN), Titanium Carbonitride (TiCN), and Alumina (Al_2O_3) are some of the commonly used coating materials in cutting tools. Single-layer coating and multilayer coating (more than 2 layers) are common types of coating for cutting tool inserts. The coating material and type is selected based on the type of machining operation and workpiece material.

The two common methods used for coating cutting tools are Physical Vapor Deposition (PVD) and Chemical Vapor Deposition (CVD). The PVD process is a vacuum deposition process in which one or more of the depositing species are evaporated or atomized from a solid source in the coating chamber and are deposited on the substrate material. The CVD process is also a vacuum deposition process in which the substrate material reacts with the coating material to form a thin film on the surface of the substrate. In the CVD process, the coating material is deposited on the substrate in a gaseous or vapor form. A detailed explanation of PVD and CVD processes can be found in reference [30].

2.2 Surface Integrity

Field and his co-workers were the first to introduce the term surface Integrity (*SI*) and made a significant contribution to the subject. Their preliminary efforts laid the foundation for future research in this field [31–34]. According to Field, the term *SI* is defined as the *inherent or enhanced condition of a surface produced in machining or other surface generation process* [31]. Field and his coworkers [35] carried out a comprehensive study on the *SI* of machined structural components and published a 362-page report. The work emphasized the different characteristics of *SI* and presented a comprehensive *SI* dataset as shown in Table 2. This ground breaking achievement in the field of *SI* lead to the establishment of an American National Standard on *SI* [36] in the year 1986. Even the most recent studies in the field of *SI* in machining [37-40] are based of the *SI* dataset developed by Field and his co-workers. From Table 2, it is clear that *SI* is not concerned only with the topographical characteristics of the surface but it reflects a combination of their physical, mechanical, metallurgical, chemical, and biological properties and characteristics [34].

Table 2 Surface Integrity (*SI*) Data Sets (adapted from [35])

Minimum *SI* data set	Standard *SI* data set	Extended *SI* data set
1. Topography/Surface Feature Surface Roughness Lay Designation/Texture Macrostructure (10x or less) Macrocrack Indications 2. Microstructure Microcracks Plastic Deformation Phase Transformation Intergranular Attack Pits, Tears, Laps Built-up Edge Melted/Redeposited Layers Selective Etching 3. Microhardness	1. Minimum *SI* Data Set 2. Residual Stress 3. Fatigue Test	1. Standard *SI* Data Set 2. Fatigue Test (extended to obtain design data) 3. Additional Mechanical Tests Tensile Stress Rupture Creep Other Component-Specific Tests

As stated in the previous chapter, the attributes and state of the manufactured surface that influences its performance (fatigue, corrosion, and wear) are called Surface Integrity [2]. The functional performance of a machined component is heavily influenced by the quality and reliability of the surface machined, both in terms of the topography as well as the metallurgical and mechanical state of the subsurface layer [37]. Hence in this thesis, the *SI* dataset will be split into three categories and analyzed as: 1. Topographical Characterization, 2. Mechanical Characterization, and 3. Microstructural Characterization. Fatigue experiments and other mechanical tests are a direct measure of the functional performance of the machined surface state. A complete *SI* study will include these mechanical tests. However, due to the time and costs of these mechanical tests, this thesis will focus only on the three characteristics (as listed above) of *SI* and their interactions.

2.2.1 Topographical Characterization

Topographical characterization of the machined surface includes surface roughness, waviness, lay and macrocracks (surface defects). The presence of macrocracks in a machined surface is not likely unless abusive machining (machining with extremely high machining parameters (f, V, a_p) and/or a severely worn-out tool) is carried out. For a facing/turning operation, the machined surface is expected to have a rectilinear parallel lay class [2]. Hence, most of the researchers only report the surface roughness parameters when it comes to topographical characterization of the machined surface.

Thomas [41] was among the first to publish a work on the effect of the workpiece surface topography on the fatigue life and that laid the foundation for the development of metrology instruments to measure surface topography quantitatively. In early fatigue models, a component's performance was completely attributed to its surface topography. However, later studies on surface integrity proved that the assumption was wrong and that the functional performance of a component depended on other *SI* parameters such as the workpiece's final mechanical and microstructural

state.

The standard terminologies and parameters used to describe a surface can be found in ASME B46.1 [42]. Some of the most commonly used surface topography/roughness parameters are amplitude height parameters (R_a , R_t), amplitude distribution (R_{sk}), and shape (R_{ku}) parameters. Of these parameters, arithmetic average height (R_a) is the parameter that most of the researchers use in SI studies of machined workpieces and it is defined as the average absolute deviation of the surface irregularities from the mean line over a considered sampling length. In other words, it is the measure of the average geometric deviation of the final surface from an ideal flat surface along one direction over a sampling length. This deviation of the final surface is mainly due to the workpiece-tool interface and partly due to factors such as tool wear, machine tool vibration, cutting fluid application and so forth.

The correlation between workpiece surface roughness and fatigue life has not been clearly established. Most *SI* studies have reported that low surface roughness will result in relatively higher fatigue life, but some studies suggest that for the surface roughness values in the range of 2.5–5 µm (R_a), the fatigue life is primarily dependent on workpiece residual stress and surface microstructure rather than roughness [43]. These conflicting results make surface roughness measurements and subsequent analysis an essential part of any *SI* study.

There are several methods used to measure surface roughness parameters. The surface roughness measurement methods can be broadly classified into two types: 1. Contact method and 2. Noncontact method. In this thesis, a noncontact optical profilometer is used to measure the surface roughness. A typical optical profilometer uses the wave properties of light to form dark and light interference fringes which are used to measure the 3-dimensional state of the surface. They measure the height (Z axis) over an area (X and Y axis) as shown in Figure 5. The red and pink spots in Figure 5 are the peaks (high spots) whereas the blue spots are the valleys (low spots), which are created due to machining. Additional information about other surface roughness measurement methods can be found in reference [2].

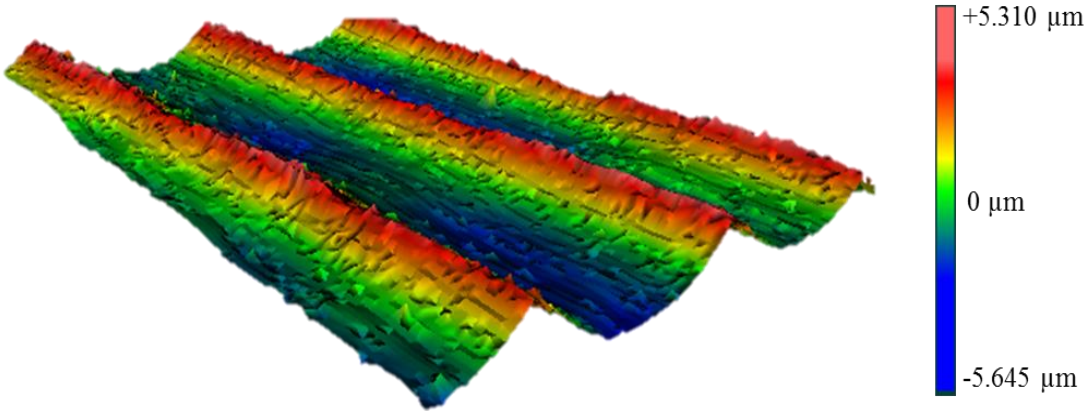

Figure 5 Topography of a Machined Surface Obtained From Surface Analysis Software - MetroPro (Red and blue color indicates highest and lowest point on the surface respectively)

2.2.2 Mechanical Characterization

The microhardness profile and residual stress profile along the subsurface of the machined component constitutes the typical mechanical characteristics of *SI*. These properties define the machined surface state that has the most significant influence on the functional performance of the machined component. On reviewing the literature, it can be seen that most of the SI studies in machining focus on either microhardness or the residual stresses profile along the machined subsurface. To obtain a completed picture of the mechanical characteristics of the machined surface state, it is essential to measure both these properties and the correlation between them.

The measurement of hardness is a simple but useful technique for characterizing the mechanical properties of the surface. The hardness measurement in the machined subsurface is an indication of the level of strain hardening that a surface has undergone due to a machining operation. Hardness is a property that is related to the plastic flow of a material [1]. Microhardness measurements starting near the surface and subsequently along the depth of the machined surface will help in evaluating the machining condition. Generally, in machining, the hardness profile of the machined surface/subsurface will show a significant increase in hardness at the surface when compared to the bulk undeformed material hardness. A typical hardness profile in a machined surface is shown in Figure 6.

Residual stresses are the most significant parameter in any *SI* study. The stresses that remain in the material/component even after removing all the external loads such as forces, stresses, acceleration and thermal loads are called residual stresses [44]. Residual stresses are present in almost all machined components. Even though the residual stresses induced in machined components are found in only a very thin layer (usually less than 1mm from the machined surface), they have a significant effect on the functional performance of the component. Residual stresses are either tensile or compressive in nature. Tensile residual stresses are undesirable, especially for parts that are under cyclic loading. The presence of tensile residual stresses accelerates the growth of fatigue cracks when compared to a compressive residual stress.

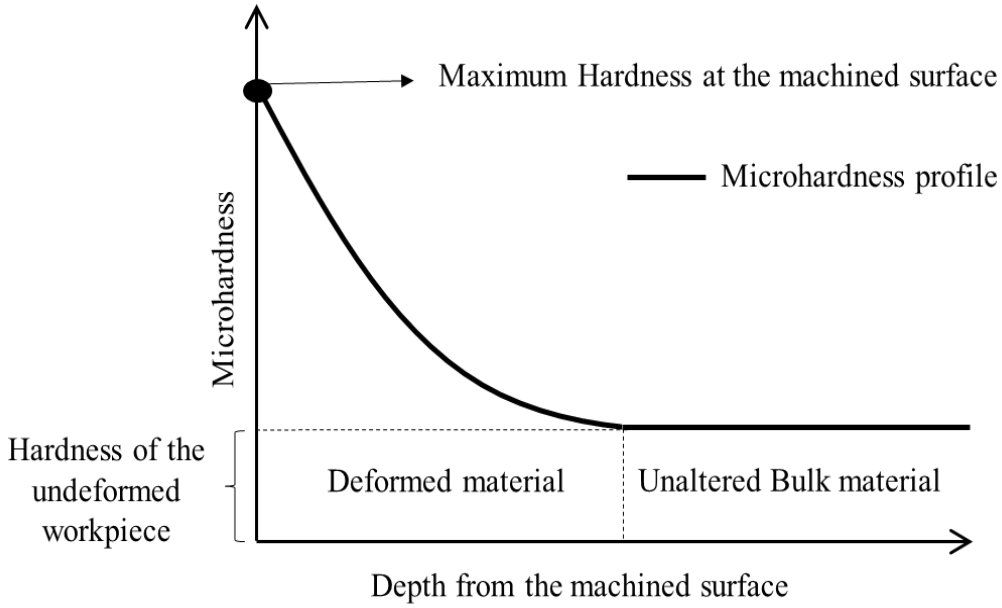

Figure 6 A Typical Microhardness Profile Obtained From Machined Surface/Subsurface

Residual stresses generated in machining can be attributed predominantly to three mechanisms: 1. Thermal phase transformation mechanism. 2. Thermal and plastic deformation mechanism. 3. Mechanical deformation mechanism [2]. In a facing/turning operation, the residual stresses are generated due to the combination of these three mechanisms. This makes it difficult to optimize the machining conditions to obtain a desired residual stress profile. A typical residual stress profile generated in a machined/processed surface is shown in Figure 7.

Vickers microhardness measurement is the most commonly used method to measure hardness in the machined subsurface whereas there are several residual stress measurement methods. Residual stresses are not directly measured. The strains in the surface are measured and then the residual stresses are calculated. The brittle lacquer method, dissection method, curvature method, hole drilling method, X-ray diffraction method, and neutron diffraction method are some of the methods that can be used to measure residual stresses. In this thesis, the hole drilling method is used to measure the residual stresses. The hole drilling method is a semidestructive method for measuring the residual stresses. In this method, a small, shallow hole is drilled on the machined surface through a strain gage, thereby relieving the strains. These relieved strains are then measured by a specially configured three element strain gage rosette. The measured strain data set is then processed with the help of the principles of solid mechanics to obtain relaxed residual stresses present in the machined component. Further explanation about the hole drilling method and other methods used to measure residual stresses can be found in the reference [45].

2.2.3 Microstructural Characterization

Neailey [46] was among the first to present a comprehensive study on the microstructural characteristics of *SI* and its influence on the functional performance of the machined component. The term microstructure may be defined as all the internal features/structure of the material that affect the material properties. These features are confined to a microscopic level.

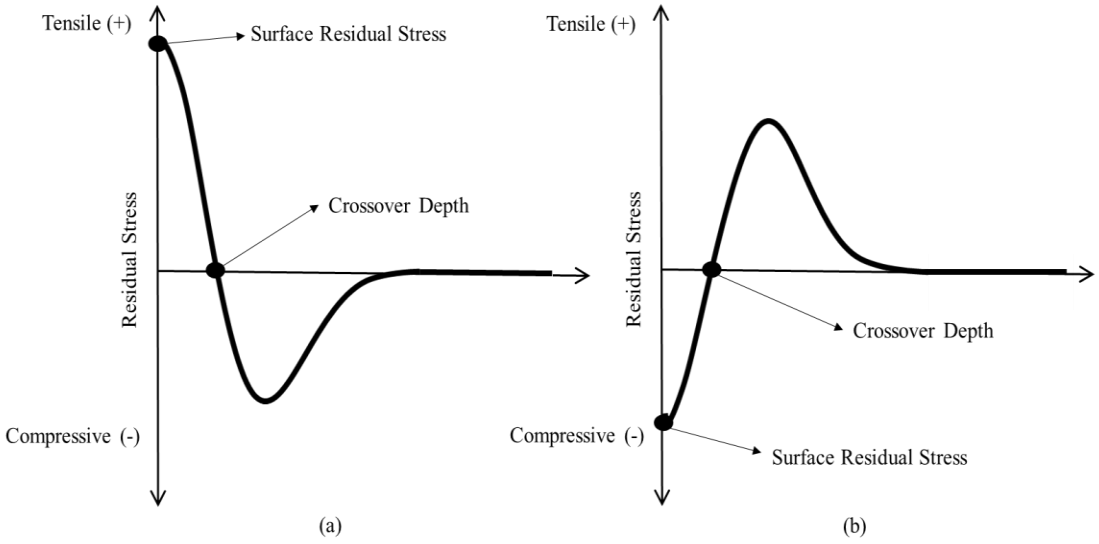

Figure 7 Typical Residual Stress Profile (a) Tensile (b) Compressive

Grain size, grain orientation, phase transformation, microcracks, degree of plastic deformation and distribution of low and high angle grain boundaries are some of the microstructural features that play an important role in the *SI* of machined components. The changes in microstructural features will be predominant near the machined surface and the changes will reduce along the depth of the machined surface until it reaches the unaltered bulk microstructure. This variation is similar to that found in the microhardness and residual stress profile.

Microstructural characterization can be performed using different tools. Optical microscope, scanning electron microscope (SEM), transmission electron microscope (TEM), atomic force microscope (AFM), and X-ray diffraction (XRD) method are some of the most commonly used tools to perform microstructural characterization in machined components. In this thesis, a scanning electron microscope (SEM) with electron backscatter diffraction (EBSD) technique and an optical microscope were used to study the microstructural changes in the subsurface of the machined workpiece.

Some of the commonly used terms in this thesis to carry out microstructural characterization are defined below:

1. Grain boundary: The boundary that separates two grains may be defined as the grain boundary. Grain boundaries play a vital role in recrystallization, phase transformation and also in some case strength of the metal [47]. The difference in the orientation of the two adjacent grains at the grain boundary is called the misorientation angle. In other words, misorientation may be defined as the difference in the crystal axes between the two adjacent grains. The misorientation of the grains along the machined surface is measured in this thesis using scanning electron microscopy (SEM). Grain boundaries can be further classified into two types:
    a. Low angle grain boundary: If the misorientation angle between the two grains is less than 15°, then the grain boundary is called a Low Angle Grain Boundary (LAGB).

b. High angle grain boundary: If the misorientation angle between the two grains is greater than 15°, then the grain boundary is called a High Angle Grain Boundary (HAGB)

2. Phase Transformation: All metals exist in different crystal structures or phases based on various external factors like temperature and pressure. The high temperature that is generated in machining may cause a metal to transform from one phase to another. The phase in which a metal exists will dictate its mechanical, thermal, and electrical properties. Discussion on various mechanisms and classifications of phase transformation is beyond the scope of this thesis.
3. Pole figure and inverse pole figure map: A pole figure (PF) map is a schematic representation of the crystallographic orientation that uses the crystallographic direction in the sample coordinate system, whereas an inverse pole figure (IPF) plots the sample directions in the crystallographic coordinate systems. IPF maps are preferred over the conventional pole figure maps for studying crystallographic orientations. Discussing the construction of pole figure maps and inverse pole figure maps are beyond the scope of this thesis and a detailed explanation on these can be found in the reference [47].

An optical microscope can be used to investigate the changes in the microstructure qualitatively. Orientation imaging microscopy (OIM) is a tool that can be used to determine the orientation of the crystal with respect to a particular axis/direction. SEM with the electron backscatter diffraction (EBSD) technique can be referred to as Orientation imaging microscopy (OIM). EBSD is a complementary characterization tool to SEM for quantitative analysis of the microstructural features to obtain crystallographic information such as phase transformation, grain size, and grain orientations. A flat and a highly polished sample is required for EBSD analysis. The polished sample should be tilted at a 70° angle with respect to the primary incident electron beam coming from the electron source as shown in Figure 8. The phosphorus screen is used as the EBSD detector and it is placed at 90° to the primary electron beam.

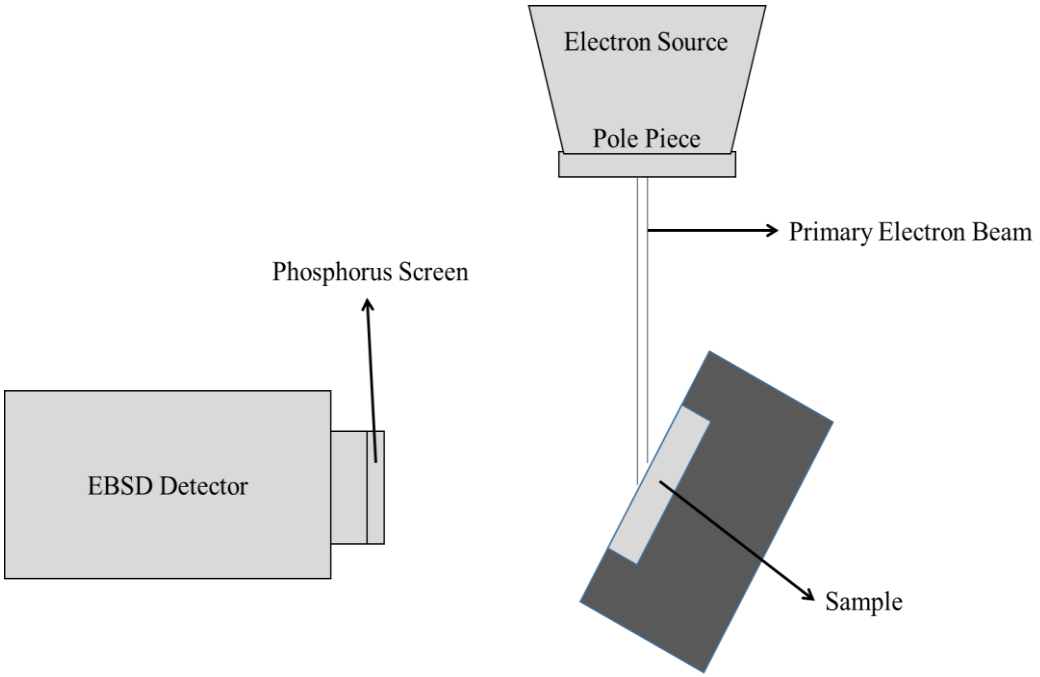

Figure 8 Schematic Arrangement of Sample Orientation in the SEM for EBSD. (Adapted from [47])

An electron beam with an accelerating voltage of 10–50 kV and an incident current of 1–50 n A interacts with the sample surface (crystal lattice) and generates low energy loss backscattered electrons. These backscattered diffracted electrons form a pattern on the phosphorus screen. The diffraction pattern (also known as an EBSD pattern) is characteristic of the crystal structure and orientation in the sample region where it was generated. Hence the EBSD patterns that are produced on the phosphorus screen are used to obtain the crystallographic information (phase and orientation) of the scanned region. A detailed explanation of the working of the EBSD technique and its application in material science can be found in reference [47].

The use of the EBSD technique for studying microstructural changes produced by machining is relatively new. To et al. [48] used the EBSD method to study the orientation changes due to precision machining of single crystal aluminum and Zn-Al-based alloy. Yamamoto et al. [49] detected the presence of slip bands and small angle grain boundaries near the machined surface in austenitic stainless steel. M'Saoubi and Ryde [50] measured the depth of the plastic deformation zone below the machined steel surface using the EBSD technique.

In one of the most recent studies, Bissey-Breton et al. [51] studied the influence of machining on microstructure in low carbon martensitic stainless steel. The effect of change in feed rate (f) on the final microstructure was studied and the results show that there is formation of grain sub-boundaries for lower values of f and grain refinement for higher values of f. Zhou et al. [52] characterized the machining-induced microstructural alterations in Inconel 718 using the EBSD technique. They found the presence of a higher concentration of low angle grain boundaries (LAGB) near the machined surface. Plastic deformation due to machining results in formation of subgrain boundaries near the machined surface which in turn shows up as LAGB.

2.3 Titanium Alloys

Titanium and its alloys have an excellent combination of high specific strength and fracture toughness as well as low density and excellent corrosion resistance. They are half the density of

steels and Ni-based super alloys. Due to their unique and remarkable mechanical properties, they are used in various industries such as bio-medical, automotive, aerospace, and chemical industries. Titanium was first discovered in 1791 by the British chemist William Gregor [53].

2.3.1 Metallurgy

Titanium exists in two crystallographic forms. At room temperature, commercially pure unalloyed titanium has a hexagonal close packed (HCP) crystal structure called "alpha (α) phase." At 1621° F (883° C), this structure transforms to a body centered cubic (BCC) structure called "beta (β) phase" [53]. By controlling these crystallographic variations with the help of varying alloying additions and using different thermo-mechanical processing techniques, a wide range of titanium alloys can be developed. Titanium can be grouped into 3 different types based on their metallurgy as follows.

1. α Alloys: Unalloyed Ti and its alloys with α stabilizers such as Al, Ga, and Sn constitute this group of alloys. These α stabilizing elements work by either preventing change in the phase transformation temperature or by causing it to increase [7]. Ti-5Al-2.5 Sn is the most common α alloy that is used commercially. They are predominantly used for high temperature application. They are most often used in the annealed or recrystallized condition to eliminate residual stresses caused by working [7].
2. β Alloys: This group of alloys generally contain large amounts of one or more β stabilizers such as V, Nb, Ta, and Mo. These stabilizers tend to decrease the temperature of α to β phase transition and thus promote development of the BCC (body centered cubic) β phase [7]. These alloys have excellent forgeability over a wide range of forging temperatures. However, these alloys are prone to brittle-ductile transformation and are not suitable for low temperature applications. An example of this group is Ti-10V-2Fe-3Al [7].
3. α + β Alloys: These alloys, usually at room temperature, contain both α and β phases. This group has a composition that contains both α and β stabilizers. Solution treating and aging

can increase the strength of alpha-beta alloy from 30% to 50% or more, over the annealed or over-aged condition [6]. This group of alloys can be further divided into near α and near β alloys based on the amount of α and β stabilizers present in them. The properties of these alloys can be controlled through heat treatment, which is used to adjust the amounts and types of phases present in the alloy. An example of this group is Ti-6Al-4V [7].

As mentioned in the previous chapter, Ti-6Al-4V was selected as the work material in this thesis. Ti-6Al-4V is an α + β titanium alloy (near α alloy) containing around 6% aluminum (α stabilizer) and 4% vanadium (β stabilizer). At room temperature, the Ti-6Al-4V titanium alloy consists mostly of the hexagonal closed packed (HCP) α structures with some retained β structure. Ti-6Al-4V is by far the most common and widely used titanium alloy, which accounts for more than 50% of the total weight of all titanium alloys that are commercially used [7]. It has an excellent combination of high strength, toughness, and corrosion resistance. This alloy may be used over a broad range of temperatures from cryogenic to about 427 °C (800 °F) for long term applications [7]. This alloy has the perfect balance of the properties of α alloys and β alloys due to the presence of both α and β stabilizers.

A wide variety of processing techniques are applied to T-6Al-4V to produce a range of products exhibiting a wide range of microstructures. Depending on the cooling rate and prior heat treatment, the microstructure of Ti-6Al-4V titanium alloy obtained can be of different types as shown in Figure 9. The β phase transforms into a globular type of α structure when the cooling rate is slow whereas an increase in the cooling rate will promote the formation α platelets. In this thesis, Ti-6Al-4V is β-annealed (995^{o} C ± 20^{o} C) to remove any stresses due to previous operations. The starting microstructure of the Ti-6Al-4V titanium alloy consists of α platelets/lamellae forming α colonies. The β phase was present only along the α grains. Some ‘coarsened α’ structures were also present in the microstructure due to cooling defects. The annealed Ti-6Al-4V titanium used in this study has a structure similar to Figure 9 (f) with some “coarsened α” structures. The length of the α platelets also primarily depends on the heat treatment procedure.

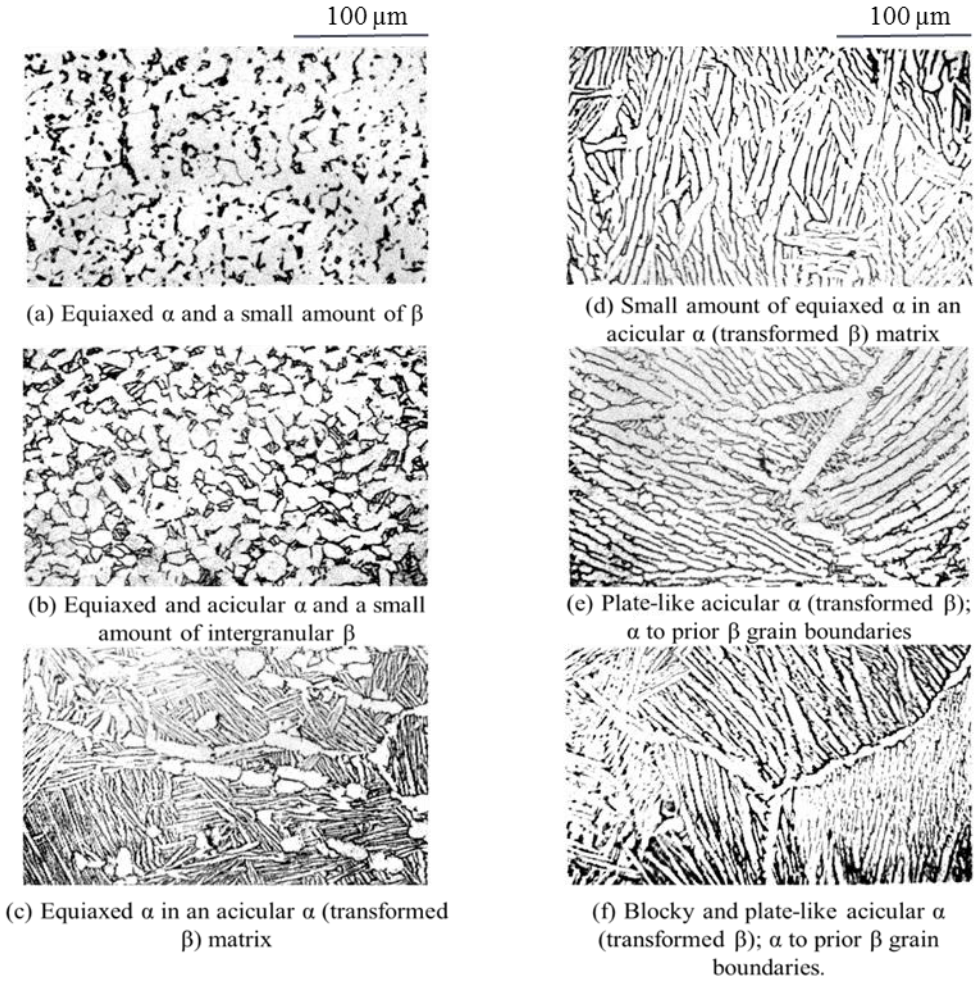

Figure 9 Optical Microstructures of Ti-6Al-4V Titanium Alloy in Six Representative Structures [54]

2.3.2 Machining

Titanium alloys, in particular Ti-6Al-4V, are classified as difficult to cut materials due to several reasons, such as low thermal conductivity, high chemical reactivity, and low elastic modulus [55]. Titanium alloys, due to their high chemical reactivity, react with oxygen, nitrogen, carbon and so on, at higher temperatures, which makes them susceptible while machining because of the abundance of these gases in the air. Due to formation of titanium oxide on the surface, it is difficult to lubricate the surface while machining [1]. Lower cutting speeds are recommended while machining titanium alloys to prevent high temperatures while machining. Due to the low thermal conductivity of titanium alloys, a large temperature rise occurs while machining titanium alloys.

Machinability of a material is usually determined based on criteria such as tool wear, tool life, cutting force, cutting temperature and surface integrity. Machinability of titanium is deemed poor based on the above-mentioned criteria. The most commonly used cutting tools for machining titanium alloys are uncoated and coated cemented carbides (WC/Co). TiAlN coated carbide tools are predominately used for machining titanium [56]. Titanium alloys react with most cutting tool materials and that hinders the life of the cutting tool. Ezugwu et al. [57] performed machining of titanium in an inert gas enriched environment and observed better tool life. According to [49] and [50], the tool coating in carbide tools rapidly fails during machining titanium alloys due to the high temperature generated between the tool and chip. Zareena and Veldhuis [60] machined Ti-6Al-4V titanium alloy using a diamond tool and found that the tool wear was primarily due to the built up edge (BUE) and chemical interaction between workpiece and tool. Recently, Rashid et al. [61] studied the tool wear mechanism in an uncoated carbide tool when machining Ti-6Al-4V titanium alloy.

The use of a cutting fluid is highly recommended while machining titanium alloys as they generate high temperatures and also to ensure reasonable tool life as an enormous amount of heat goes into the tools. The increasing demand for environmentally friendly machining has urged researchers to investigate high pressure cooling, MQL machining, cryogenic machining, and dry

machining. Palanisamy et al. [62] investigated the effect of high pressure coolant application on tool life while turning Ti-6Al-4V alloy. The highly pressurized coolant application on the rake and flank face of the cutting tool increased the tool life by three times and also generated smaller chips. Sadeghi et al. [63] evaluated the grindability of Ti-6Al-V titanium alloy with MQL using synthetic and vegetable oil. MQL grinding with synthetic fluid produced a better surface finish (roughness) and lower grinding forces whereas MQL with vegetable oil showed a better cooling effect in the grinding zone. According to Fujiwara et al. [64], a longer tool life was obtained while machining titanium alloy under mist application when compared to a dry condition. Rotella et al. [65] studied the effect of dry, MQL, and cryogenic cooling conditions on surface roughness and subsurface hardness of machined Ti-6Al-4V titanium alloy. MQL and cryogenic cooling conditions produced better surface finish when compared to dry machining. Cryogenic cooling produced higher surface/subsurface hardness indicating that it has a better cooling effect than MQL. The correct selection of lubrication and cooling conditions is essential while machining titanium alloys as it has large influence on tool life and surface integrity of the machined part.

2.3.3 Surface Integrity

Titanium alloys are used in critical components of aircraft and automobiles. Hence, surface integrity of the component is an essential aspect as it directly influences its functional performance. Surface integrity characteristics such as topographical characteristics (surface roughness, texture), mechanical characteristics (residual stresses and hardness), and microstructural characteristics (grain size, grain orientation, phase transformation, microcracks) of titanium alloys are largely affected during the machining operation [56].

Riberio et al. [66] optimized the machining of Ti-6Al-4V titanium alloy by conducting a series of experiments and evaluating the final machined surface roughness. Results showed that the surface roughness was largely influenced by built-up edge formation on the cutting tool. Ramesh et al. [67] carried out a surface roughness analysis in the machining of titanium alloys. Tests were

conducted using a CVD-coated carbide tool under different cutting conditions (feed (f), cutting speed (V) and depth of cut (a_p)). Results showed that increasing cutting speed (V), and depth of cut (a_p) decreased the surface roughness (Ra). Ginting and Nouari [58] machined titanium alloys using an uncoated and CVD-coated carbide cutting tool and found that the uncoated tool produced a better surface finish than the CVD-coated tool. Recently, Sargade et al. [68] analyzed the surface roughness generated during turning of Ti-6Al-4V under varying cutting conditions. After analyzing the results, they concluded that the optimum cutting conditions for machining Ti-6Al-4V ELI titanium alloy were: cutting speed (V) – 66.97m/min and feed rate (f) – 0.08 mm/rev.

Sun and Guo [69] performed an experimental study on the machining-induced surface integrity of Ti-6Al-4V titanium alloy and found that the cutting speed and feed had a significant influence on the surface residual stresses. Hughes et al. [70] worked on the effects of tool edge preparation on the surface integrity of a Ti-6Al-4V work piece and reported that significant microstructural damage was visible along the cutting direction. Puerta-Velasquez et al. [71] analyzed the surface and subsurface of orthogonally machined Ti-6Al-4V titanium alloy under varying cutting conditions and found that there was no phase transformation along the machined surface/subsurface as the composition of the α and β phases remained the same. Che-Haron and Jawaid [72] worked on the effect of dry machining on the surface integrity of Ti-6Al-4V alloy. They carried out microstructural analysis and found severe tearing and plastic deformation along the machined surface/subsurface in Ti-6Al-4V titanium alloy. Ibrahim et al. [6] and Colafemina et al. [73] claimed to have worked on surface integrity in machined titanium alloys but neither included the residual stresses aspect of surface integrity in their study. Arisoy and Ozel [74] adapted a machine learning based predictive model to predict microhardness and grain size in machined Ti-6Al-4V titanium alloy under a dry environment.

Ulutan and Ozel [40] published a comprehensive review of machining-induced surface integrity in titanium alloys. Some of the important conclusions from the review were:

1. The subsurface microstructure of machined titanium alloys is altered significantly due to plastic deformation and, in some cases, white layer formation.
2. Due to high mechanical and thermal loads, the surface and immediate subsurface of the material becomes harder because of work hardening.
3. Surface roughness was also largely influenced by the high temperature generated during machining.
4. In most cases, increase in cutting speed, feed rate, and depth of cut has a negative impact on machining-induced residual stresses.
5. Carbide tools are still the most commonly used material for machining titanium alloys. Coated tools have a delamination problem while machining titanium alloys and that affects the final machined surface state and tool life.

2.4 Summary

The background and literature survey on machining, surface integrity, and titanium alloys, presented in this chapter helps in framing the objectives and the experimental plan for this thesis. As shown in Figure 3 (Chapter 1), this thesis will focus on all three characteristics of surface integrity (topographical, mechanical, and microstructural) unlike most of the previous research in the field of machining-induced surface integrity. This thesis will also evaluate the effect of different cutting-fluid applications on the difficult to machine titanium alloy. A systematic study of machining-induced surface integrity will be planned and executed in the following chapters.

CHAPTER 3

RESEARCH PLAN

The purpose of this chapter is to provide a detailed description of the research plan that includes the machining experimental plan and the methodology used in measuring dependent variables such as machining forces, chips obtained from machining, surface roughness, subsurface residual stresses, microstructural characterization, and subsurface microhardness profile.

3.1 Objectives

The research plan was constructed in order to meet the following objectives:

- To establish a fundamental relationship between the machining-induced microstructural deformation and mechanical characteristics of surface integrity.
- To investigate the effect of cutting fluid application (dry, flood, TMQF) on final surface state.
- To study the interaction between cutting tools (uncoated and coated carbide tools) and cutting fluid application.
- To investigate the effect of cutting tool coatings on subsurface microstructural deformation.
- To investigate the effect of cutting fluids (synthetic fluid and vegetable oil) used in Targeted Minimum Quantity Fluid (TMQF) application on the final surface state.
- To complete a well-defined multiscale surface integrity study on machined Ti-6Al-4V titanium alloy.

3.2 Overview

The experiments were designed with the view of achieving the objectives of this research. Based on the literature survey and the research objectives, the variables to be measured were identified. Machining forces, chips, surface roughness (texture), residual stresses, microhardness, and microstructural deformation are the parameters that were identified as necessary to fulfill the main objectives of this thesis.

Machining temperatures would have been another variable that would help in evaluating the different cutting fluid applications used in this research study. Due to the difficulty involved in measuring the temperature in machining, machining temperatures were not measured. Tool wear measurement was also omitted as it requires a different experimental study which is time consuming; however, such a study can be performed as future work.

Since a surface integrity study was carried out in this research, machining parameters such as feed, cutting speed, and depth of cut were chosen to represent a finishing operation and are maintained constant for all experiments. Another reason to keep these parameters constant was that a large amount of prior research has been focused on these parameters alone. Eight facing operation experiments were designed with cutting tools and cutting fluid application modes being the only variables. Two different cutting tools and four different cutting fluid application modes were used in this study such that all the major research objectives were addressed. The multiscale surface integrity study that were carried out in this study can be broadly classified into study of external features and internal features as shown in Figure 10.

A facing operation was carried out to conduct the surface integrity study. A flat machined surface was generated by the facing operation. The reasons for choosing facing operation are:

1. The hole drilling strain gage residual stress measurement method is generally limited to flat surfaces [75].
2. A flat surface is ideal for surface roughness measurement. Surface curvature could provide an additional distortion to the measured surface.

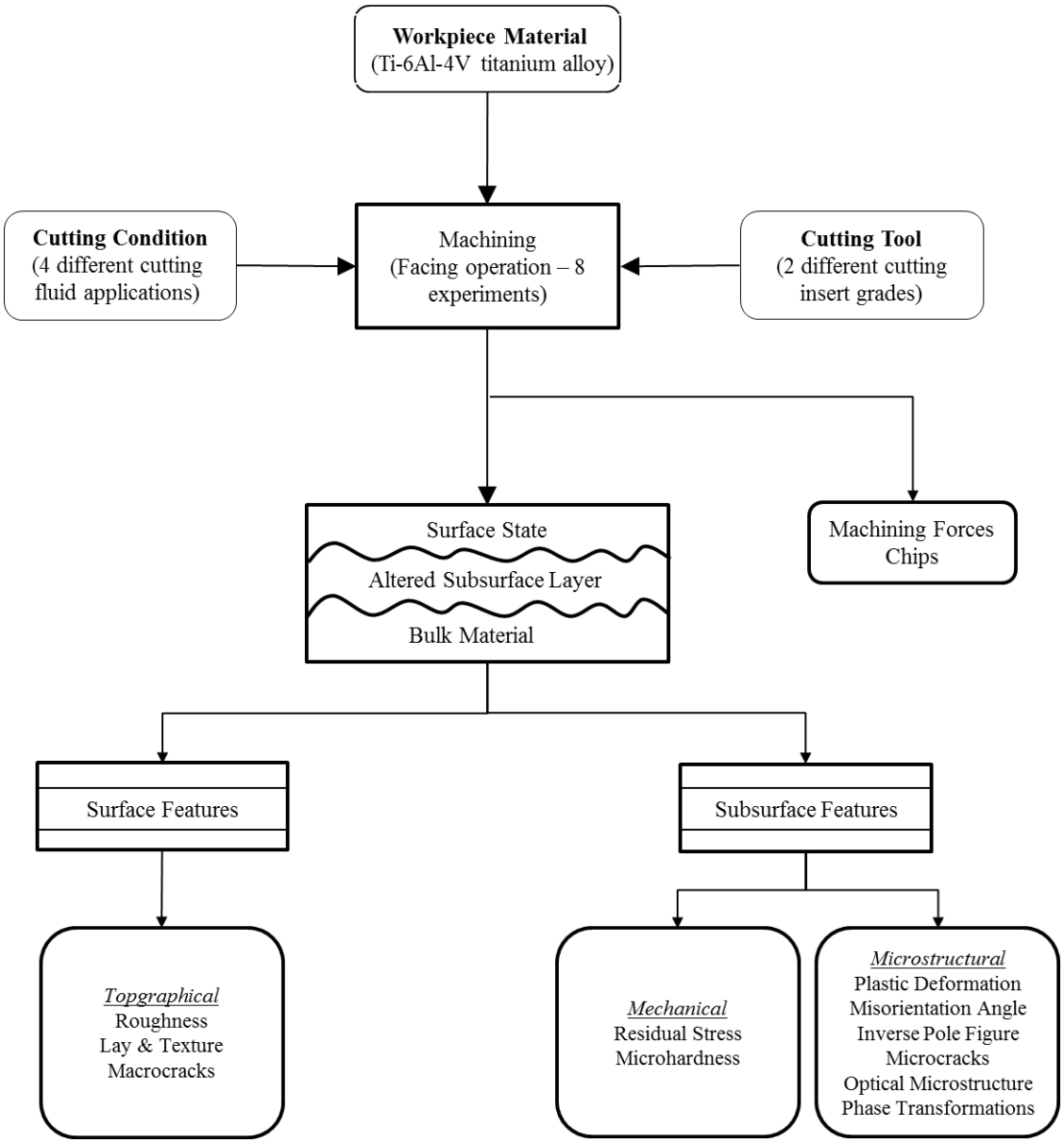

Figure 10 Surface Integrity Study Plan for This Research

Ti-6Al-4V annealed titanium alloy (grade 5) was used in this study. The material elements, properties, and thermal and mechanical data for Ti-6Al-4V can be found in Tables 3 and 4. Machining forces are in-situ measured during the machining process – by using a cutting tool dynamometer - while chips are collected using a chip collecting tray. All other parameters were measured after the machining experiments were completed. The procedure to measure all the parameters will be discussed in this chapter.

3.3 Machining Experiments

All the machining experiments were carried out on a HAAS SL-20 CNC turning center, with a travel of 20" and maximum cutting diameter of 10.3" under a single fixed cutting condition (feed, cutting speed, and depth of cut). Titanium machining involves facing a cylindrical surface to produce a new flat machined surface. Figure 11 shows the dimensions of the work piece used in all the experiments (4" in diameter and 2" in length). A prior facing operation was carried out to make the workpiece flat and void of any band saw marks. Since a surface integrity study was to be carried out in this research, the workpiece needed to be free from residual stresses due to prior machining. Hence, a stress-relieving heat treatment process was carried out to remove the residual stresses that may have been induced due to prior machining and other prior processing. The typical stress-relieving process involves heating the material to a certain temperature, maintaining it at that temperature for a suitable time, and then cooling in a furnace. The stress-relieving conditions for Ti-6Al-4V titanium alloy were obtained using the time-temperature-transformation (TTT) chart [76]. All eight workpieces used in this research study were premachined and held at 550^{o}C for 2h using a Lindberg laboratory box furnace (Model: BF51842 – Figure 12). The workpieces were then furnace cooled. The cutting conditions such as feed rate and cutting speed were chosen to represent a finishing operation as it was deemed appropriate for this study (since the immediate subsurface integrity is the focus of the thesis).

Table 3 Material Component Constituents for Ti-6Al-4V Titanium Alloy [76]

Constituents	Aluminum, Al	Oxygen, O	Iron, Fe	Titanium, Ti	Vanadium, V
Weight Percentage	6.00%	<=0.25%	<=0.20%	90.00%	4.00%

Table 4 Mechanical Properties of Ti-6Al-4V Titanium Alloy [76]

Mechanical Properties	**Ti-6Al-4V (unit)**
Ultimate tensile strength	950 MPa
Tensile yield strength	880 MPa
Modulus of elasticity	113.8 GPa
Poisson's ratio	0.342
Vickers hardness	334 HV
Density	4.42 g/cc
Thermal conductivity	6.70 W/m-K
Melting point	1604 – 1660 °C

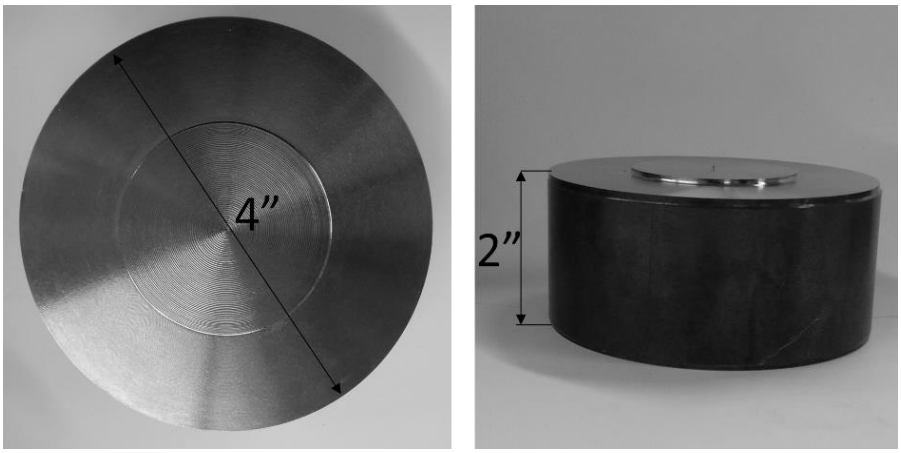

Figure 11 Dimension of the Workpiece

Figure 12 Lindberg Box Furnace Used for Heat Treatment

The typical feed rate (f), cutting speed (V) and depth of cut (a_p) used for Ti-6Al-4V titanium alloy machining are 0.2mm/rev (0.0079 in./rev), 1.2 mm (0.0472 in.) and 75 m/min (246 surface feed per min) respectively and these cutting conditions were used in this study. The three stages of the workpiece-pre-machined, heat treated, and postmachining experiments are shown in Figure 13a, 13b, and 13c, respectively. The CNC program used for the machining experiment can be found in Appendix A.

3.3.1 Cutting Tools

Two different cutting tool insert grades were chosen to study the interaction between coated and uncoated inserts with cutting fluid applications and their effect on final surface state. Tungsten carbide cutting inserts are the most commonly used cutting inserts for titanium machining. CNMG 432 AH KW10-Grooved uncoated tungsten carbide cutting insert and CNMG 432 TK PR1125-Grooved (TK) single-layered PVD (TiAlN) coated tungsten carbide insert (Figure 14) manufactured and supplied by Ceratip-Kyocera were used for this research study as per the industry recommendation for finishing operation of Ti-6Al-4V titanium alloy [77]. Only the grooved cutting insert geometry was used in all experiments in order to reduce the number of variables in the study. A groove is a design feature in cutting tools to enable effective chip breaking and chip formation. Both the tools used in this research have a rake and inclination angle of -5° and major cutting edge angle of 90° which is appropriate for the facing operation (machining experiment) conducted as part of this thesis. Each letter on the cutting insert grade has its own significance. The reader is directed to the Kyocera cutting manual for a detailed explanation of each letter in the insert designation [77].

The cutting insert tool holder used for the experimentation was manufactured by Kennametal. The ISO designation of this tool holder is given by MCFNR 124B. The ISO tool holder identification system can be found in the Kennametal cutting tool manufacturer's catalogue [78].

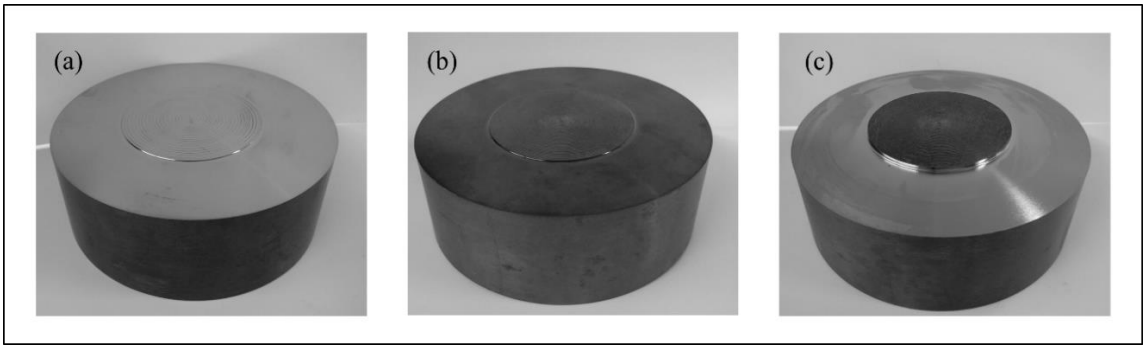

Figure 13 Three Stages of Workpiece (a) Premachined (b) Stress Relieved by Heat Treating (c) After Machining Experiment

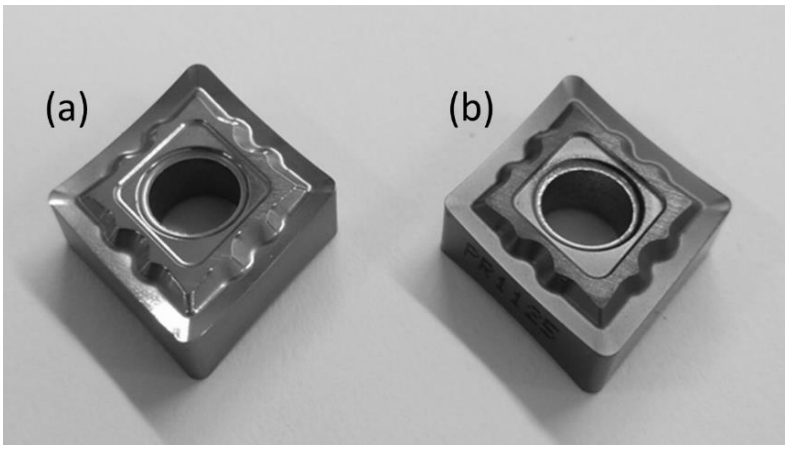

Figure 14 Cutting Tools (a) Uncoated Tungsten Carbide Cutting Tool b) PVD-Coated Carbide Tool

3.3.2 Cutting Fluid Application

Three different cutting fluid application conditions were chosen for this research with the view of evaluating the effect of cutting fluid application on the final surface state in Ti-6Al-4V titanium alloy. The three different conditions are as follows:

- Dry machining: No cutting fluid is used in this type of machining. Generally, titanium machining is carried out with copious amounts of cutting fluid [53]. However, dry machining was chosen to study the effect of temperature on the final surface state as there is no cooling involved in this process. Figure 15 shows machining in a dry environment.
- Flood machining: The most commonly used cutting fluid application for titanium machining is flood machining, in which a high-volume stream of fluid is applied on the approximate rake face zone (untargeted) at a predefined flow rate. In this study Cimtech 310, which is a synthetic cutting fluid, was mixed with water in the ratio of 1:9 and was applied on the rake face zone during machining at a flow rate of 6 liters/min.
- Targeted minimum quantity fluid application (TMQF): TMQF is a new cutting fluid delivery system that was developed at the Sustainable Manufacturing Laboratory at the University of Utah [80]. In this system, the cutting fluid is strategically targeted at the rake face and flank face of the tool to vary and optimize the usage of cutting fluid as shown in Figure 16. A recent study carried out using this cutting fluid delivery system has shown that it can produce compressive residual stresses in the machined subsurface [9]. A flow rate of 300ml/h was chosen for all experiments that use TMQF application. Two different cutting fluids along with compressed air were used in this application to further validate the effect of TMQF application on final surface state. The two different cutting fluids used in this application will be discussed in the following section. Figure 17 shows the TMQF setup used in this research.

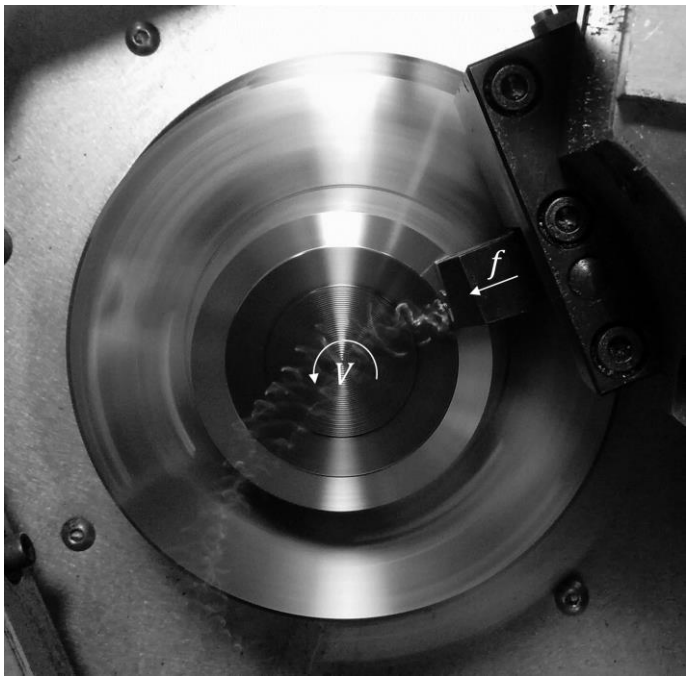

Figure 15 A Picture of Machining Experiment (Dry Condition)

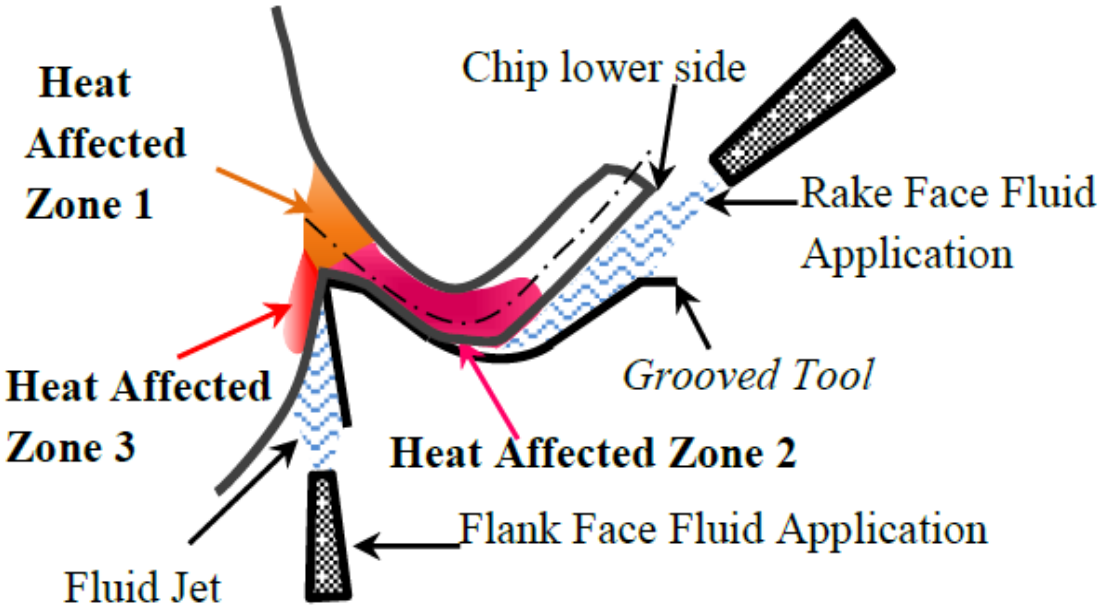

Figure 16 Schematic Representation of Targeted Minimum Quantity Fluid (TMQF) Application [9]

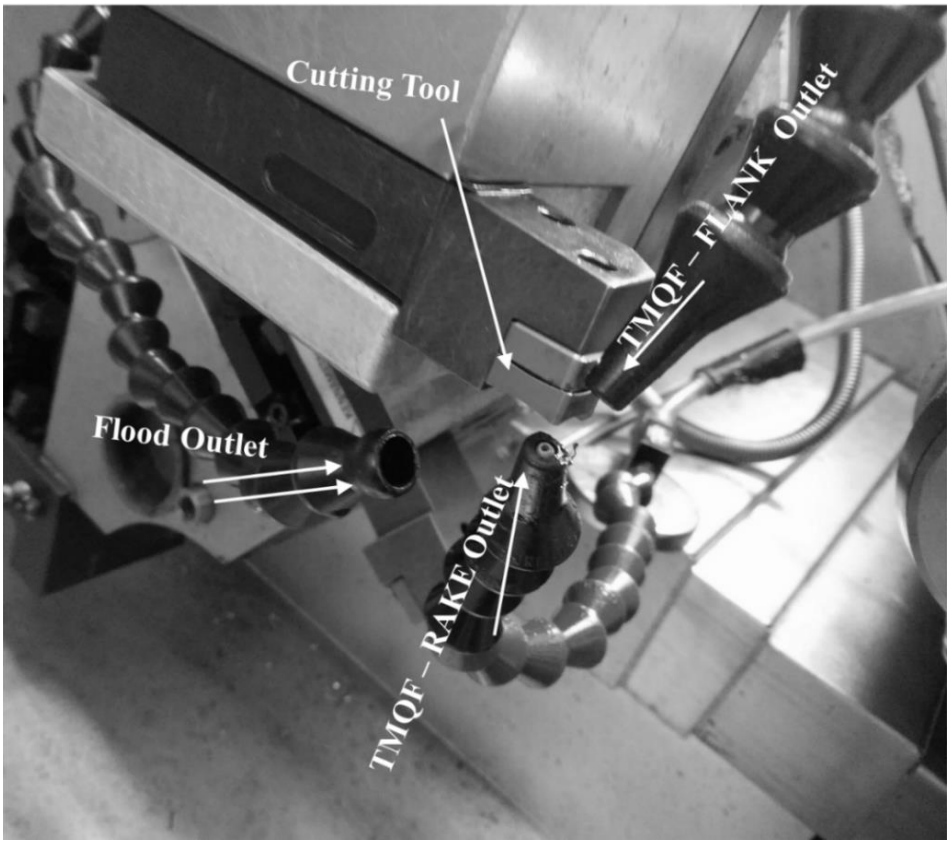

Figure 17 Targeted Minimum Quantity Fluid (TMQF) Application Setup and Flood Outlet Used in the Experiments

3.3.3. Cutting Fluids

Two different cutting fluid were used in the TMQF application whereas flood machining was carried out using only one cutting fluid, which was chosen based on the industry standard. Both cutting fluids used in the research were produced by Cimcool Fluid Technology Ltd, a leading cutting fluid manufacturer. Table 5 shows the comparison between the two fluids.

- CIMTECH 310: This metalworking fluid is a unique, low pH synthetic fluid designed to use for machining and grinding of titanium alloys [79]. It has relatively high lubricity, tool life and surface finish properties. This water-soluble synthetic fluid ***was mixed with water at the ratio of 1:9 to produce a cutting fluid*** which was used ***both in the flood application and the TMQF application***. In the TMQF application, the cutting fluid is used along with compressed air at the pressure of 0.689 MPa.
- CIMFREE VG-703ES: This is a vegetable-based metalworking oil that is recommended for minimum quantity lubricant (MQL) application [18]. This vegetable oil ***is used neat (100%) and not mixed with water.*** CIMFREE VG-703ES is used in the TMQF application along with compressed air at a pressure of 0.689 MPa.

3.4 Machining Chips and Force Measurement

Machining chips are produced in metal cutting process. The form of chips produced during the machining process has important implications for the cutting forces, machining temperatures, surface roughness, and tool life [1]. It is necessary to analyze the chips to better understand the dynamic actions that take place during the machining process. The chips were collected from all machining experiments using a chip collecting tray shown in Figure 18. The collected chips were later photographed to conduct further analysis. The determination of the cutting force components is essential for analyzing the machining process and it is one of the most common parameters that are measured during a cut. The most common method of measuring machining forces is using a dynamometer.

Table 5 Comparison Between Cimtech 310 and Cimfree VG 703 ES

Properties/Features	**CIMTECH 310**	**CIMFREE VG-703 ES**
Type of Fluid	Synthetic fluid	Vegetable oil
Solubility in water	100% miscible	Insoluble
Viscosity @ 100^{O} F (Saybolt Universal Seconds)	110	50
Appearance	Clear	Clear
Cost per gallon[1]	$36.22	$52.80
Effective cost in TMQF machining (per hour)	$0.86	$4.17
Industry Recommendation	Flood machining	Minimum quantity application

Note: Data from DGI supply – authorized cutting fluid distributors.

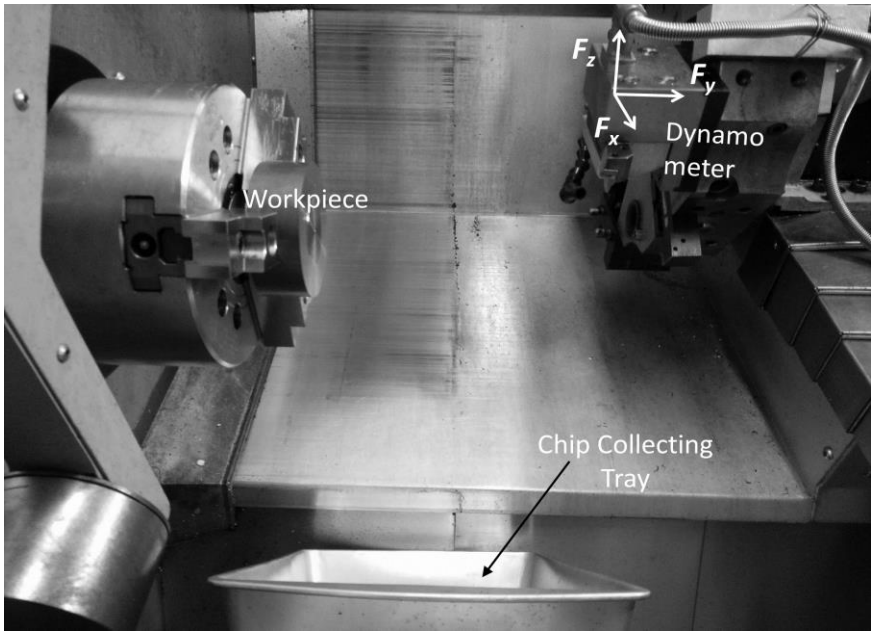

Figure 18 Machining Force Component Overlaid on Kistler Dynamometer and Chip Collecting Tray in CNC Lathe

A Kistler® three-component force dynamometer (type: 9121) and charge amplifier (type: 5010) coupled with National Instruments Lab View based data acquisition system were used to measure the cutting forces for this study. The three force components measured in this study are the feed force (F_x), the radial force (F_y), and the cutting force (F_z). The dynamometer is installed on the tool holder of CNC machine as shown in Figure 18. The three force components were measured before, during and after the cut. All three force components that were measured by the dynamometer have a level of noise associated with them due to tool vibration and other external elements. Additionally, the machining operation takes a few microseconds to reach a steady state and hence there is more fluctuation in the measured machining forces. Therefore, the average force measured during the machining operation is recorded as the mean force of the operation and this is applicable for all three force components. The machining forces (F_x, F_y, and F_z) were measured for all eight machining experiments.

3.5 Surface Roughness Measurement

Surface roughness (texture) an important surface physical property that has a direct influence on fatigue failure, wear failure, and corrosion failure [2]. All machining operations create a pattern or texture on the machined surface that is a function of the tool geometry and relative motion of the tool and workpiece. Surface roughness is defined as the geometric deviation of the final surface from the desired surface [1]. Surface roughness can be measured using different methods such as the stylus method (contact), optical instruments, and scanning probe microscopy. The ASME B46.1 [42] standard for surface roughness measurements can be referred to for a detailed explanation of all possible methods of measuring surface roughness.

In this study, a Zygo® NewView 5000 series optical interferometry-based surface profilometer was used to measure the surface roughness values of the machined workpieces. The surface roughness was measured at three different spots on the machined surface using a 20x magnification

lens on the Zygo Optical Profilometer as shown in Figure 19. The MetroPro metrology software package was used to investigate and quantify the surface roughness in the machined surfaces.

Figure 20 shows the Zygo profilometer setup that was used to measure the surface roughness and it also shows the fringes that are obtained as a result of geometric deviation in the machined surface. The dark bands in the fringes represent the feed marks. For all experiments, the two-dimensional roughness average (R_a) in the feed direction with a 0.8 mm cutoff length was calculated with +/- one standard deviation displayed. Note that the variation indicated by the standard deviation was a result of the variation in the surface profile between the three sample locations and cutting speed direction variation. R_a values were considered for comparison in this present research as it is a very commonly used surface roughness measurement reported in the literature.

3.6 Residual Stress Measurement

Generally, all machining operations leave the surface in a stressed state. Even though such residual stresses induced by machining are limited to a thin surface layer, they have a significant effect on the functional performance of the machined part [2]. Residual stresses are a significant aspect of the final surface state in a machined component. There are different methods [81] to measure the residual stress such as the X-ray diffraction technique, hole drilling method, ultrasonic-based measurement and the curvature method.

In this study, the hole drilling strain gage method was used to measure the residual stresses in all machined Ti-6Al-4V titanium alloy samples. The procedure that was utilized to measure the residual stresses using the hole drilling method is in accordance with a standard testing method-ASTM E837 [75]. The hole drilling strain gage method involves an incremental drilling of holes through a strain gage that is bonded to the workpiece surface. The strain gage measures the strain due to the residual stress that is released or relaxed while drilling the holes. The measured strain was post processed using the H-drill software package to yield the residual stress in the surface.

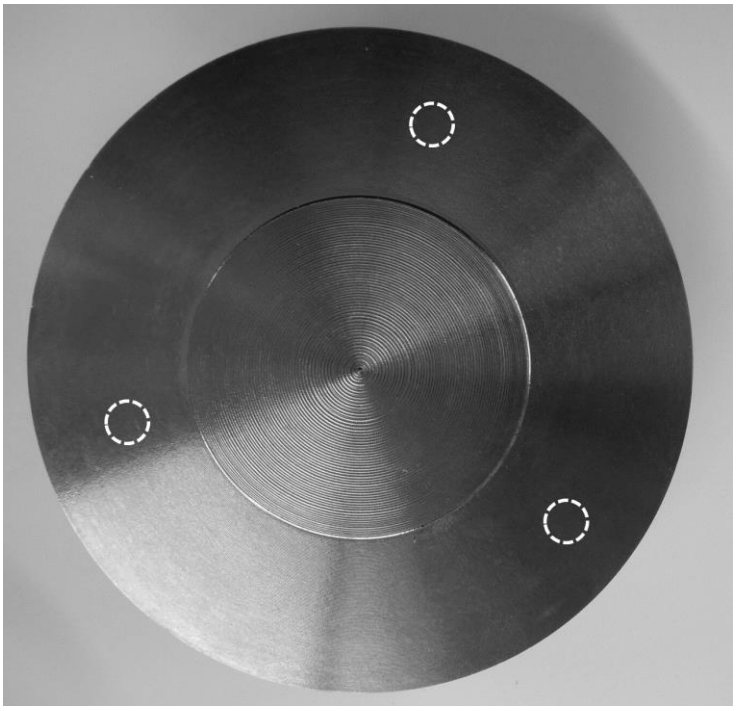

Figure 19 Three Approximate Positions (White Circles) on the Machined Surface Where the Surface Roughness Was Measured

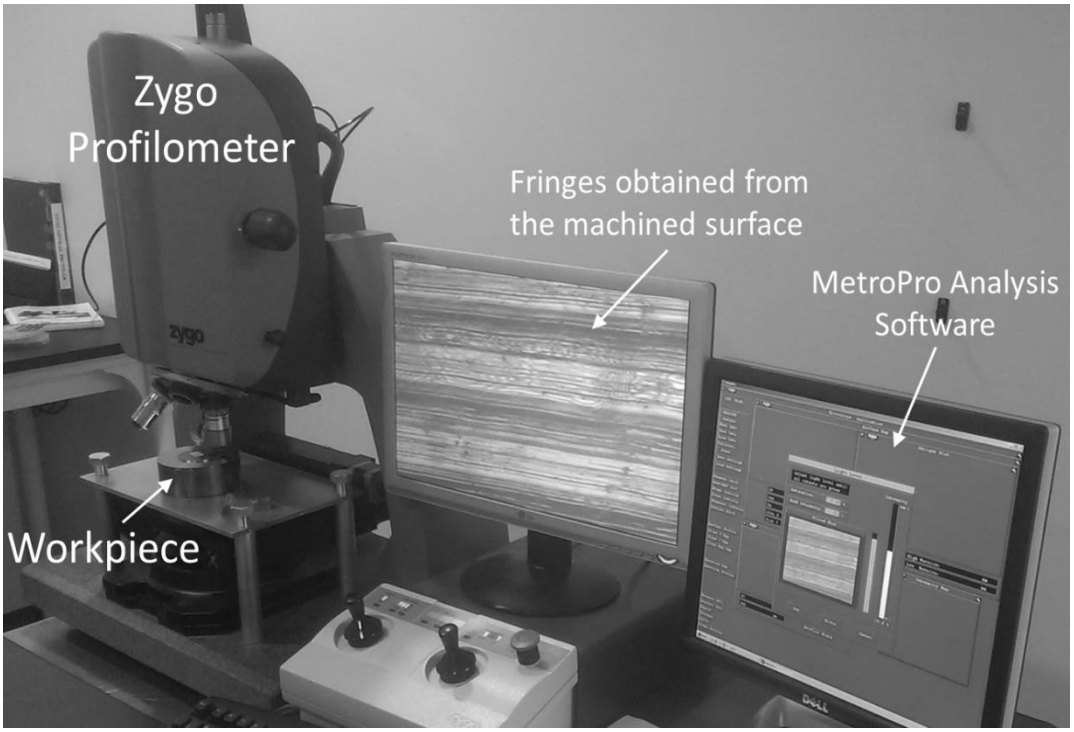

Figure 20 Zygo Profilometer Setup

A HAAS TM-1 CNC mill running at a spindle speed of 2000 rpm and a feed rate of 1.0 in./min was used to drill the holes. A two-flute tungsten carbide end mill with a diameter of 0.0625 inches was used for drilling the hole. The process of measuring the residual stress using hole drilling starts with the selection of a strain gage, which depends on the material under investigation. A CEA-06-062UL-120 type strain gage, shown in Figure 21, is recommended for measuring residual stresses in steel and titanium alloys. The strain gage is manufactured and supplied by Vishay Measurement Inc. A detailed explanation for the designation of the strain gage can be found in [81]. Once the strain gage is selected, there are various steps involved in determining residual stress using the hole drilling method which can be subdivided into the following sections:

- Strain gage bonding
- Soldering the strain gage
- Obtaining strain data by hole drilling
- Processing the strain data using H-drill software to determine the residual stresses

A brief description of each section of the hole drilling strain gage method is discussed below. A detailed explanation of each section can be found in [75].

1. Strain Gage Bonding:
    a. Select an appropriate spot on the workpiece where the residual stress is to be measured. Clean the selected spot using acetone to remove any dirt. Then, clean the surface further using a conditioner and a neutralizer recommended by Vishay Measurement Inc. for residual stress measurement.
    b. Bond the strain gage to the cleaned surface on the workpiece using a gage tape, an adhesive, and a catalyst as shown in Figure 22.
2. Soldering the strain gage:
    a. Tin should be applied to the soldering dot using the Iron tip in the Mark V Soldering Station. Figure 21 shows the strain gage used in this thesis.
    b. Solder the lead wires to the tinned solder dots on the strain gage.

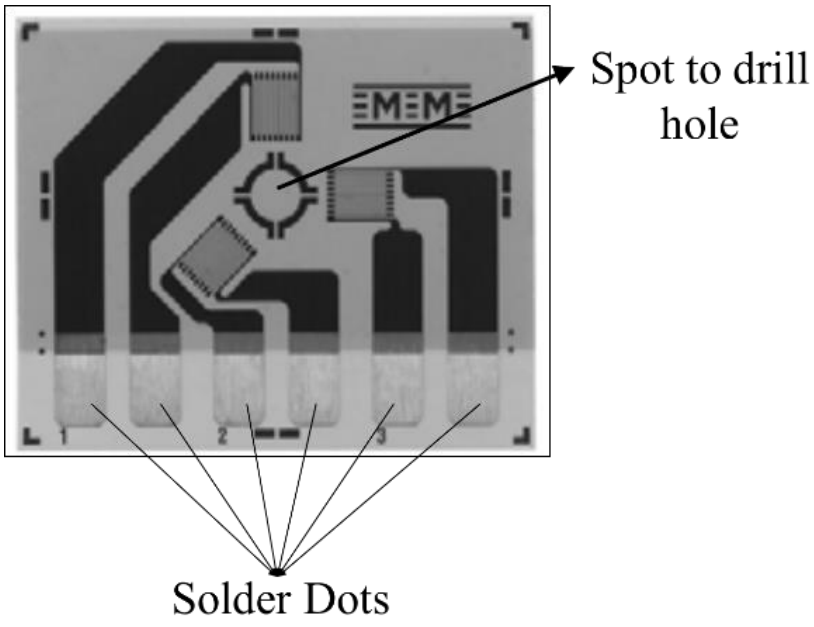

Figure 21 CEA-06-062UL-120 Type of Strain Gage [82]

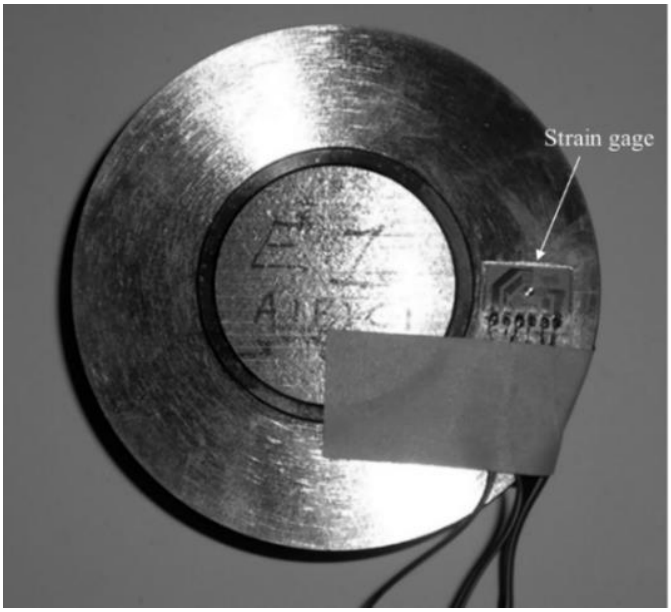

Figure 22 Strain Gage Bonded to the Machined Surface

3. Obtaining strain data from hole drilling experiments
    a. Load the workpiece into the HAAS CNC mill and the other end of the lead wires should be connected to the strain gage instrumentation as shown in Figure 23. Null the instrument to zero strain as closely possible and record any deviation from zero strain.
    b. Zero the end mill at the surface of the sample using a shim of known thickness and align the end mill to the center of the strain gage.
    c. Drill holes incrementally through the strain gage at depths shown in Table 6. Record strains in all three directions after each hole is drilled.
4. Processing the strain data in H-Drill software to determine the residual stresses
    a. Import the strain data to the H-Drill software and use the integral method to determine the residual stress profile as a function of depth.

The maximum principal stress profile calculated in the H-Drill software was considered the residual stress profile for the machined sample [83]. A detailed procedure to use H drill software can be found in reference [84]. The CNC program used for the hole drilling experiment can be found in Appendix A. Appendix B provides information about the H-Drill software and integral method that was used to determine the residual stress at each depth.

3.7 Sample Preparation and Microstructural Analysis

Microstructural analysis of the machined subsurface is an important characteristic for understanding the final surface state of the machined sample. The various steps involved in preparing samples for microstructural analysis are as follows:

1. Cut a small sample of 5 mm x 5 mm x 10 mm size using a waterjet cutting machine and band saw.
2. Mount the sample on a Phenolic resin by using a hot compression mounting press from Pace Technologies.

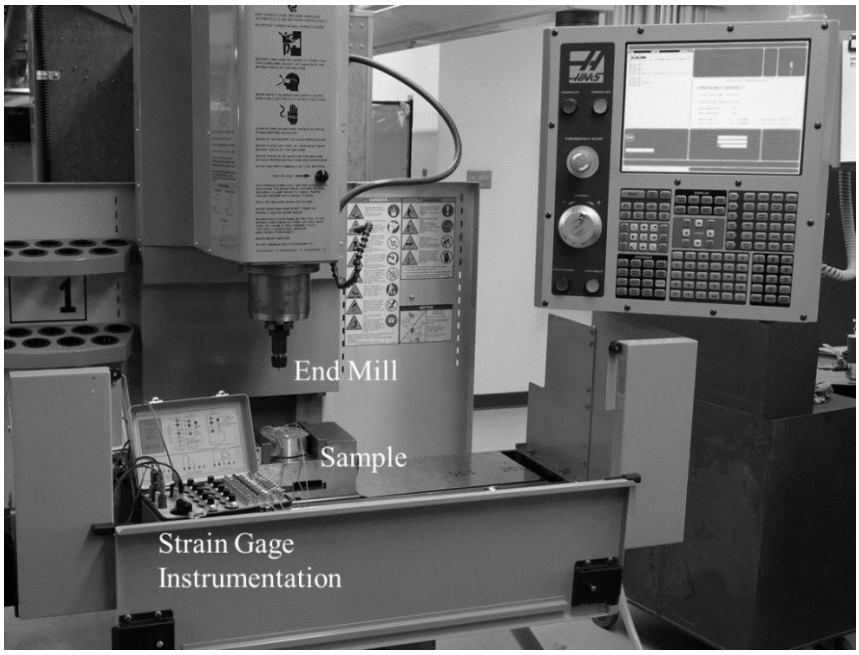

Figure 23 HAAS CNC Mill With a Sample Ready for the Hole-Drilling Procedure. [85]

Table 6 Hole Depth Steps Used for Hole-Drilling Strain-Gage Method

(in)	(mm)
0.0005	0.0127
0.0010	0.0254
0.0015	0.0381
0.0020	0.0508
0.0025	0.0635
0.0030	0.0762
0.0035	0.0889
0.0040	0.1016
0.0045	0.1143
0.0050	0.1270
0.0055	0.1397
0.0060	0.1524
0.0065	0.1651
0.0070	0.1778
0.0075	0.1905
0.0080	0.2032
0.0090	0.2286
0.0101	0.2565
0.0202	0.5131
0.0303	0.7696
0.0404	1.0262

3. In the press, the temperature and time to cure is set to 290^0 C and 10 min, respectively. A schematic representation of sample preparation for microstructural analysis is shown in Figure 24.
4. Polish the mounted sample using carbide abrasive papers ranging from 240 grit size to 1200 grit size (240, 360, 600, 800 and 1200 grit sizes).
5. Polish the sample using diamond particles of size 5 μm for 15 min using a semiautomatic polisher.
6. Finally, polish the sample on a velvet cloth using an alumina slurry of particle sizes 0.05 microns for 20-30 min until a mirror surface is obtained.

The polished samples were now ready for scanning electron microscope (SEM) study. A FEI Quanta 600 FEG SEM with EDAX electron backscatter diffraction detector, shown in Figure 25, was used for this study. The electron back scatter diffraction (EBSD) technique in SEM is used to perform quantitative analysis on the microstructure [47]. No etching is required to carry out EBSD analysis. OIM data acquisition software and TSL OIM analysis software was used to collect and analyze the data. In this study, grain misorientation data and inverse pole figure map obtained from EBSD analysis were used for further analysis. The general steps involved in EBSD analysis are shown in Figure 26 with a brief description. Figure 27 shows an image taken from inside an SEM. A detailed explanation for EBSD analysis can be found in [47] [86].

To perform optical microscope imaging, the polished surface of the samples were etched with Kroll's reagent for about 15 sec by dipping the sample in the Kroll's reagent solution. Kroll's reagent is prepared by mixing 92 ml of distilled water with 6 ml of HNO_3 (Nitric acid) and 2 ml of HF (Hydrofluoric acid) for each 100ml of Kroll's reagent preparation. A fresh solution was used for each sample to prevent any contamination. An Olympus GX51 optical microscope (Figure 28) capable of imaging up to 1000X magnification was used to obtain optical microscope images. The images were then used for later analysis.

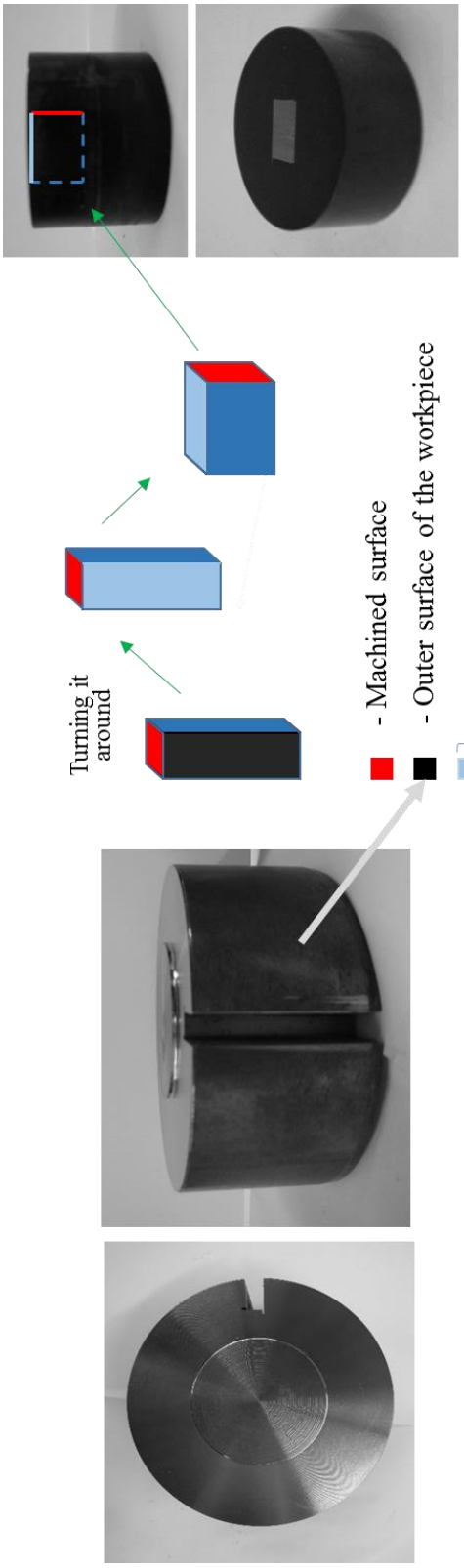

Figure 24 Schematic Representation of the Sample Preparation Process for Microstructural Analysis

Figure 25 FEI Quanta 600 FEG Scanning Electron Microscope

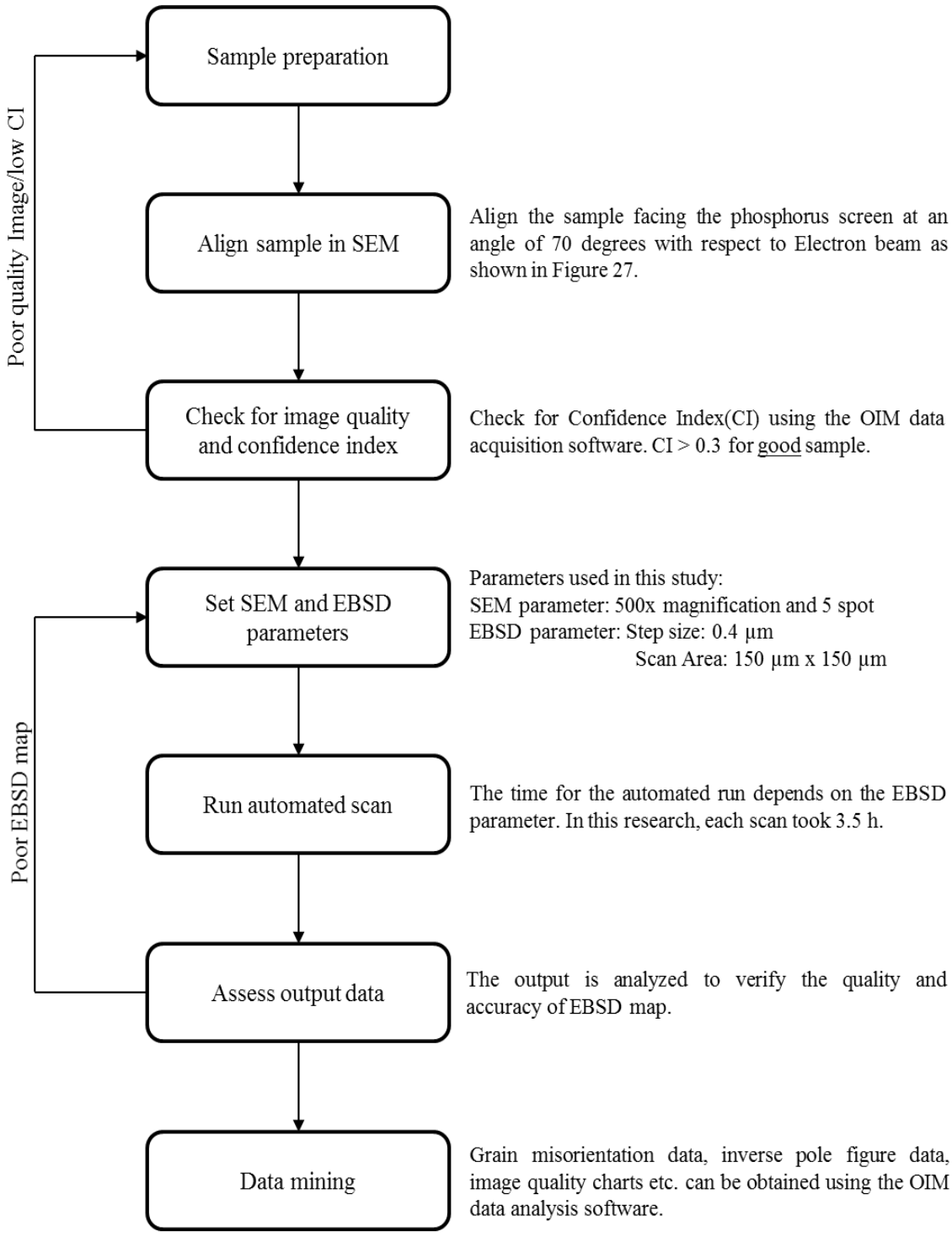

Figure 26 Flow Chart Representing the Steps Involved in a Typical EBSD Analysis

.

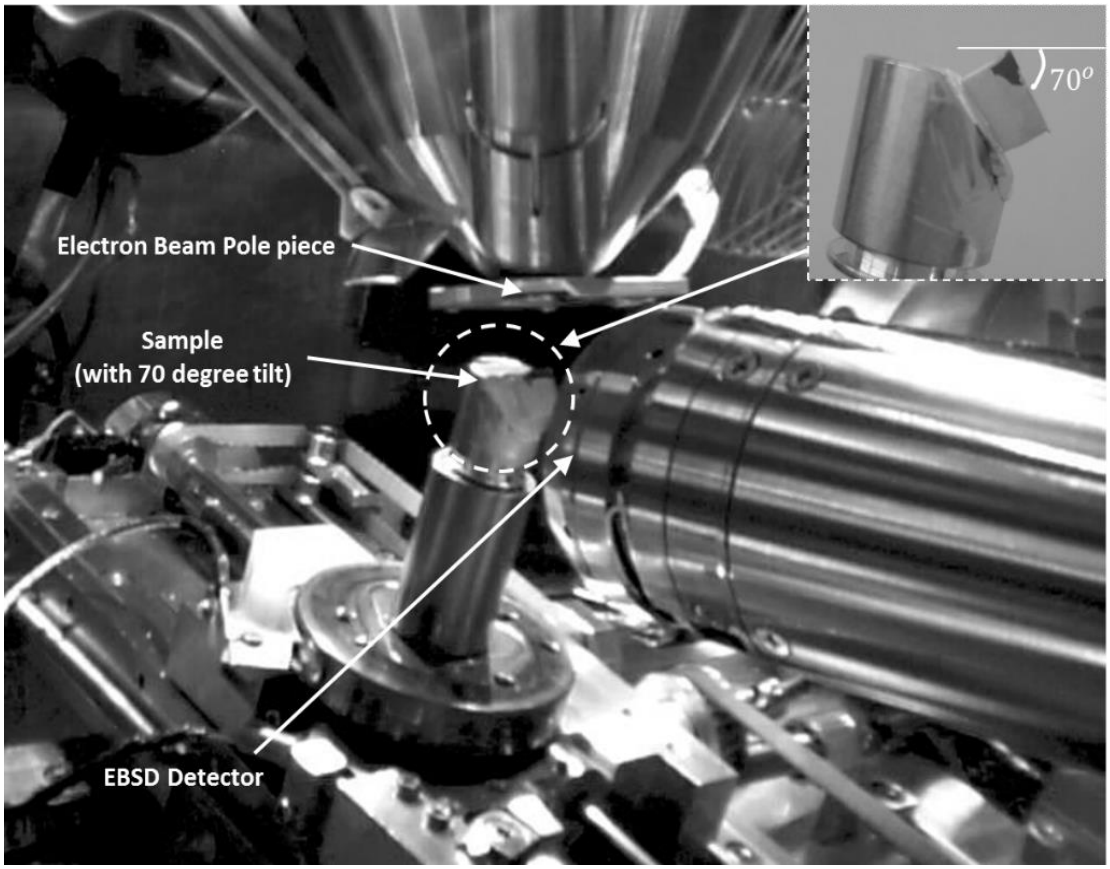

Figure 27 An Image From Inside the SEM Chamber

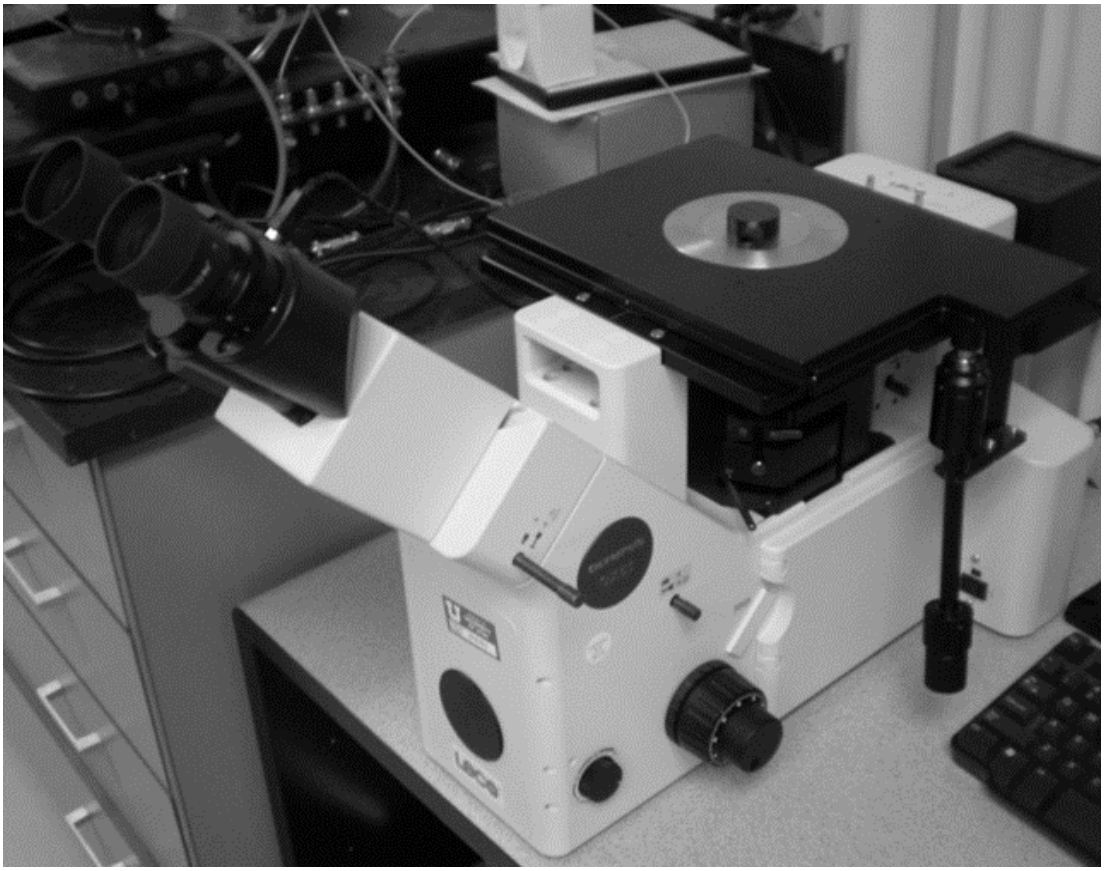

Figure 28 Olympus GX51 Optical Microscope

3.8 Microhardness Measurement

In machining, the material around the cutting edge is plastically deformed and dragged in the cutting direction. As Titanium alloys are known for their work hardening characteristics [56], the variation in the microhardness along the depth of the machined surface is an important aspect in this surface integrity study. The microhardness measurement was carried out using the Leco M-40 hardness tester shown in Figure 29. The tester has a 10x and a 40x magnification lens attached with a camera to focus on the surface. A diamond Vickers indenter was used to measure the microhardness. A 100-gram load and dwell time of 10 seconds were used.

The microhardness measurement was carried out after the sample was cut and polished as described in the previous section. The steps involved in measuring microhardness are as follows:

1. Clamp the sample between the vice in the hardness tester.
2. Using the 10x magnification lens, bring the edge of the sample into focus by moving the sample.
3. Set the load and dwell time for the indenter and press the start button.
4. Once indenter retracts from the surface, switch to the 40x magnification.
5. Measure the diagonals of the indenter mark as shown in Figure 30.
6. Calculate the microhardness using the equation given below.

$$Vickers\ Hardness\ Number = \frac{1.8544L}{d^2}$$

L = load in kilograms

d = Mean diagonal length (mm)

7. Repeat the above steps to measure the microhardness along the depth of the machined surface.
8. The depth from the machined surface at which the measurements will be taken is shown in Table 7.

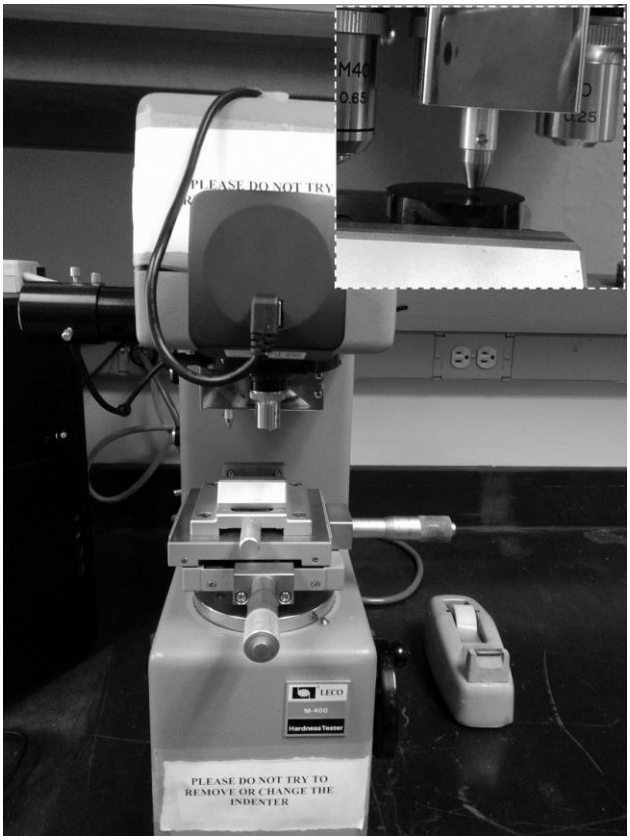

Figure 29 Microhardness Tester (Right corner: Indentation Image)

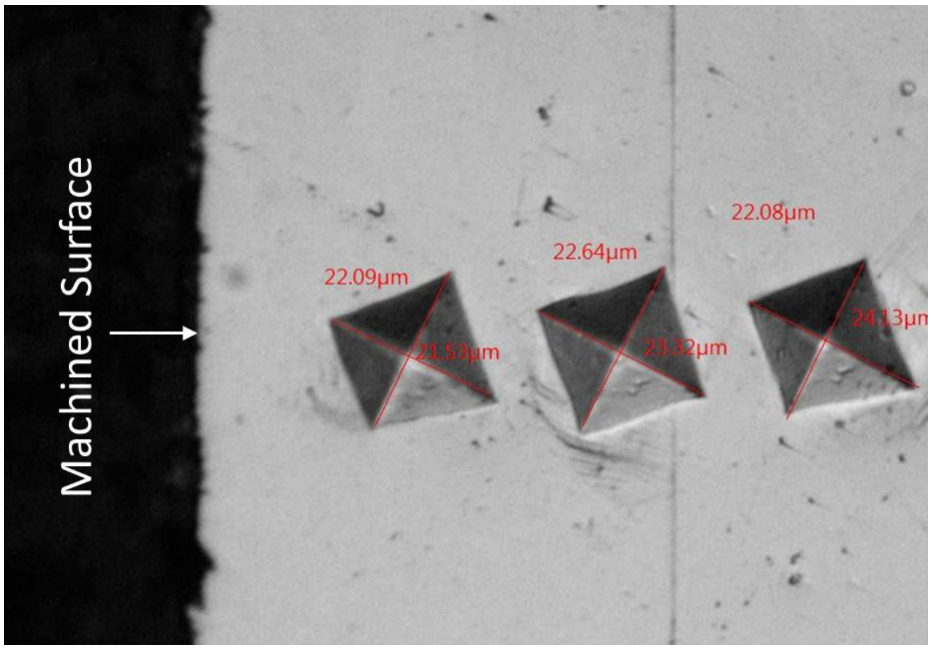

Figure 30 Sample Indentation Marks Along the Depth of the Machined Surface

Table 7 Depth From the Machined Surface Where Microhardness Will Be Measured

Reading No.	Depth from Machined Surface (μm)
1	25
2	60
3	100
4	135
5	175
6	215
7	275
8	325
9	395
10	500

3.9 Summary

A complete experimental plan and the methodologies used to measure various parameters to evaluate machining performance (machining chips and forces) and surface integrity (surface roughness, residual stresses, microhardness, and microstructural analysis) were presented in this chapter. The complete experimental setup used in this thesis is provided in Table 8. A total of eight machining experiments were carried out. Chapter 4 will provide a detailed explanation of the results obtained from all eight experiments.

Table 8 Summary of the Experimental Plan

<table>
<tr><td colspan="3">EXPERIMENTAL PLAN</td></tr>
<tr><td colspan="2">Workpiece</td><td>Ti-6Al-4V-Titanium Alloy (Annealed)</td></tr>
<tr><td colspan="2">Cutting Tool (2)</td><td>Grooved Uncoated Tungsten Carbide
(CNMG 432 AH KW10)
PVD-Coated (TiAlN) Tungsten Carbide
(CNMG 432 TK PR1125)</td></tr>
<tr><td colspan="2" rowspan="4">Cutting Fluid Application (4)</td><td>Dry Machining (No fluid)</td></tr>
<tr><td>Flood Machining (6 l/min) - Synthetic fluid (10%) + Water (90%) (directed approximately along the rake face)</td></tr>
<tr><td>TMQF (300 ml/h) - Synthetic fluid (10%) + Water (90%) + Compressed Air (CA) at 0.689 MPa (Both rake and flank face)</td></tr>
<tr><td>TMQF (300 ml/h) - Vegetable Oil (100%) + Compressed Air (CA) at 0.689 MPa (Both rake and flank face)</td></tr>
<tr><td colspan="2">No. of Experiments (2x4)</td><td>8</td></tr>
<tr><td colspan="2"><u>Machining Conditions</u>
Feed (mm/rev) (f)
Cutting Speed (m/min) (V)
Depth of cut (mm) (a_p)</td><td>
0.2 mm/rev
75 m/min
1.2 mm</td></tr>
<tr><td colspan="3">MEASURED VARIABLES</td></tr>
<tr><td colspan="3">Machining Performance Evaluation</td></tr>
<tr><td colspan="3">1. Machining Chips
2. Machining Forces</td></tr>
<tr><td rowspan="3">Surface Integrity Study</td><td>Topographical Characterization</td><td>Surface Roughness</td></tr>
<tr><td>Mechanical Characterization</td><td>Residual Stresses
Microhardness</td></tr>
<tr><td>Microstructural Characterization</td><td>Optical Microstructure
EBSD Analysis</td></tr>
</table>

CHAPTER 4

RESULTS AND DISCUSSION

The purpose of this chapter is to provide the results from all eight experiments outlined in Chapter 3 and also provide a detailed discussion of all the results. Initially, the machining process is evaluated by analyzing the chips and machining forces for all eight experiments. The results obtained from different aspects of topographical, mechanical, and microstructural characterization of the machined surface will be analyzed individually. A detailed analysis of the correlation between the three characteristics of surface integrity (topographical, mechanical, and microstructural) will be presented in the discussion section of the chapter. The effect of four different cutting fluid application conditions (dry, flood, TMQF-synthetic fluid, and TMQF–vegetable oil) and two different cutting tools (uncoated and PVD-coated tungsten carbide tool) on the final surface state of the machined samples will also be discussed in detail.

4.1 Machining Chips

Analyzing the machining chips is a direct way to evaluate the metal cutting/machining process. Machining chips were collected and photographed after each experiment. Table 9 shows the images of the chips that were produced from machining Ti-6Al-4V titanium alloy using two different cutting tools (uncoated and PVD-coated tungsten carbide tool) and four different cutting fluid application conditions (dry, flood, TMQF-synthetic fluid, and TMQF–vegetable oil). As both tools used in this study had a chip breaker, no significant difference in chips is observed depending on the cutting tool used for machining. However, it can be clearly seen that the cutting fluid application plays a significant role in the type of chip that is being produced during machining.

Table 9 Ti-6Al-4V Titanium Alloy Chips From the Eight Machining Experiments

Cutting Tool / Cutting Fluid Application	Uncoated Tungsten Carbide Cutting Tool	PVD-Coated Tungsten Carbide Cutting Tool
Dry Machining		
Flood Machining (10% Synthetic fluid + 90 % water at 6l/min along rake face)		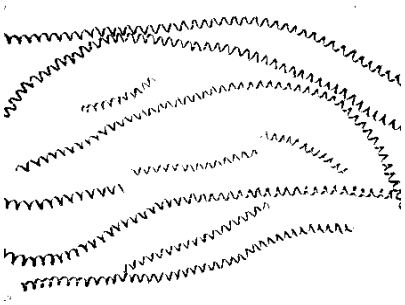
TMQF machining (10% Synthetic fluid + 90 % water +Compressed Air (CA) at 300 ml/hr and 0.689MPa along rake and flank face)		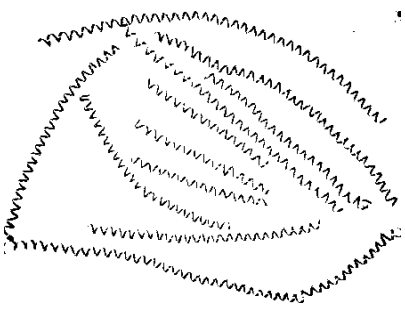
TMQF machining (100% Vegetable Oil + Compressed Air (CA) at 300 ml/hr and 0.689MPa along rake and flank face)	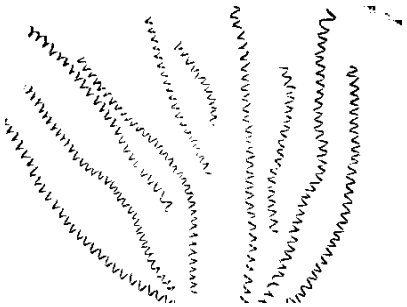	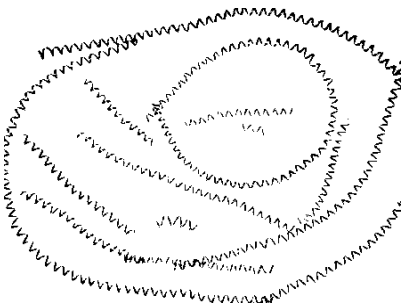

Machining at low cutting speeds usually produces discontinuous chips [1]. Titanium and its alloys are known for their low thermal conductivity and hence usually produce serrated chips with adiabatic shear bands due to machining [56]. Dry machining produced long and continuous chips irrespective of the cutting tool used. Flood and TMQF machining produced relatively smaller (in terms of length) discontinuous chips as the use of the cutting fluid assisted in chip breaking. Since flood machining does not involve targeting the fluid at a specific location, inconsistent chip formation is observed when machining with uncoated and PVD coated cutting tools.

4.2 Machining Forces

The three components of the machining forces were measured using the force dynamometer for all the machining experiments. The feed, radial, and cutting forces are the three components of the machining forces that were measured as described in Chapter 3. The feed force is aligned with the direction of the feed, the radial force is aligned along the direction of the depth of cut, and the main cutting force is aligned along the direction of the cutting speed. Average feed force, average radial force, and average cutting force measured for all machining experiments are shown in Figure 31, Figure 32, and Figure 33, respectively. The determination of the cutting force component is one way of determining the wear behavior of cutting tools during the machining process. The increase in forces during the machining process, in many cases, is an indication of tool wear [87]. The increase in all three force components were observed in only one experiment. The PVD-coated tool under dry condition showed such behavior. However, no conclusion on tool wear can be drawn without completely analyzing the cutting tools, which is beyond the scope of this thesis.

On analyzing all three components of machining forces for all experiments, no clear tends were observed, and hence no significant conclusions can be drawn from machining forces. However, on close examination, machining using a PVD-coated carbide tool produces relatively higher forces (all three components) at all cutting fluid application conditions when compared with those obtained using an uncoated tungsten carbide cutting tool. This may be attributed to the relatively

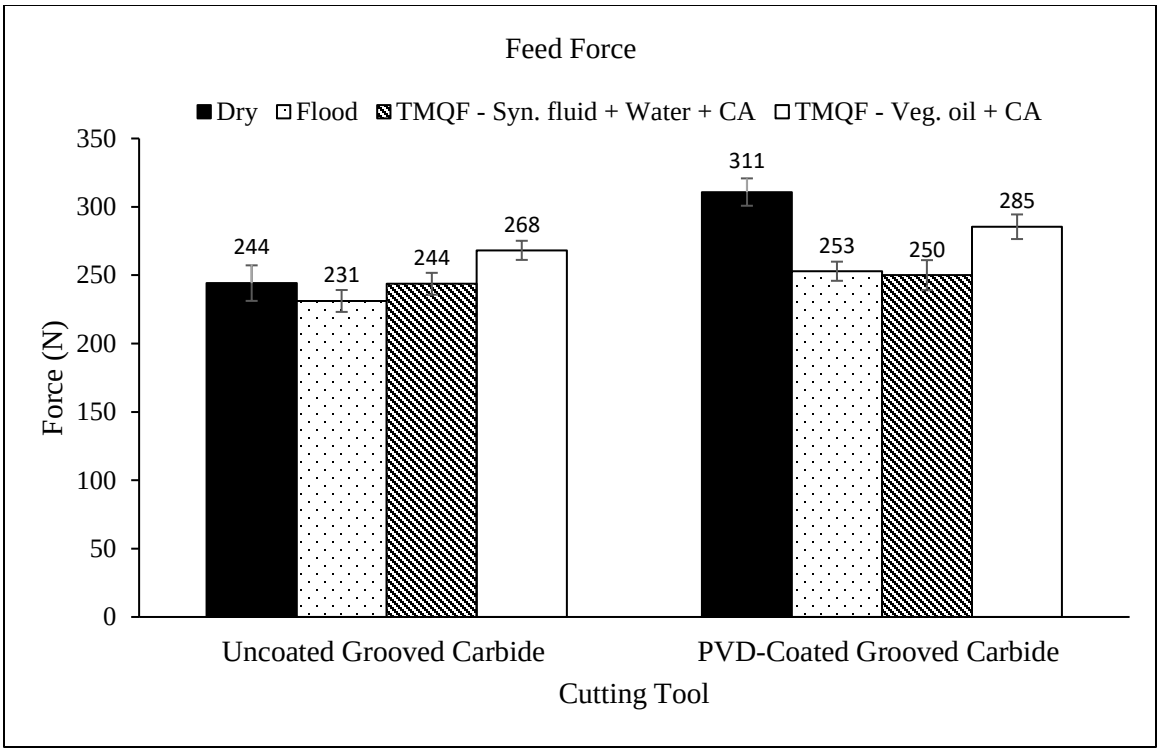

Figure 31 Average Machining Feed Forces

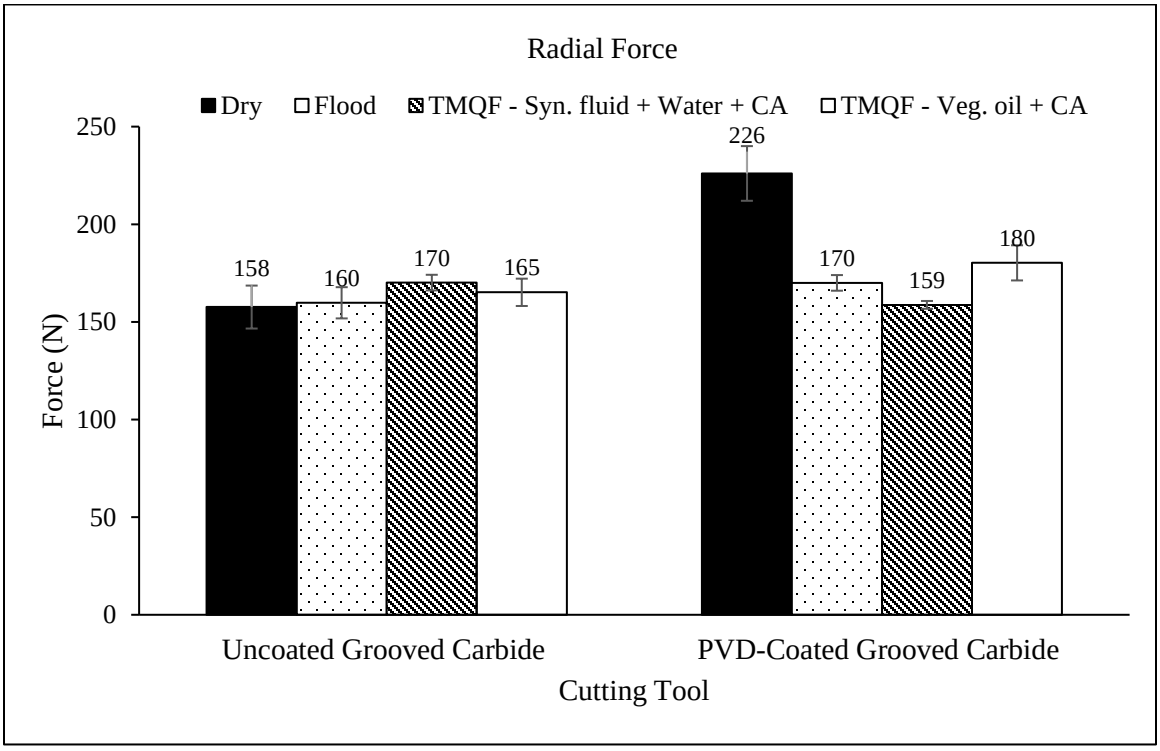

Figure 32 Average Machining Radial Forces

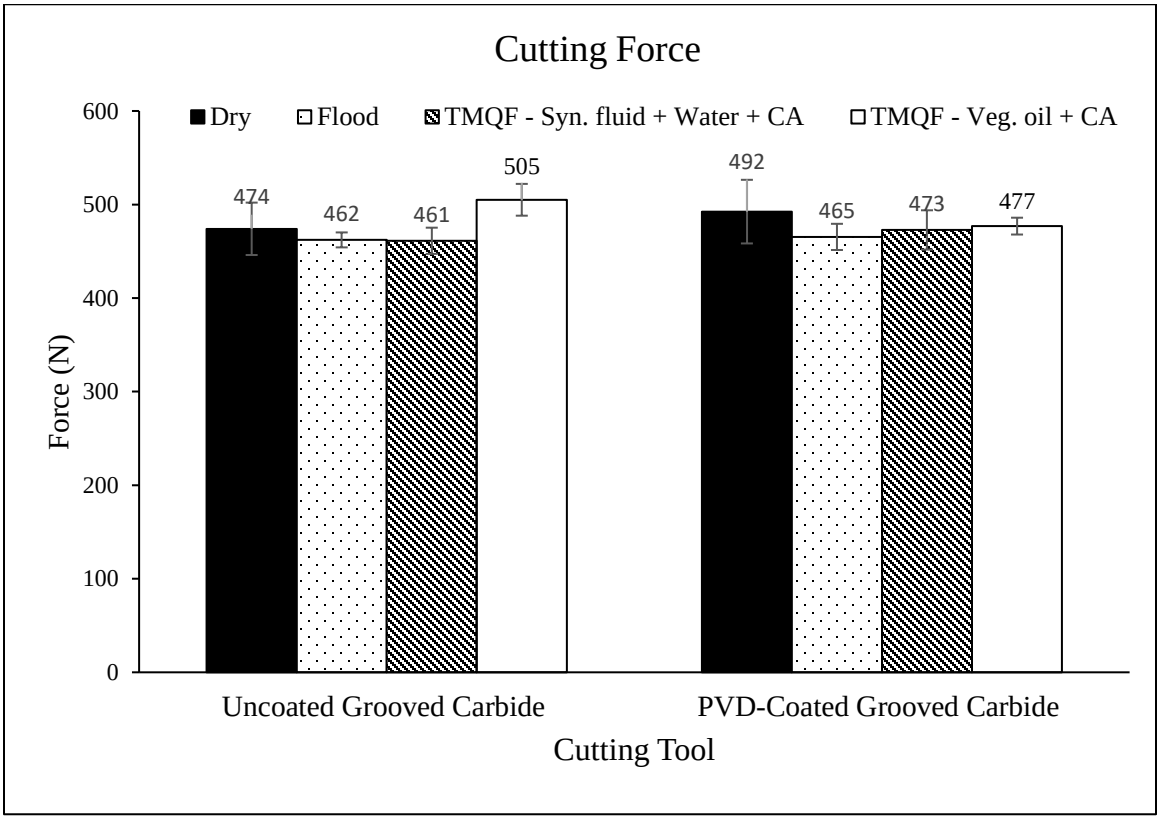

Figure 33 Average Machining Main Cutting Forces

low thermal conductivity of TiAlN coating compared to the thermal conductivity of the tungsten carbide substrate in an uncoated tool.

4.3 Topographical Characterization - Surface Roughness

The topographical characteristics of machining-induced surface integrity include macrocracks, lay, and surface roughness. On visual inspection, no macrocracks were present in any of the machined surfaces. All machined (turning/facing) surfaces should have a rectilinear parallel lay surface feature due to the feed marks [2]. The parallel lines were clearly visible in all eight machined samples when analyzed using a Zygo noncontact Profilometer. Surface roughness is the most commonly measured topographical feature on the machined sample. Hence, for this study, topographical characterization of the machined surface will involve analyzing only the surface roughness on the machined samples for all eight machining experiments.

The roughness average (R_a) is a one-dimensional surface roughness parameter that is commonly used for analyzing the quality of the machined surface. It is known that the higher the R_a value, the rougher the machined surface. In this study, the roughness average (R_a) is obtained for all eight machining experiments using a Zygo® NewView 5000 series surface profilometer. Figure 34 shows the roughness values measured from the machined Ti-6Al-4V titanium alloy under varying cutting fluid applications and cutting tools. The error bars in Figure 34 represent the standard deviation in roughness values obtained from three spots on the machined surface.

From Figure 34, it is clear that machining with the PVD-coated tool yielded lower average surface roughness values when compared to those obtained from the uncoated tool for all cutting fluid applications. The PVD-coated tool has a relatively larger edge radius due to the coating than the uncoated tool which may have resulted in a lower surface roughness value. Dry machining had relatively higher R_a when compared with those from the other three cutting fluid applications, which is a typical beneficial effect of some cutting fluid application [58]. TMQF with straight vegetable oil and TMQF with synthetic fluid + water showed little or no difference in the surface

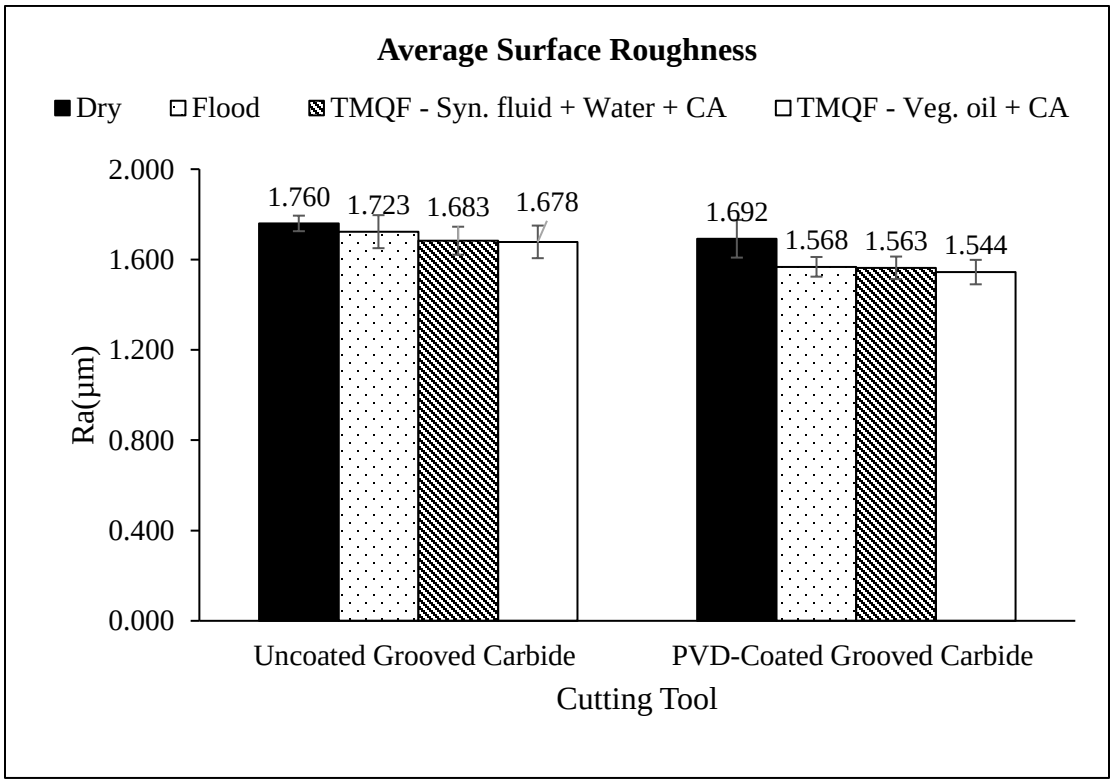

Figure 34 Average Surface Roughness (R_a)

roughness values. However, **both TMQF machining conditions performed better than the flood machining**, underlining its effectiveness using only 300 ml/min of cutting fluid compared to flood conditions which employs 6 l/min or more of cutting fluid.

4.4 Mechanical Characterization

Residual stresses and microhardness are two mechanical characteristics of machining-induced surface integrity. Residual stresses and microhardness are measured along the depth of the machined sample as discussed in Section 3.6 and Section 3.8, respectively. Residual stresses are one of the most commonly considered surface integrity parameters as they have a direct influence on the fatigue life of the component. A high tensile residual stress profile is known to increase the probability of crack nucleation, thereby reducing the fatigue life of the component. Hardness also is an important measure of machining-induced surface integrity that can clearly indicate the effect of a cutting fluid application [65].

4.4.1 Residual Stresses

The hole drilling strain gage method was employed in this study to measure the residual stresses along the depth of the machined surface for all machining experiments. The hole drilling strain gage method indirectly measures the residual strains in the surface, which are then converted to residual stresses using H-drill software (integral method). The maximum principal residual stress obtained from processing the residual strain was chosen to represent the state of the residual stress at each depth. The residual stress plots for flood and dry machining were obtained from a previous thesis [88] where the same cutting conditions, cutting fluid, and cutting tools were used for machining Ti-6Al-4V titanium alloy.

Figure 35 shows the residual stress profile obtained for all cutting fluid application conditions using the uncoated tool. A positive value indicates a tensile residual stress while a negative value indicates a compressive residual stress. As far as machining with uncoated tool is considered, only dry machining yielded tensile surface residual stresses whereas flood and both TMQF machining

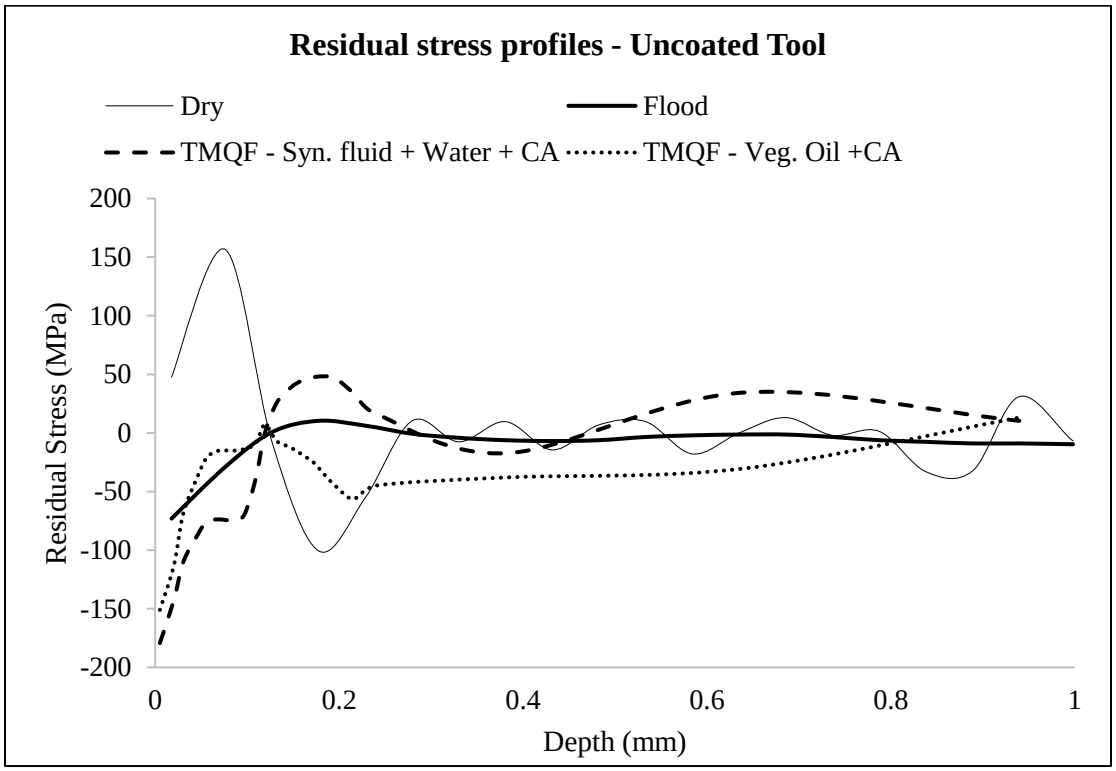

Figure 35 Maximum Principal Residual Stress Profiles - Uncoated Tool

conditions yielded compressive surface residual stresses. Typically, tensile residual stresses are attributed to thermal loads whereas compressive residual stress are attributed to mechanical loads [23], [89]. High temperature is generated while dry machining and the corresponding increased thermal loads probably induce tensile residual stresses on the surface whereas the temperature is much reduced whenever a cutting fluid is used. Both the TMQF machining conditions produced higher compressive surface residual stress and a desirable compressive residual stress profile than the flood machining, which seemingly underlines the effectiveness of strategically targeting the cutting fluid. TMQF with synthetic fluid + water and TMQF with straight vegetable oil did not show significant difference in the residual stress profile even though the viscosity of the two fluids is different.

Figure 36 shows the residual stress profile obtained for all cutting fluid application conditions using the PVD-coated (TiAlN) carbide tool. Like the uncoated tool, dry machining with the PVD-coated tool yielded the highest surface tensile residual stress. It is interesting to note that flood machining with the PVD-coated tool yielded tensile residual stress profile. TiAlN has a relatively lower thermal conductivity when compared to the tungsten carbide substrate [83]. Correspondingly, the PVD coated tool will absorb less heat during machining process when compared to the uncoated tool. The combination of low thermal conductivity of the TiAlN coating on the cutting tool and the nontargeted cutting fluid application in flood machining could be the reason for the tensile residual stress profile. However, both the TMQF machining conditions produced the desirable compressive residual stress profile when machined with PVD-coated tool, further validating its ability to effectively control the localized heat produced in the cutting zone and transferred to the newly machined work surface during the machining process. Like the uncoated tool, no significant difference in residual stress profile was seen for TMQF machining with synthetic fluid +water and with straight vegetable oil.

From both the plots (Figure 35 and Figure 36), it can be seen that the peak residual stress for all TMQF machining conditions is at the surface, which is highly desirable for fatigue performance.

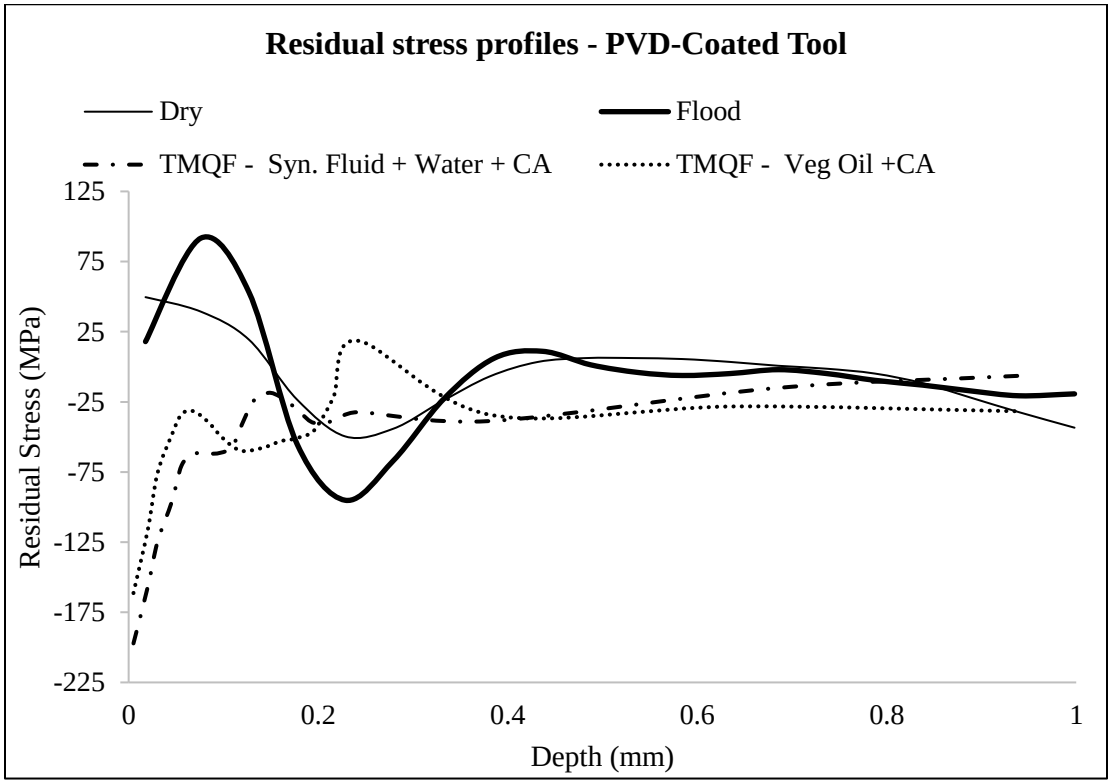

Figure 36 Maximum Principal Residual Stress Profiles – PVD-Coated tool

Furthermore, the residual stress profile obtained from all four TMQF machining conditions is predominantly in the compressive stress region (negative values). These results clearly indicate that TMQF machining is able to eliminate any negative influence of the cutting tool on the surface integrity of the machined sample by effectively cooling the cutting zone and the newly machined works surface, which flood machining is unable to effectively achieve. The interaction between the cutting tool and cutting fluid application and its effect on residual stresses will be discussed further in Section 4.6.2.

4.4.2 Microhardness

A Vickers microhardness tester (Leco M-40) was used to measure the microhardness along the depth of the machined surface. The microhardness profiles for machined subsurface when using the uncoated tool and the PVD coated tool are shown in Figure 37 and Figure 38, respectively. At each depth, three readings were recorded at different locations along the machined surface depth (into the machined surface). The average microhardness obtained at each depth is represented in Figure 37 and Figure 38.

The results from both the microhardness profiles (uncoated and PVD-coated tungsten carbide tool) clearly demonstrated that both flood and TMQF cutting fluid applications produces a higher subsurface hardness. It was also observed that this increased hardness is maintained up to a greater depth compared to dry machining irrespective of the cutting tool used. No significant difference in microhardness profile was found when varying the type of cutting fluid (synthetic fluid + water and straight vegetable oil) used in TMQF application. It is widely reported in literature ([65], [72], [90]) that the increase in hardness due to machining is a result of plastic deformation which in turn work-hardens the surface. Dry machining produces high temperatures which does not allow an increase in microhardness while flood and TMQF machining produce lower temperatures which promotes a higher subsurface hardness. In dry machining, the generated high temperature also weakens the effect of work hardening [90].

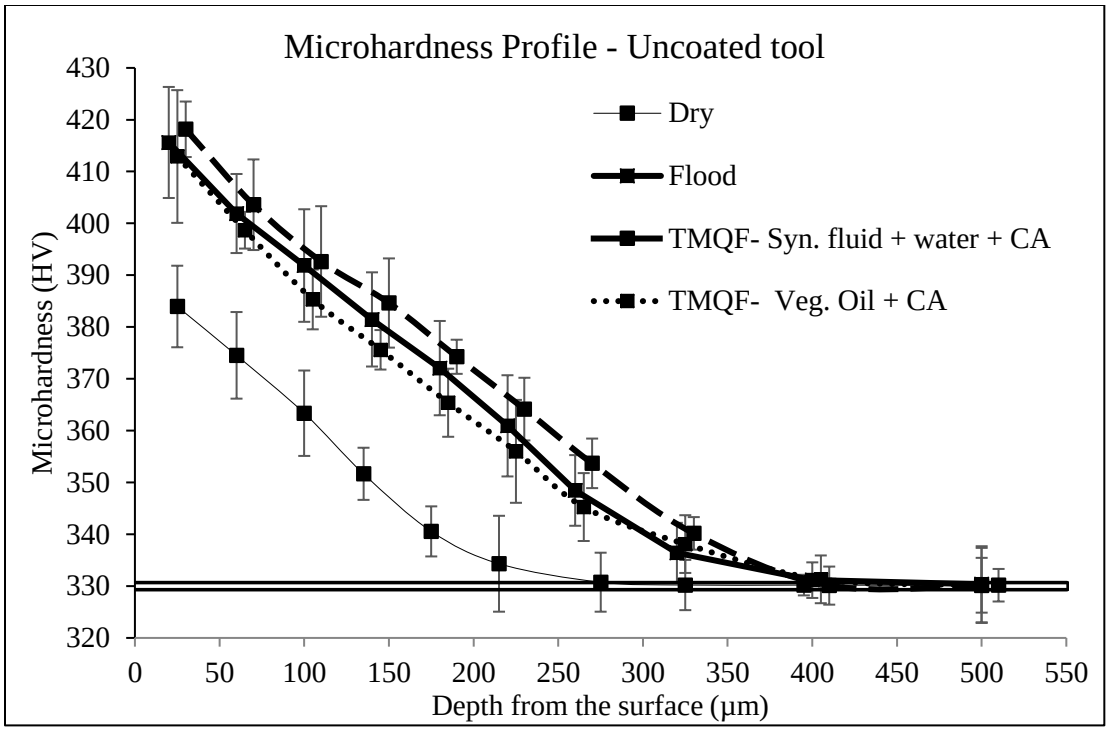

Figure 37 Average Microhardness Profile Along Subsurface Depth - Uncoated Tool

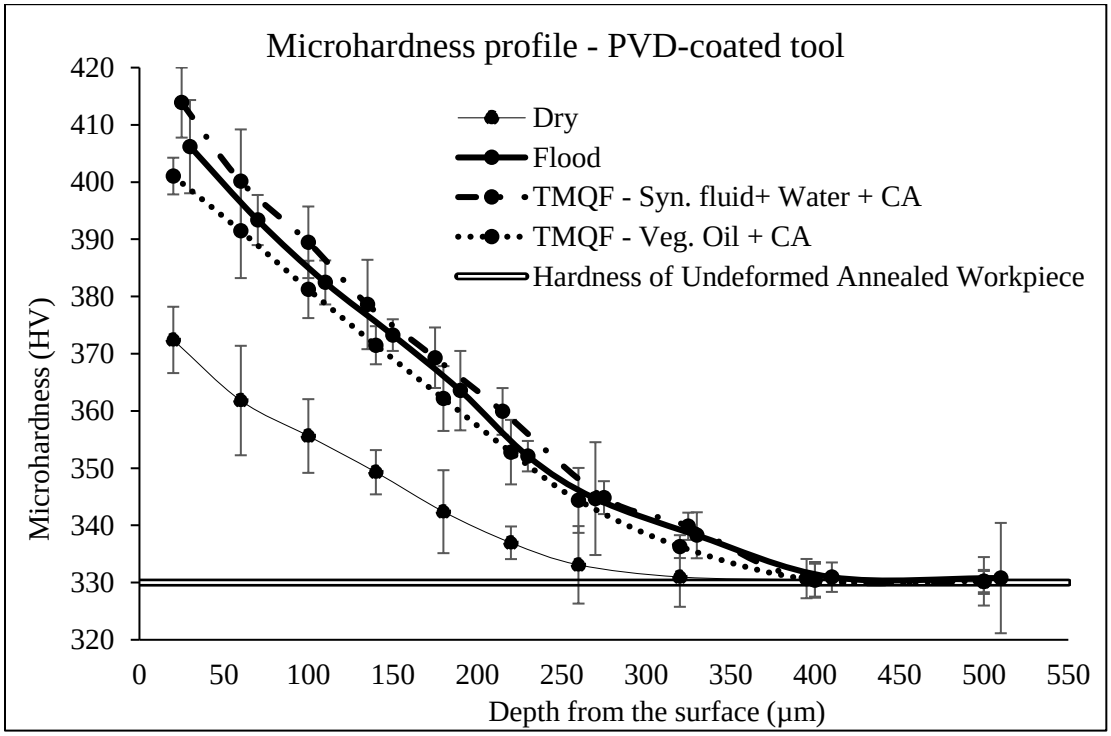

Figure 38 Average Microhardness Profile Along Subsurface Depth – PVD-Coated Tool

Interestingly, both the TMQF machining conditions produce a similar hardness profile to flood machining, suggesting that traditional cutting fluid application in a flood manner is grossly over used. A drastically reduced volume of strategically targeted cutting fluid appears to provide the same subsurface hardness benefits as that provided by flood machining.

Figure 39 provides a plot comparing the microhardness profile for individual cutting fluid application conditions with two different cutting tools. On closer examination of the effect of the cutting tool, it can be seen that the uncoated tool has a slightly higher hardness, which may be due to its higher thermal conductivity compared to the PVD-coated tool. The PVD-coated tool, due to its low thermal conductivity, will absorb less heat compared to the uncoated tool. Thus, in machining with the PVD-coated tool, the workpiece will be exposed to more heat than the workpiece that is machined with an uncoated tool. This clearly explains the reason behind the slight decrease in microhardness when the material is machined with the PVD-coated tool.

4.5 Microstructural Characterization

As discussed in Chapter 2, most of the recent literature on machining-induced surface integrity either completely ignored or only partially addressed microstructural characteristics of surface integrity. In this study, both optical microstructural images and data from Orientation Imaging Microscopy (OIM - SEM/EBSD) of the machined subsurface will be analyzed to evaluate the effects of cutting fluid applications and cutting tools on surface integrity. Optical microstructural images were obtained using an Olympus GX51 optical microscope (20x magnification lens) while the OIM data was obtained using a FEI Quanta 600 FEG Scanning Electron Microscope with Electron Backscatter Diffraction (EBSD) detector and analyzed using TSL OIM Analysis 7 software.

4.5.1 Optical Microstructure

Ti-6Al-4V is a two-phase titanium alloy containing both α (alpha) and β (beta) phases. The α phase is a low-temperature phase with an HCP crystal structure whereas β phase is a high-

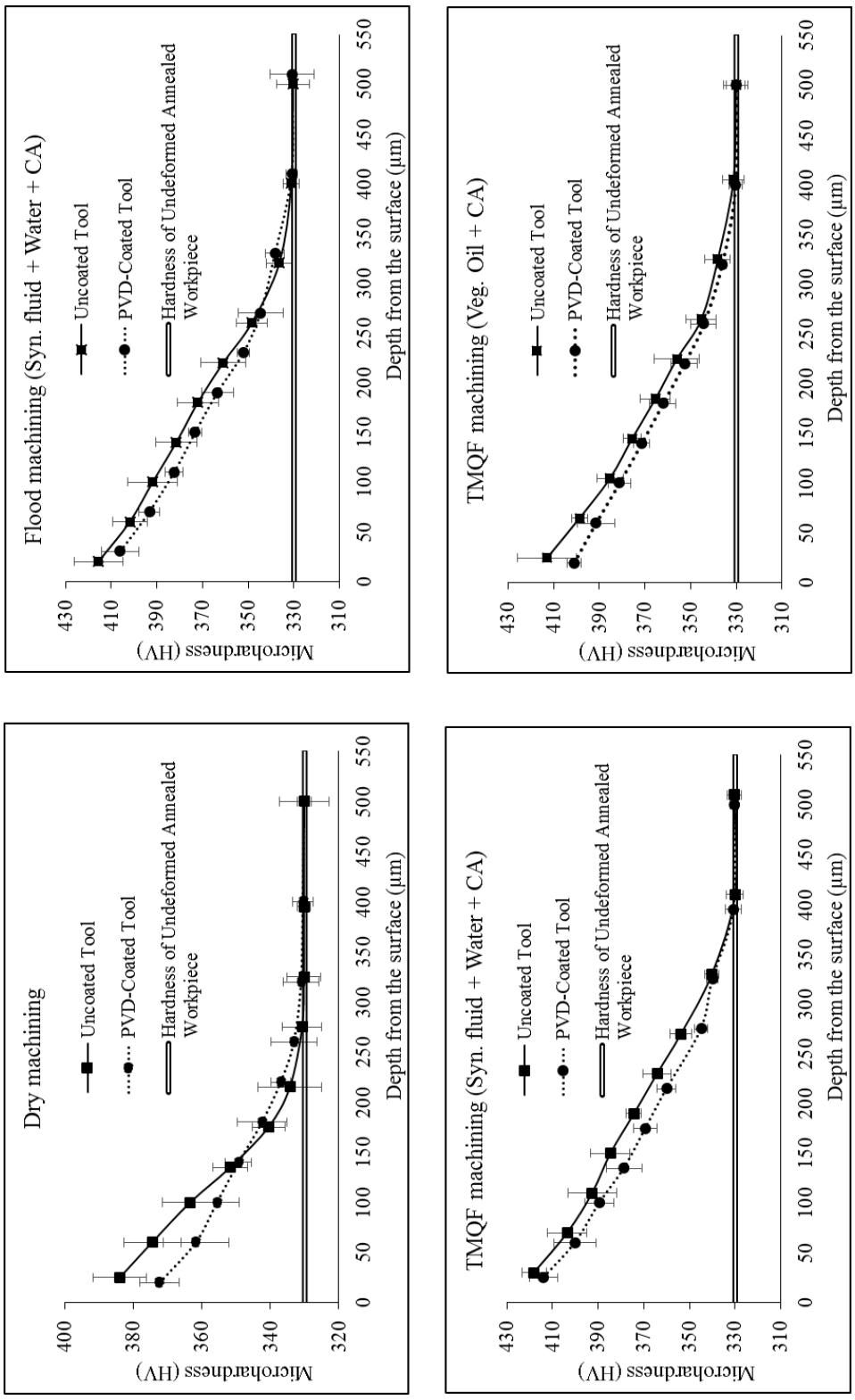

Figure 39 Subsurface Microhardness Profile for Individual Cutting Fluid Application

temperature phase with BCC crystal structure The microstructure of Ti-6Al-4V titanium alloy is highly dependent on the processing history and heat treatment [53]. The microstructure of annealed Ti-6Al-4V titanium alloy contains platelets of α in colonies with traces of the β phase along the grain boundaries. The annealed Ti-6Al-4V titanium alloy contains ~2% of β phase. Figure 40 and Figure 41 show the optical microstructural images of the subsurface of the machined Ti-6Al-4V titanium alloy under varying cutting fluid application conditions using the uncoated cutting tool and the PVD-coated cutting tool, respectively. The light colored region in the optical microstructure images represent the α phase whereas the dark regions represent the β phase. Visual analysis of Figure 40 and Figure 41 clearly shows that there is no significant difference in the microstructure for all eight experiments. Figure 42 represents a zoomed image from one of the dry machining experiments. The images clearly shows grain bending/kinking along the machining direction. The grain bending is visible in all eight machined samples.

The most important microstructural parameter determining the mechanical properties of α and β titanium alloys is α lamella/colony size [91] . However, on visual inspection of the microstructural images, no significant change in the grain size near the machined surface is seen. Grain bending /kinking will result in subgrain boundary formation and in turn may lead to low angle grain boundaries (grain misorientation angle less than 5°). EBSD analysis will provide quantitative evidence of low angle grain boundary formation near the machined surface and is discussed in the following section.

4.5.2 EBSD Analysis

An approximately 150 µm x 150 µm area below the machined surface was mapped and analyzed for all eight samples using the EBSD technique in the SEM. The EBSD analysis was carried out to get four different features of microstructural alterations due to machining. Phase distribution, grain size distribution, pole figure analysis (texture), and grain misorientation angle are the four features.

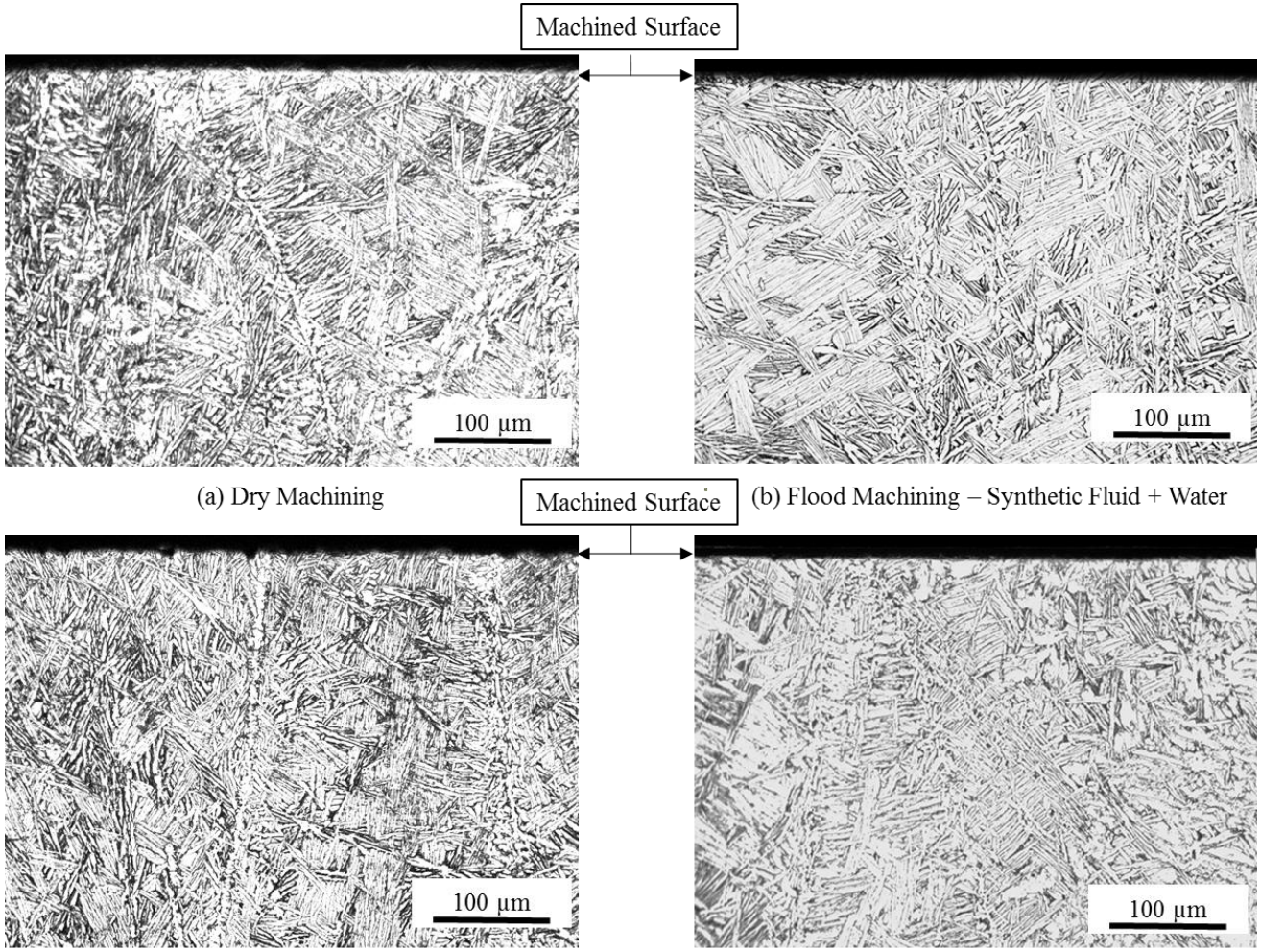

Figure 40 Optical Microstructural Images of Machined Ti-6Al-4V Titanium Alloy Using the Uncoated Tool

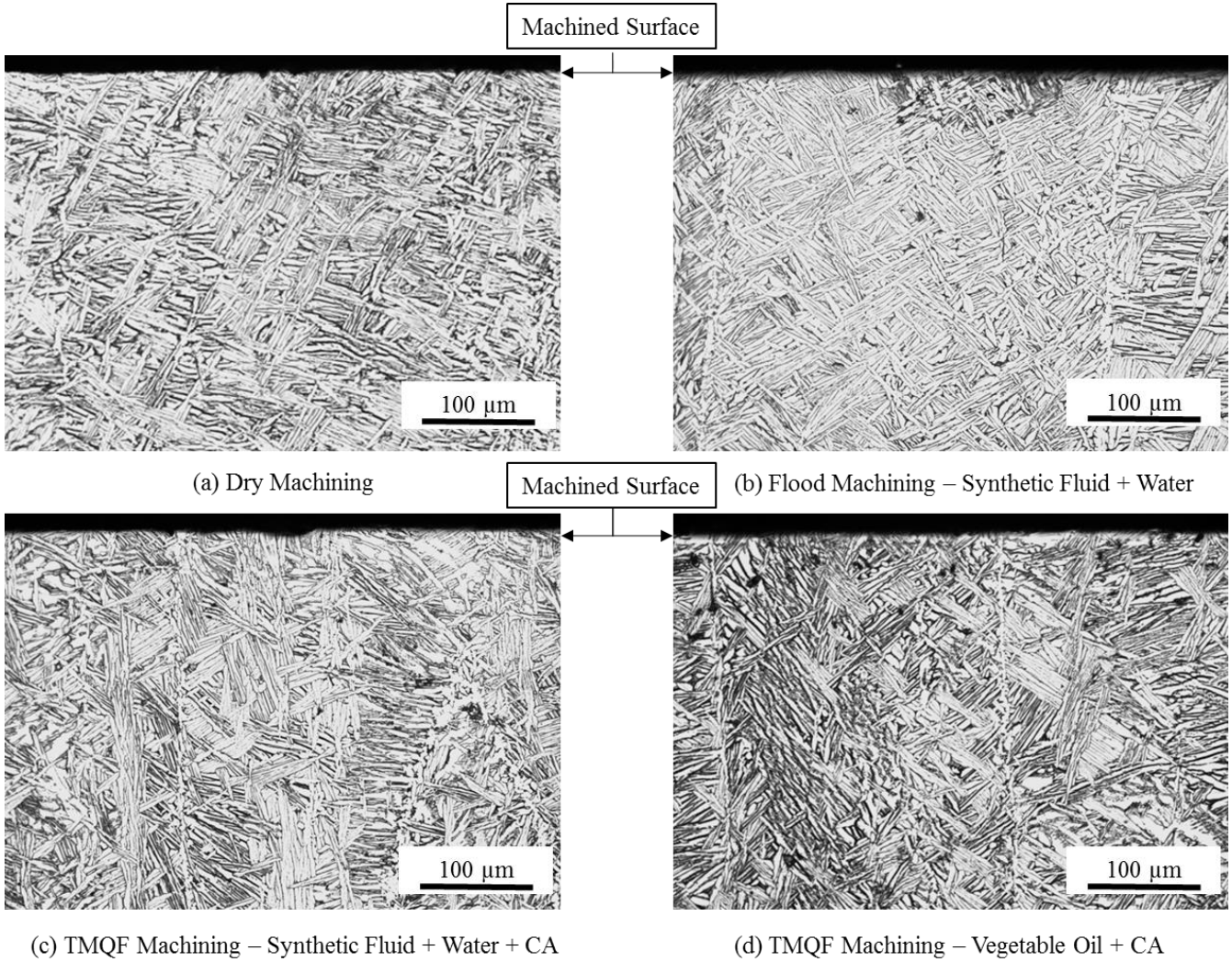

Figure 41 Optical Microstructural Images of Machined Ti-6Al-4V Titanium Alloy Using PVD-Coated (TiAlN) Tool

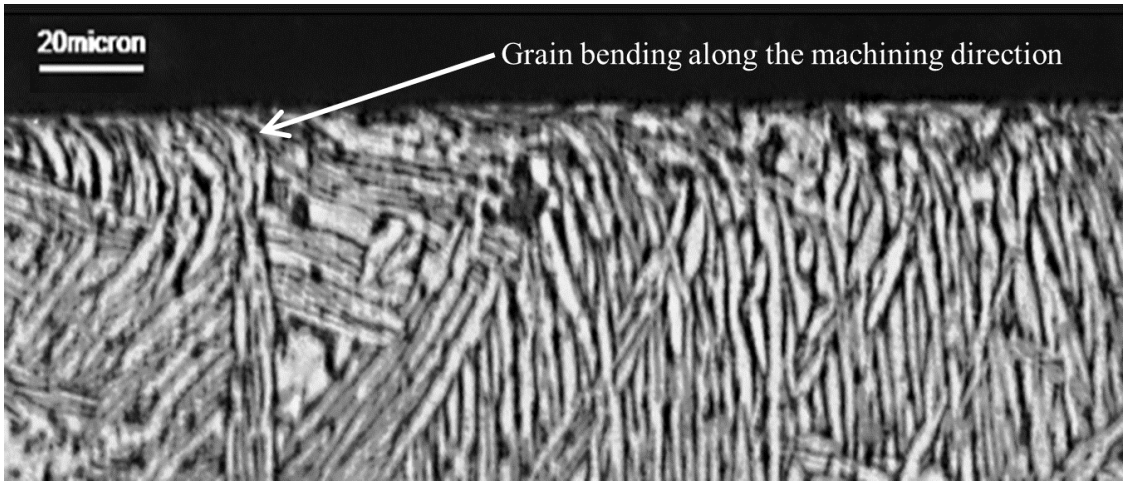

Figure 42 Zoomed Optical Image From Dry Machining Using Uncoated Tool

1. Phase distribution: The relative amount of phases present at the edge of the machined surface will provide a clear insight regarding any phase transformation due to machining. Since the β phases are present only along the boundaries of α lamellae (in the range of 100-500 nm), the resolution of the SEM used in this study was unable to detect β phases with consistency. Hence, the phase distribution data obtained from the EBSD analysis was not used further in this study to evaluate the phase transformation phenomena. The optical microstructure, albeit with its limitations in resolution at that very small scale near the surface, is unable to indicate any phase transformation due to machining in any of the eight machining experiments.
2. Grain size distribution: Each grain can be differentiated based on its orientation. EBSD analysis provides the grain size distribution data using the grain orientation map. In β annealed Ti-6Al-4V titanium alloy, all the α lamellae/platelets (needle structure) present within an α colony have the same grain orientation. A group α lamella/platelets with the same orientation form an α colony and the α lamellae/platelets are separated only by the presence of β phase in between them. As the resolution of the SEM used in this study was not enough to detect the β phase along the boundaries of α lamellae, the grain orientation data was not able to accurately provide the grain size distribution data. The grain size distribution data obtained from this analysis is representative of the α colonies rather than the α lamellae. Hence, in this study, the grain size distribution data will not be utilized to characterize the machining-induced microstructure alterations.
3. Pole figure map (Texture): Since the EBSD analysis was not able to detect the β phases present in the microstructure, the pole figure analysis was carried out using only the data from the α phase. On analyzing the pole figures obtained from all eight samples, no crystallographic texture (grains having similar orientation) was created due to machining. The pole figure maps obtained from all eight machined samples are provided in Appendix C.
4. Grain misorientation angle: The grain misorientation angle is the difference in crystallographic orientation between two crystallites in a polycrystalline material. The

misorientation within a grain caused by plastic deformation will also be detected by the EBSD analysis. The grain misorientation angle distribution data for α phase is the only data from the EBSD analysis that will be used in this study to characterize the machining-induced microstructural alterations. Figure 43 and Figure 44 shows the misorientation angle distribution data obtained for all cutting fluid application conditions for the uncoated cutting tool and the PVD coated cutting tool, respectively. It can be clearly seen that there is no significant difference in the grain misorientation distribution irrespective of cutting tool or cutting fluid application. Hence, in order to assess this issue more closely, the grain misorientation angle distribution analysis was carried out by splitting the ~150 µm x 150 µm area into four different zones to eliminate any bulk effects. A detailed analysis on the grain misorientation angle distribution data obtained for all eight experiments will be provided in the next section.

4.5.3 Grain Misorientation Angle

As no significant difference in grain misorientation angle distribution data obtained from the ~150 µm x 150 µm area for all eight machining experiments was found, the ~150 µm x 150 µm area was split into 4 zones to better analyze the data. Figure 45 shows the approximate location of the 4 zones below the machined surface in an optical microstructural image. Splitting the area into 4 zones will help in analyzing the effects of cutting tools and cutting fluid application on grain misorientation along the depth of the machined surface. Figures 46 - 49 show the grain misorientation angle distribution data in all four zones for varying cutting fluid application conditions using the uncoated tungsten carbide cutting tool and the PVD-coated tungsten carbide cutting tool.

The results obtained from the four zones are first analyzed individually and then together to get a better understanding of the microstructural alterations due to cutting fluid application and the cutting tool.

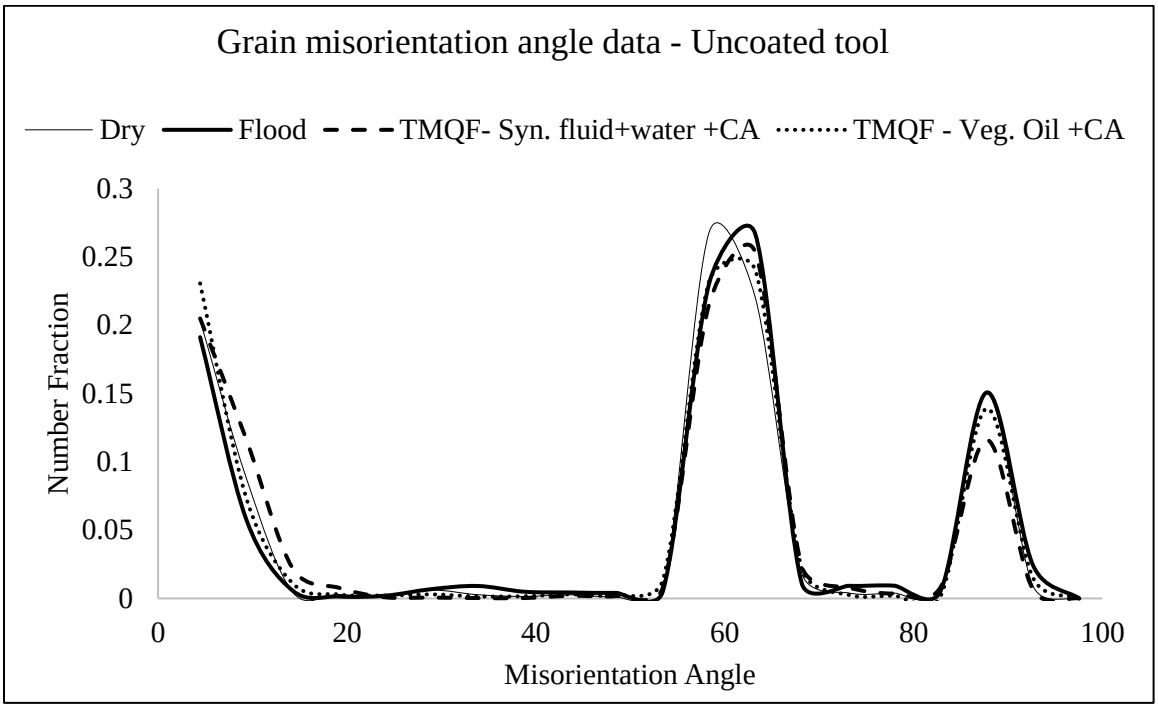

Figure 43 Grain Misorientation Angle Data – Uncoated Tool

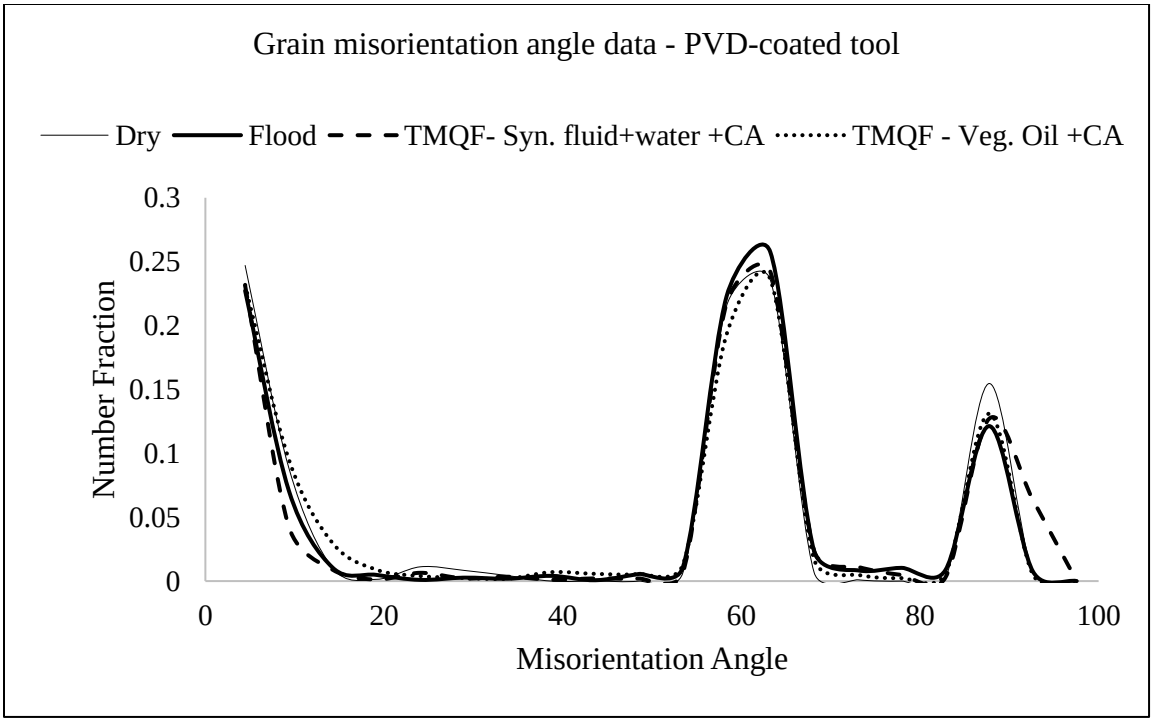

Figure 44 Grain Misorientation Angle Data – PVD-Coated Tool

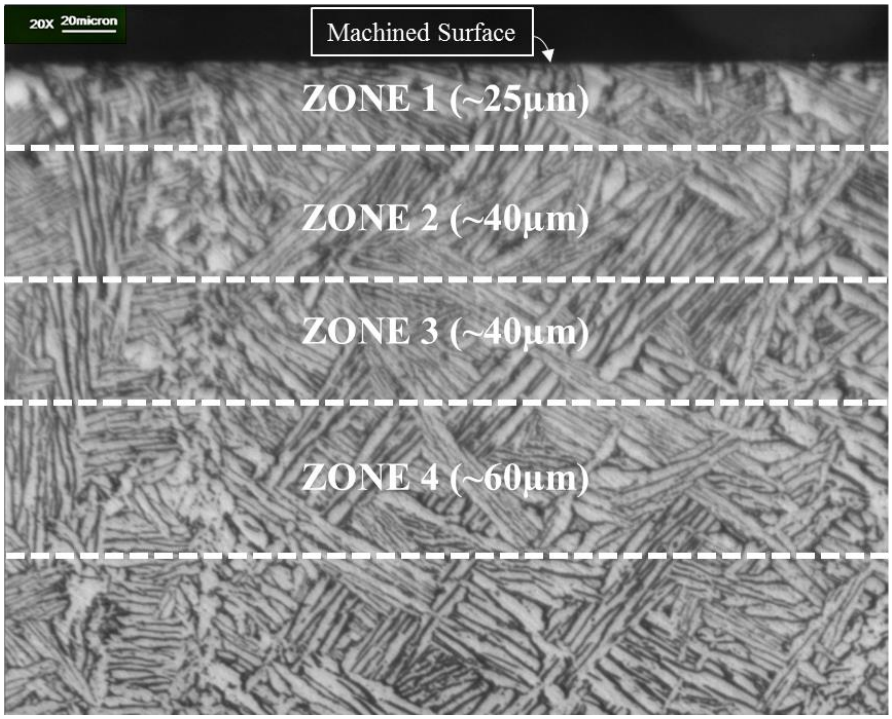

Figure 45 An Approximate Location of the Four Subsurface Zones for Misorientation Angle Analysis (shown on an optical microstructural image of machined Ti-6Al-4V titanium alloy)

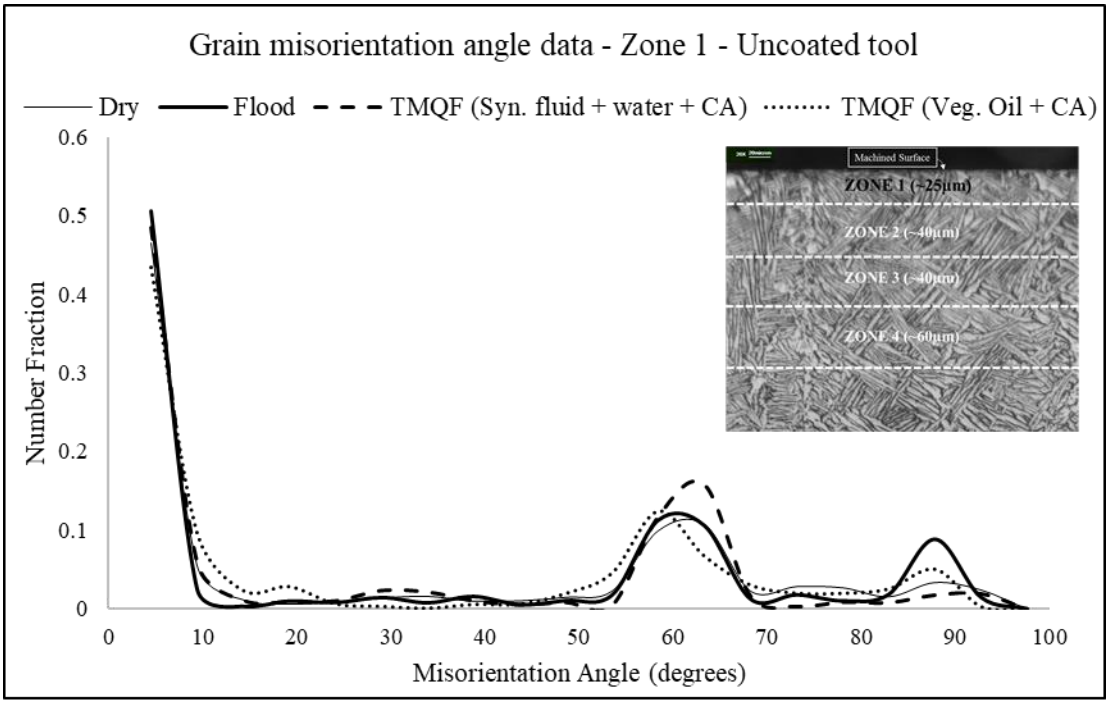

(a)

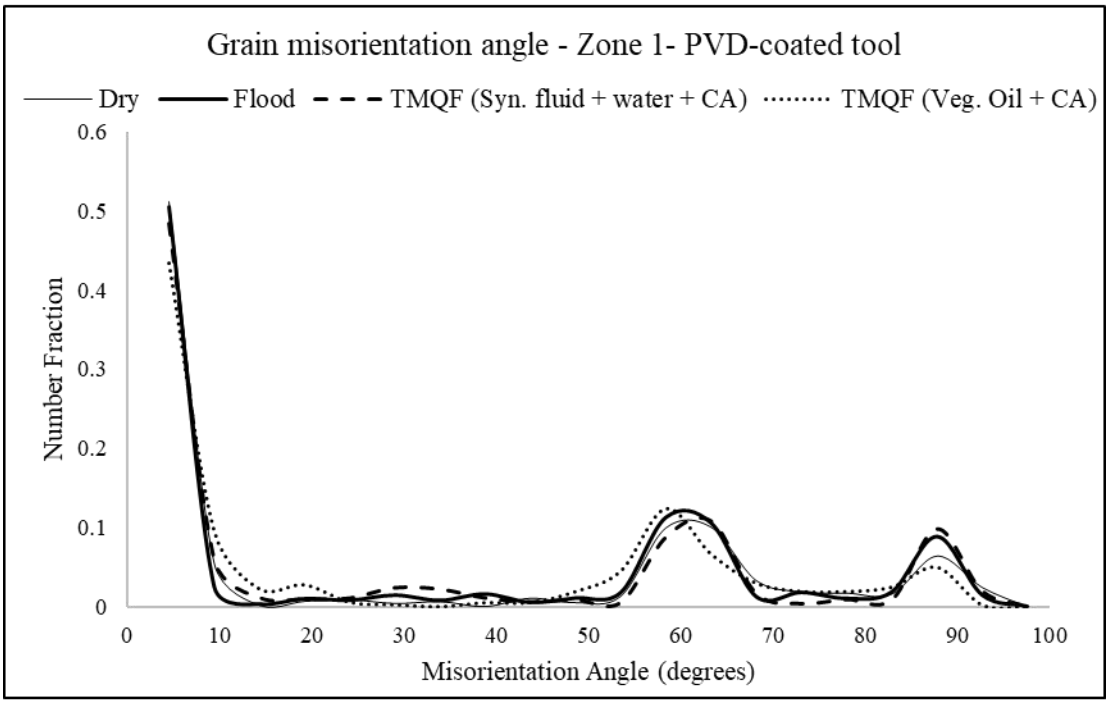

(b)

Figure 46 Grain Misorientation Angle Data for Zone 1: (a) Uncoated Tool, (b) PVD-Coated Tool

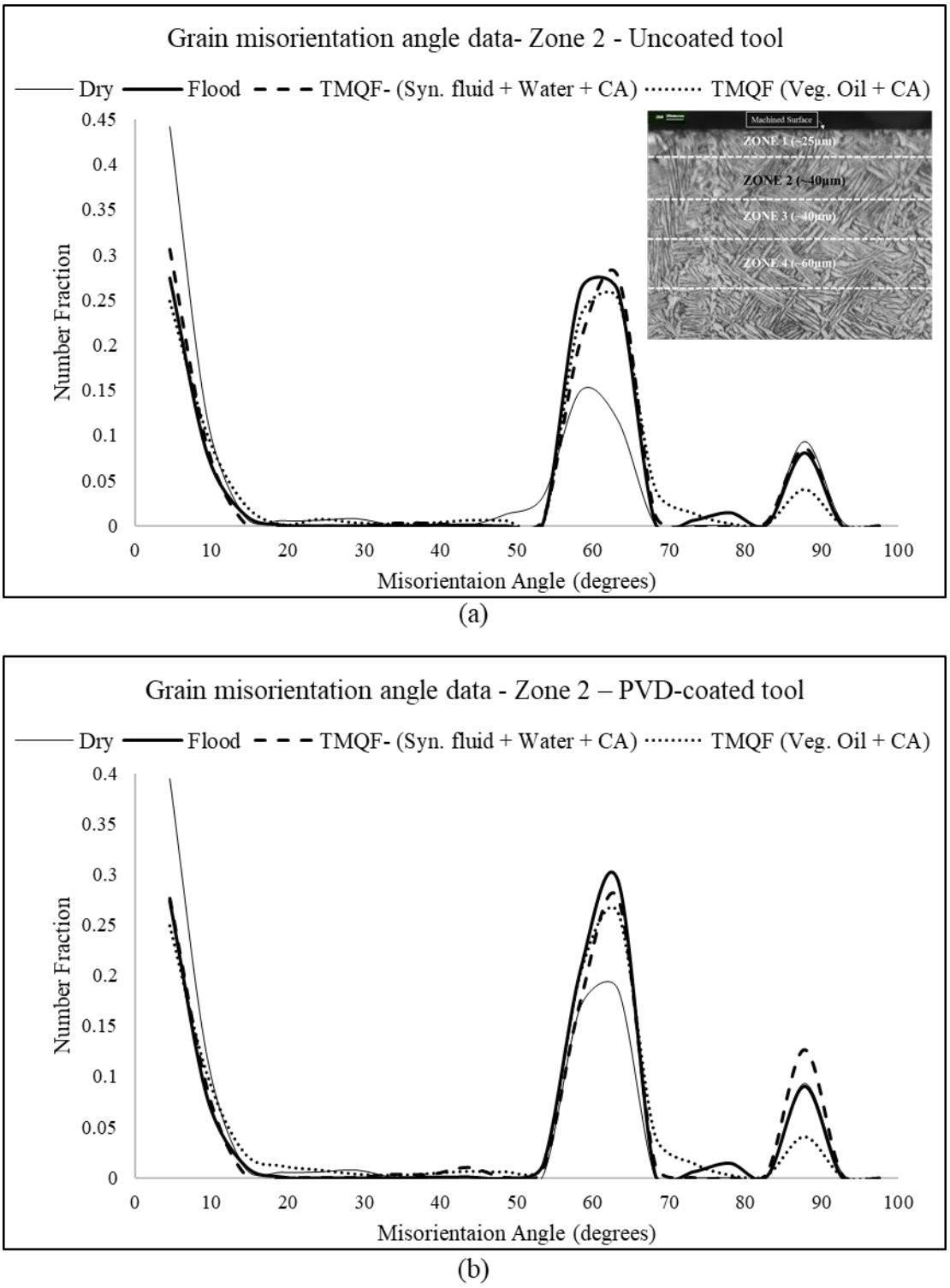

Figure 47 Grain Misorientation Angle Data for Zone 2: (a) Uncoated Tool, (b) PVD-Coated Tool

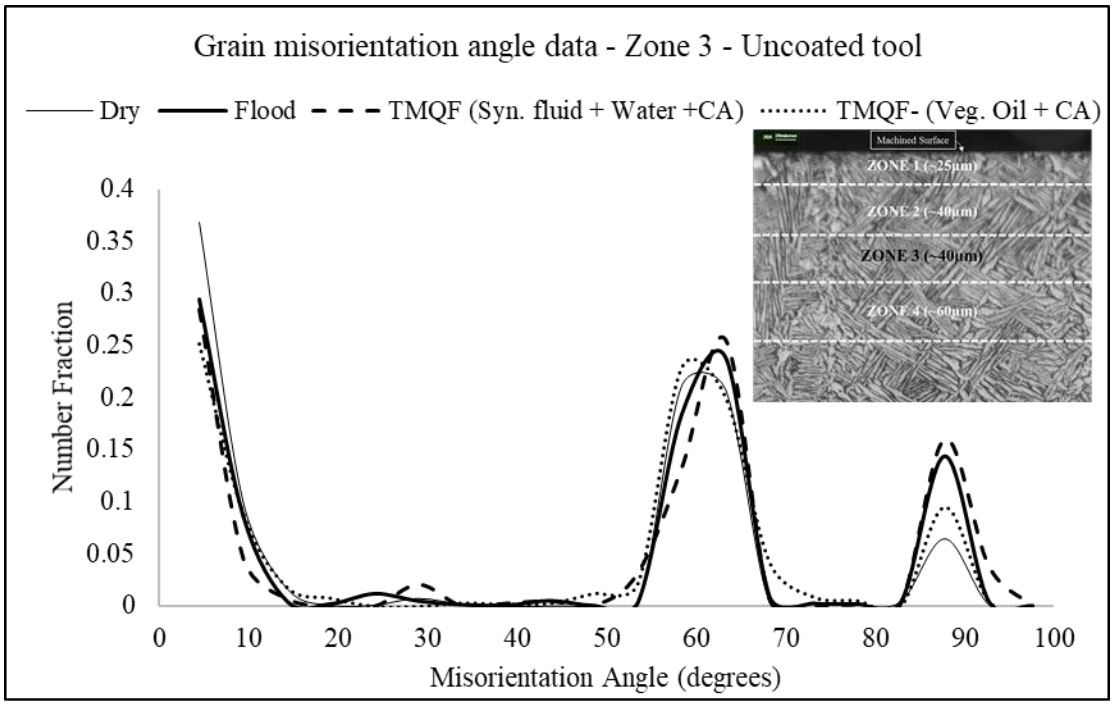

(a)

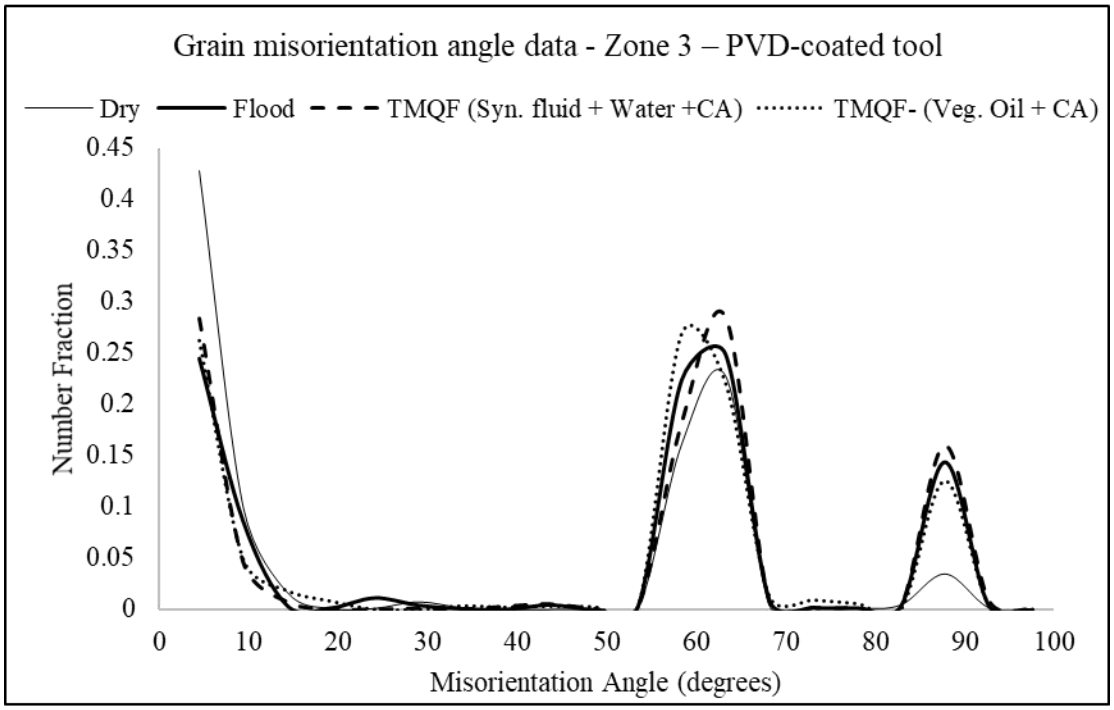

(b)

Figure 48 Grain misorientation Angle Data for Zone 3: (a) Uncoated Tool, (b) PVD-Coated Tool

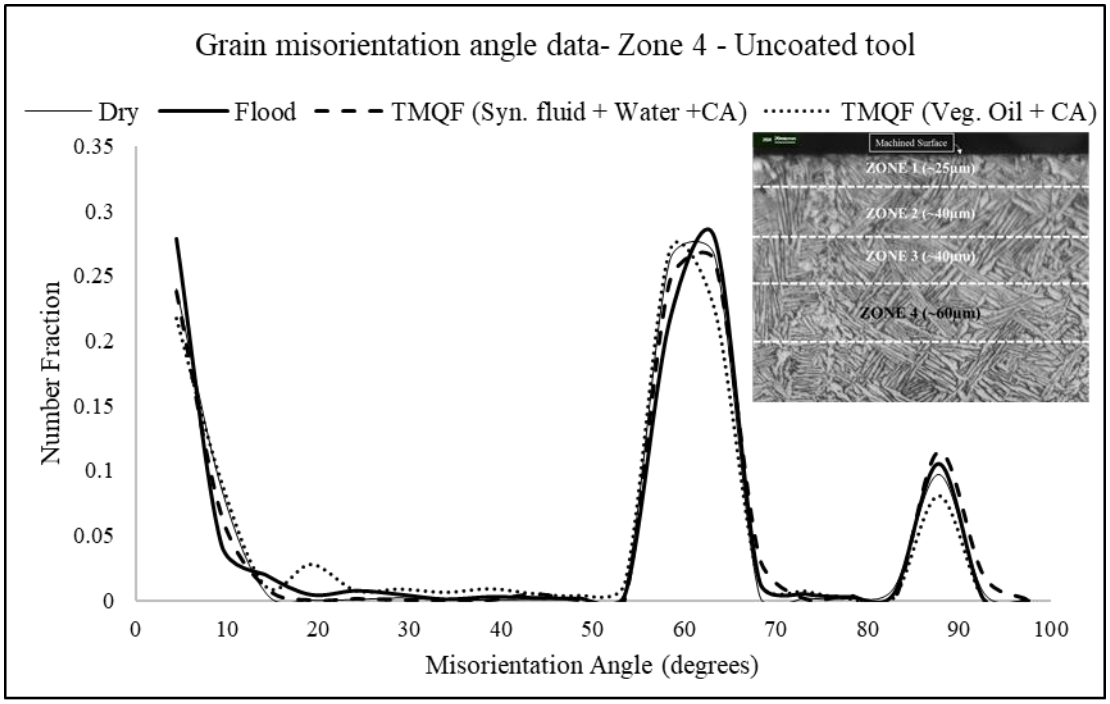

(a)

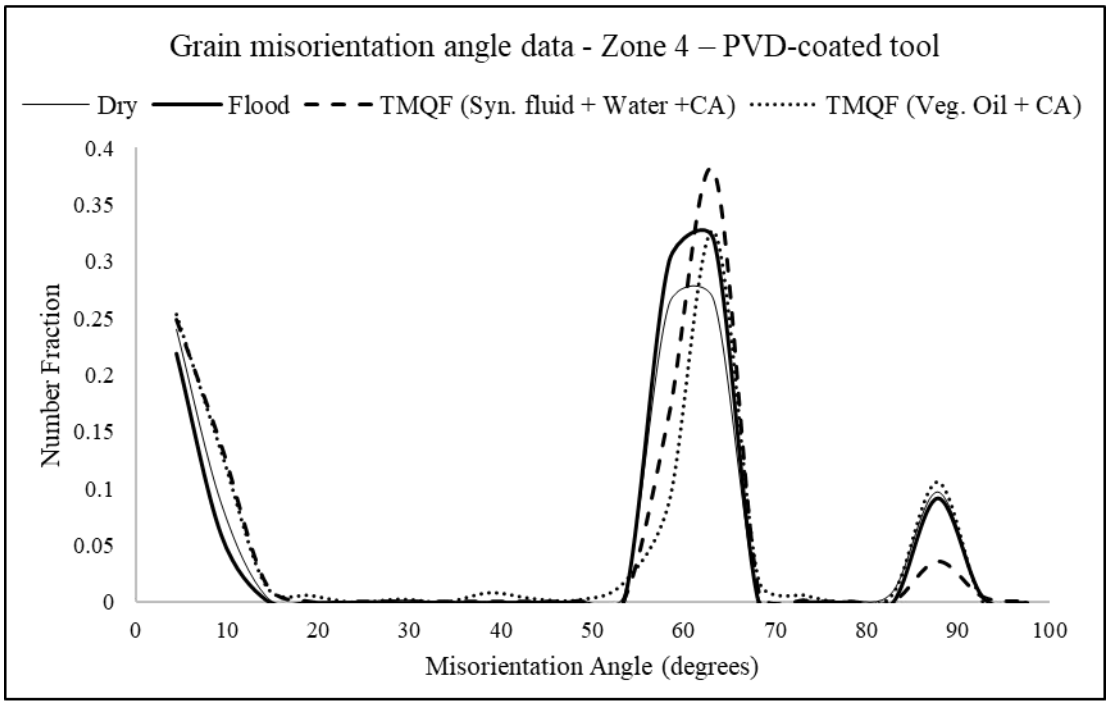

(b)

Figure 49 Grain Misorientation Angle Data for Zone 4: (a) Uncoated Tool, (b) PVD-Coated Tool

a) Zone 1: (25µm in length and 150 µm in width) This area is directly below the machined surface. From Figure 46 it can be clearly seen that the relative amount of low angle grain boundaries (5 degrees or less) is high for all eight machining experiments. The high presence of low-angle grain boundaries is primarily attributed to severe plastic deformation occurring near the machined surface, which results in formation of subgrain boundaries within a grain. The area near the machined surface is usually affected by severe plastic deformation as also reported by other researchers [50], [52].

b) Zone 2 and Zone 3: (each 40 µm in length and 150 µm in width) The Zone 2 and Zone 3 grain misorientation angle data, from Figure 47 and Figure 48, respectively, show that dry machining has relatively higher amounts of low-angle grain boundaries compared to the other three cutting fluid application conditions for both the cutting tools under investigation. This is primarily due to the relatively high temperature generated during dry machining. Due to high temperature and high strain rate in dry machining, there is a higher possibility of formation of subgrain boundaries within a grain. In this case, the subgrain can be formed within each α lamella/platelet. Hence, there is a relatively higher percentage of low-angle grain boundaries in dry machining.

c) Zone 4: (50-60 µm in length and 150 µm in width) The grain misorientation angle data for the final zone in this analysis is shown in Figure 49. As can be seen, the grain misorientation angle data in this zone has a similar profile for all eight machining experiments. Dry machining also has a similar profile to those obtained from the other cutting fluid application conditions. Hence, at this depth, it is safe to assume that there is no significant effect of high temperature and high strain rate on the microstructure.

On analyzing the grain misorientation data (α phase only) along the depth of the machined surface for all eight experiments, it can be concluded that dry machining, irrespective of the cutting tool used, produced a higher concentration of low angle grain boundaries compared to those from other cutting fluid application conditions. This is primarily due to the combination of high

temperature that is generated during dry machining and also severe plastic deformation (high strain rates). Furthermore, this result validates the importance of using controlled and precise amounts of cutting fluids in machining.

4.6 Discussion

The individual results from the three characteristics (topographical, mechanical, and microstructural) of machining-induced surface integrity were provided in the previous sections. As there is no significant difference in the topographical characteristic of surface integrity (surface roughness data – Figure 34), it is not considered for the following discussion. Thus, only the correlation between mechanical and microstructural characteristics of surface integrity will be addressed in this section. Furthermore, the interaction between cutting tool and cutting flood application on the final surface state (all three characteristics of surface integrity) will also be discussed in this section.

4.6.1 Correlation Between Mechanical and Microstructural Characteristics of Surface Integrity

The data from the residual stress profile, microhardness profile, and misorientation angle distribution for all eight machining experiments do not show any immediate, direct correlation. However, an in-depth analysis of misorientation angle distribution and microhardness profile may provide some correlation between the two results. Dry machining, irrespective of the cutting tool used, yields a low microhardness profile and a higher percentage of low angle grain boundaries (until Zone 3) compared to those obtained from the other three cutting fluid applications (Figure 50). This is predominately due to the high temperature that is generated during dry machining.

The major reasons for increase in hardness is plastic deformation and work hardening. Plastic deformation in general changes the grainsize, strain-hardens the material, and increases the dislocation density. The movement of dislocations and dislocation generation are the primary reasons for the increase in the hardness of the machined surface. Furthermore, titanium alloys are

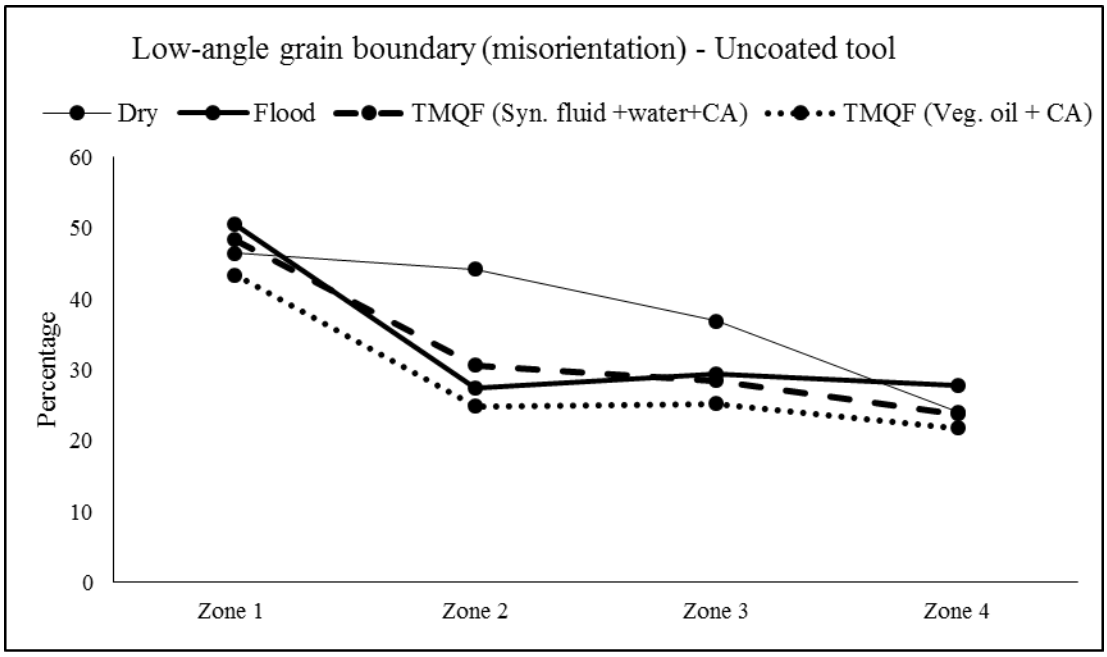

(a)

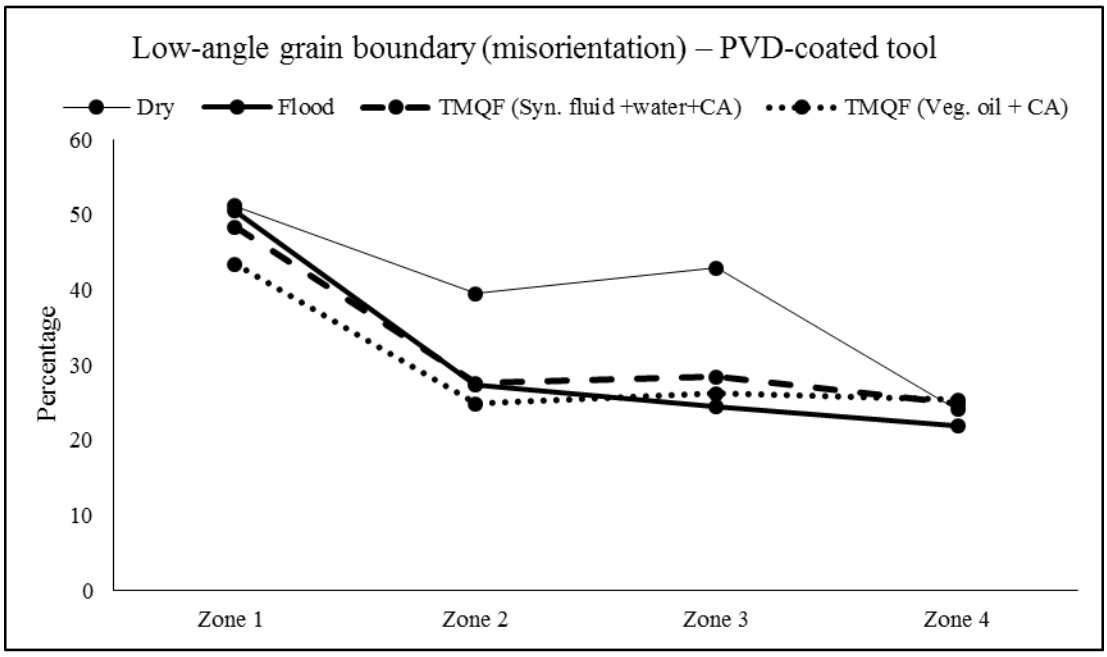

(b)

Figure 50 Percentage of Low-Angle Grain Boundaries in all 4 Zones in Machined Ti-6Al-4V Titanium Alloy (a) Uncoated Tool (b) PVD-Coated Tool

known for their work-hardening characteristics due to machining.

The low-angle grain boundaries arise primarily due to formation of subgrain boundaries within a grain. The high temperature generated due to dry machining may increase the dislocation motion. Due to high subgrain boundary formation, the probability of dislocations settling along the grain boundaries is high and that may reduce the strain-hardening phenomena. The correlation between yield strength (σ_y) and effective dislocation density (ρ) is provided in the below equation where G represents the shear modulus and b represents the Burgers vector. The dislocations reaching the grain boundaries will annihilate themselves and thus reduce the effective dislocation density.

$$\sigma_y = Gb\sqrt{\rho}$$

In dry machining, the effective dislocation density may be less due to the motion of dislocations towards the grain boundaries. This may be one of the reasons for the low hardness profile produced in dry machining. This relationship establishes some correlation between the microhardness profile and grain misorientation angle data. However, no clear conclusions can be drawn with just the misorientation angle distribution data. The above relationship can be proven only by performing extensive microstructural analysis using transmission electron microscopy (TEM).

4.6.2 Interaction Between Cutting Tool and Cutting Fluid Application

Based on the results from all eight machining experiments, it can be clearly seen that only residual stresses showed some significant changes due to the interaction between the cutting tool and cutting fluid application. Figure 51 shows the effect of individual cutting fluid application conditions on the residual stress profile. Contrasting residual stress profiles were obtained for flood machining with uncoated tool and PVD-coated tool underlining the significance of the interaction between the cutting tool and cutting fluid application, and their effect on the final surface state.

In flood machining, an uncoated cutting tool yielded compressive surface residual stress whereas the PVD-coated tool produced a tensile surface residual stress. The low thermal conductivity of the coating on the PVD-coated tool compared to the uncoated tool along with flood

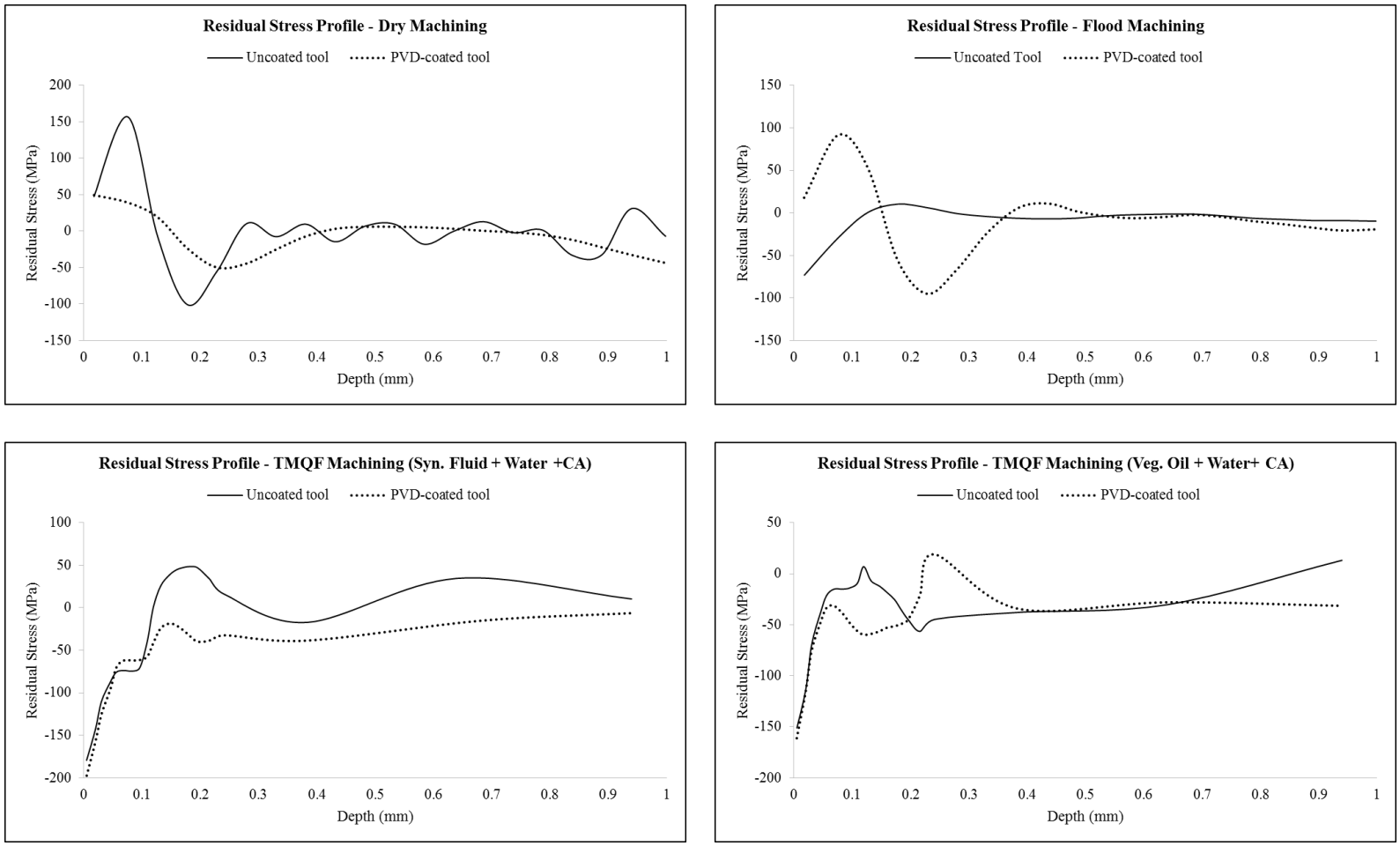

Figure 51 Residual Stress Profile for Individual Cutting Fluid Application

machining has possibly produced a tensile residual stress profile. It is possible that in flood machining using the PVD-coated tool, there is a higher percentage of heat being transferred to the workpiece than flood machining with uncoated tool. This may be the primary reason for the significant difference in the residual stress profile. However, this phenomenon is not seen in any of the TMQF machining conditions, which further validates its performance and its ability to reduce the temperature irrespective of the thermal conductivity of the tool used in machining. TMQF machining, irrespective of type of cutting fluid and cutting tool used, produces a highly desirable compressive surface residual stress suggesting that there is no significant interaction between the cutting tool and TMQF application. TMQF application significantly reduces the heat produced in the cutting zone and the newly created work surface and thereby it appears to eliminate any negative effects of the cutting tool on the final surface state. In this case, the low thermal conductivity of PVD coated tool had a negative influence on the residual stresses when machined with flood but that effect was eliminated when machined under TMQF application.

4.7 Summary

The chapter started with an analysis of the machining performance (machining chips and forces) for all eight machining experiments. No significant difference in the machining chips and forces was found. The analysis of topographical, mechanical, and microstructural characteristics of machining-induced surface integrity yielded some interesting results and correlations. Furthermore, there was enough evidence that TMQF machining performed better than flood machining, suggesting that traditional cutting fluid application in a flood manner is grossly over used. No significant difference in TMQF machining's performance (in terms of machining performance as well as final surface quality) was recorded for the two inherently different cutting fluids used even though the synthetic fluid (10%) was applied with water (90%) and concentrated vegetable oil (100%) was applied without water.

Based on analyzing all the results, it can be concluded that TMQF (Syn. Oil + Water + CA)

machining using a PVD-coated tool is the best combination for producing a highly desirable surface quality. TMQF machining (Syn. Oil + Water + CA) with PVD-coated tool produced a low surface roughness, relatively high subsurface microhardness, desirable compressive surface residual stresses, and no undesirable microstructural damages. Even though the TMQF machining with vegetable oil performed similar to the TMQF machining with synthetic fluid + water, the cost and amount of vegetable oil is high compared to synthetic fluid. Therefore, TMQF machining with synthetic fluid, water, and compressed air using a PVD-coated tool is recommended for finish machining operation of Ti-6Al-4V titanium alloy.

The next chapter summarizes all the results from this thesis and also provides recommendations for future work to answer some of the questions from this thesis.

CHAPTER 5

SUMMARY AND FUTURE WORK

5.1 Summary and Conclusions

The major aim of this thesis was to conduct a comprehensive surface integrity study by addressing topographical, mechanical, and microstructural characteristics of surface integrity in machined Ti-6Al-4V titanium alloy under varying cutting fluid application conditions and cutting tools. As reported in Chapter 2, much of the previous research on machining-induced surface integrity is focused on either one or two characteristics of surface integrity. Only a handful of researchers have looked at the orientation imaging microscopy (OIM) analysis of machining-induced microstructural alterations. Hence, this thesis was aimed at addressing all three important characteristics of machining-induced surface integrity by measuring surface roughness (using an optical profilometer), residual stresses (using the hole drilling method), microhardness (using Vickers hardness tester), and microstructural alterations (using optical microscope and SEM/EBSD). The cutting conditions (feed and cutting speed) were chosen to represent the finish machining operation of Ti-6Al-4V titanium alloy. The finishing operation dictates the final surface state of the component that goes into service. Moreover, the final surface integrity of the component directly influences the component's performance (fatigue life, stress corrosion, creep resistance, etc.) Additionally, this thesis was also aimed at evaluating the performance of the targeted minimum quantity fluid (TMQF) application in machining. Eight machining experiments using 4 different cutting fluid applications and 2 different cutting tools were designed to address all the objectives of this thesis.

First, the ***machining performance*** was evaluated by analyzing the machining chips and

machining forces for all cutting fluid applications and cutting tools under investigation. The summary of results from evaluating the machining chips and machining forces for all eight experiment are as follows:

1. Machining Chips
    a. Dry machining produces long continuous chips whereas using cutting fluid assisted in more controlled chip formation.
    b. No significant difference in chip formation was observed for machining with an uncoated cutting tool or a PVD-coated cutting tool.
2. Machining Forces:
    a. The PVD-coated cutting tool produced higher machining forces compared to those obtained from the uncoated cutting tool.
    b. No clear trend in machining forces were observed based on cutting fluid application employed.

After analyzing the machining performance, the ***surface integrity study*** was carried out by analyzing the results from surface roughness, residual stresses, microhardness, optical microstructure, and EBSD analysis. The summary of the results from the surface integrity study is as follows

1. Topographical Characterization: Surface Roughness (R_a)
    a. The PVD-coated tool produced lower surface roughness values when compared to those obtained from the uncoated tool.
    b. Dry machining in general generated higher surface roughness whereas TMQF machining with vegetable oil and compressed air had the lowest surface roughness value.
2. Mechanical Characterization: Residual Stresses
    a. TMQF machining, irrespective of the cutting fluid and cutting tool used, produced a highly desirable compressive residual stress profile.

   b. Dry machining, irrespective of the cutting tool used, produced highest surface tensile residual stress.
   c. Flood machining underlined the significance of interaction between cutting tool and cutting fluid application by yielding contrasting residual stress profile when machined with an uncoated cutting tool (compressive surface residual stress) and a PVD-coated cutting tool (tensile surface residual stress).

3. Mechanical Characterization: Microhardness
   a. Flood machining and both TMQF machining conditions produced higher subsurface hardness and they also maintained this increased hardness up to a greater depth compared to dry machining for both cutting tools.
   b. The uncoated cutting tool yielded higher hardness than the PVD-coated tool under all cutting fluid applications which may be due their difference in thermal conductivity.
4. Microstructural Characterization: Optical Microstructural Images
   a. No significant difference in optical microstructural image was observed for all eight machined samples. However, clear grain bending/kinking along the cutting direction was visible in all eight images.
5. Microstructural Characterization: EBSD Analysis – Grain Misorientation Angle
   a. A higher concentration of low-angle grain boundaries (misorientation angle) was present near the machined surface (up to 25μm) in all eight machined samples.
   b. Dry machining, irrespective of cutting tool used, had a higher concentration of low angle grain boundaries at a larger depth (~100μm) than the other three cutting fluid application conditions.

It is important to note that these results may apply only to titanium alloys. These results provide greater understanding of the state of the machined surface due to different cutting fluid applications and cutting tools. Furthermore, on analyzing the results from microhardness measurement and grain misorientation data, it can be seen that there may be some correlation between the two

characteristics (mechanical and microstructural) of surface integrity. The presence of higher concentration of low-angle grain boundaries at larger depth may lead to reduction in the effective dislocation density, which in turn reduces the hardness in dry machining compared to those obtained from other cutting fluid application conditions. However, there is no concrete evidence to prove the above assumption. Further analysis should be carried to validate the above statement and to establish a significant correlation between mechanical and microstructural characteristics of surface integrity.

5.2 Future Work Recommendations

The results from this thesis will act as a platform for further studies that are recommended below.

- It is highly recommended to perform TEM analysis of the machined surface/subsurface to establish a clear relationship between the microstructural and mechanical characteristics of machining-induced surface integrity. The mechanism for formation of low-angle grain boundaries can also be established by performing TEM analysis. The understanding of the relationship between mechanical and microstructural characteristics of surface integrity will help in evaluating the machining conditions, cutting fluid applications, and cutting fluids, cutting tools, and so on, and thereby will aid in selection of these conditions for obtaining a desired final superior surface quality that will improve the performance of the component in service.
- Future studies involving machining-induced surface integrity should consider including EBSD studies as they provide extensive quantitative details about the microstructure (grain size, misorientation angle, phase distribution data, pole figure maps, etc.) along with the mechanical and topographical characteristics of surface integrity.
- Fatigue studies may be carried out to further validate the results from this analysis. A fatigue study will be a direct measure of the machined surface state

- Different cutting fluid combinations should be used with TMQF application to evaluate its performance. More than two cutting fluid outlets can also be explored to improve the performance of TMQF application in machining.
- The performance of TMQF application should be further evaluated by performing tool life studies. The interaction between different tool coatings and TMQF application, and its effect on final surface quality should also be studied.
- Using the results from this study and future studies on machining-induced surface integrity, a finite element model can be developed to predict the microstructural changes and residual stresses due to machining under varying cutting fluid application conditions and cutting tools. This model will assist in predictively designing the machining process to obtain a desired surface integrity in the final component.

APPENDIX A

CNC MACHINING CODES

A.1 Machining Experiment– CNC Lathe

```
%
N10 (FACING EXPERIMENT – TI-6AL-4V)
N20 G18 G40 G64 G80 G97 G99
N30 T101
N40 G00 G54 X4.5 Z1.
N50 G50 S4950
N60 G96 S246 M03 (CUTTING SPEED, SFM)
N70 G00 X4.5 Z0.1
N80 G00 Z-0.0472 (DOC, IN)
N90 G01 X2. F0.0079 (FEED.IN/REV)
N100 G00 X4.5 Z0.1
N110 G00 X5.
N120 G00 Z5.
N130 M30;
%
```

A.2 Strain Gage Hole Drilling Experiment – CNC Mill

```
%
O00100
N20 (HOLE DRILLING METHOD – RESIDUAL STRESS MEASUREMENT)
N30
N40 G00 G40 G80 G90
```

N50 T1 M06

N60 (1/64 DRILL TOOL - 1 DIA. - .0625in)

N70 T1 M06

N80 G54 X0. Y0.

N90 G43 H01 Z2.

N95 S2000 M03

N100 Z0.1

N110 G81 X0. Y0. Z-0.0005 R0.1 F1. (HOLE 01)

N120 G80

N130 Z5.

N140 M00

N150 Z0.1

N160 G81 X0. Y0. Z-0.001 R0.1 F1. (HOLE 02)

N170 G80

N180 Z5.

N190 M00

N200 Z0.1

N210 G81 X0. Y0. Z-0.0015 R0.1 F1. (HOLE 03)

N220 G80

N230 Z5.

N240 M00

N250 Z0.1

N260 G81 X0. Y0. Z-0.002 R0.1 F1. (HOLE 04)

N270 G80

N280 Z5.

N290 M00

N300 Z0.1

N310 G81 X0. Y0. Z-0.0025 R0.1 F1. (HOLE 05)

N320 G80

N330 Z5.

N340 M00

N350 Z0.1

N360 G81 X0. Y0. Z-0.003 R0.1 F1. (HOLE 06)

N370 G80

N380 Z5.

N390 M00

N400 Z0.1

N410 G81 X0. Y0. Z-0.0035 R0.1 F1. (HOLE 07)

N420 G80

N430 Z5.

N440 M00

N450 Z0.1

N460 G81 X0. Y0. Z-0.004 R0.1 F1. (HOLE 08)

N470 G80

N480 Z5.

N490 M00

N500 Z0.1

N510 G81 X0. Y0. Z-0.0045 R0.1 F1. (HOLE 09)

N520 G80

N530 Z5.

N540 M00

N550 Z0.1

N560 G81 X0. Y0. Z-0.005 R0.1 F1. (HOLE 10)

N570 G80

N580 Z5.

N590 M00

N600 Z0.1

N610 G81 X0. Y0. Z-0.0055 R0.1 F1. (HOLE 11)

N620 G80

N630 Z5.

N640 M00

N650 Z0.1

N660 G81 X0. Y0. Z-0.006 R0.1 F1. (HOLE 12)

N670 G80

N680 Z5.

N690 M00

N700 Z0.1

N710 G81 X0. Y0. Z-0.0065 R0.1 F1. (HOLE 13)

N720 G80

N730 Z5.

N740 M00

N750 Z0.1

N760 G81 X0. Y0. Z-0.007 R0.1 F1. (HOLE 14)

N770 G80

N780 Z5.

N790 M00

N800 Z0.1

N810 G81 X0. Y0. Z-0.0075 R0.1 F1. (HOLE 15)

N820 G80

N830 Z5.

N840 M00

N850 Z0.1

N860 G81 X0. Y0. Z-0.008 R0.1 F1. (HOLE 16)

N870 G80

N880 Z5.

N890 M00

N900 Z0.1

N910 G81 X0. Y0. Z-0.009 R0.1 F1. (HOLE 17)

N920 G80

N930 Z5.

N940 M00

N950 Z0.1

N960 G81 X0. Y0. Z-0.0101 R0.1 F1. (HOLE 18)

N970 G80

N980 Z5.

N990 M00

N1000 Z0.1

N1010 G81 X0. Y0. Z-0.0202 R0.1 F1. (HOLE 19)

N1020 G80

N1030 Z5.

N1040 M00

N1050 Z0.1

N1060 G81 X0. Y0. Z-0.0303 R0.1 F1. (HOLE 20)

N1070 G80

N1080 Z5.

N1090 M00

N1100 Z0.1

N1110 G81 X0. Y0. Z-0.0404 R0.1 F1. (HOLE 21)

N1120 G80

N1130 Z5.

N1140 G91 G28 Z0.

N1150 M30

%

APPENDIX B

H-DRILL SOFTWARE AND INTEGRAL METHOD

Once the residual strains present in the machined subsurface were measured using hole drilling experiments, the H-drill software was used to convert those strains into stresses. The H-drill is a specialized software developed by Professor Gary S. Schajer to calculate the residual stresses from the strain data obtained by hole drilling experiment. The H-drill software uses the integral method (a constitutive model) to determine the maximum and minimum principal stresses at each measurement depth. The maximum principal stresses obtained at each depth was chosen to represent the residual stresses at that depth. The step by step procedure to use H-drill software to determine residual stresses is outlined below.

1. Open the H-Drill software. Figure 52 shows the image of the main H-Drill window.
2. Click Blind-Hole on the menu bar, to get drop down list as shown in Figure 53. Note that the strain data was collected by drilling a blind hole. Click on the Specific Material and Geometry option from the drop down list. The Material and Geometry Data window opens as shown in Figure 54.
    a. Enter Young's modulus (16.5 $*10^6$ psi), Poisson's ratio (0.342), and yield strength (126 ksi) of the Ti-6Al-4V titanium alloy in the appropriate text box.
    b. Measure the diameter of the hole using putty.
    c. Enter the value in the hole diameter text box.
    d. Check the appropriate rosette type check box in the Material and Geometry Data window and click OK.
    e. Note: Rosette type can be found in the strain gage box.

Figure 52 Main H-Drill Window

Figure 53 Image of Blind-Hole Menu Bar

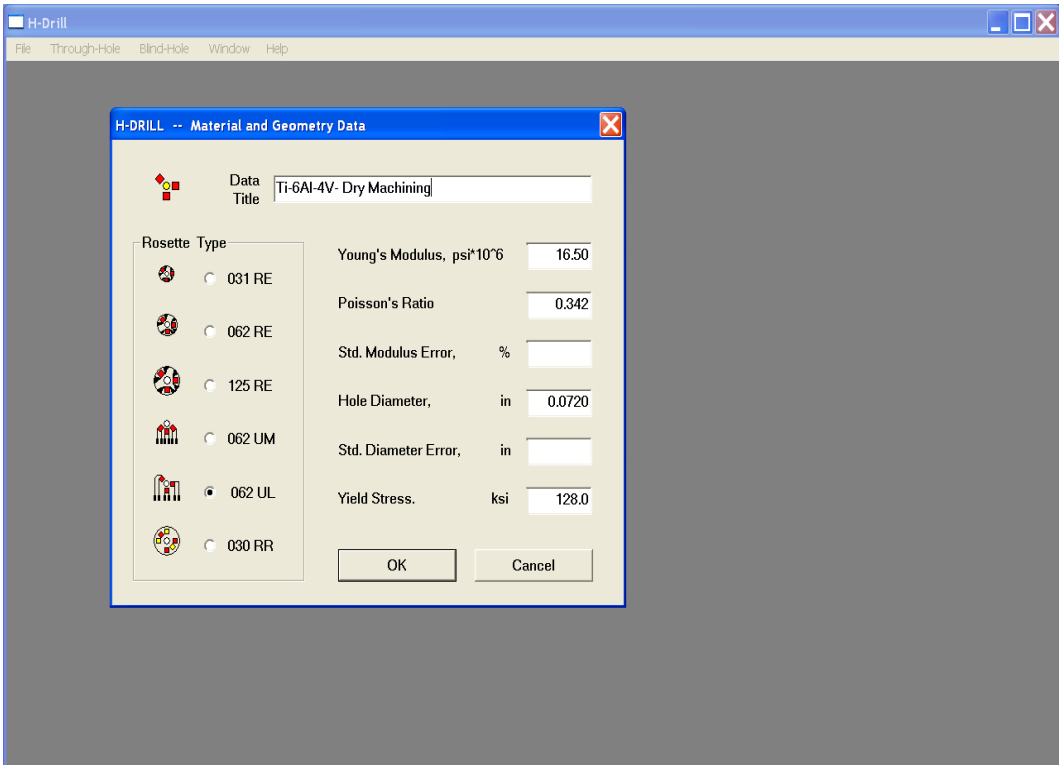

Figure 54 Material and Geometry Window

3. Click on the second option (Specify Blind-Hole strains) in the Blind–Hole drop down menu. Blind-Hole strain data window opens as shown in Figure 55.
    a. Enter the measured strain data obtained from hole drilling experiment in the window and click OK.
4. Click on the Set Calculation Options, the third option in the Blind-Hole drop down menu. The Calculation Options window opens as shown in the Figure 56.
    a. Check the maximum and minimum principal stresses check box and click OK.
5. Click on the Display Integral Method option in the blind hole drop down menu to get the results. The results are displayed as shown in Figure 57. Click on the save results option in the blind hole drop down menu to save the results in an excel sheet for further analysis.

These are the steps involved in converting the residual strains measured from hole drilling experiment to residual stresses (maximum principal stress) using H-Drill software. A brief description of the integral method used in the H-Drill software is provided below.

Machining-induced residual stresses are generally rapidly varying along the depth of the machined subsurface. The integral method is the recommended method for determining machining-induced residual stresses. This method is able to find relaxed strains that relate to highly nonuniform residual stress distribution. A great degree of precision is required while measuring the strains, as the calculations in this method are highly sensitive to strain measurement errors. “This method recognizes that the strains measured during hole drilling are the cumulative result of relieving the residual stresses that were originally present at all depth steps within the total hole depth” [45]. Hence, the integral method was chosen to determine the machining-induced residual stresses.

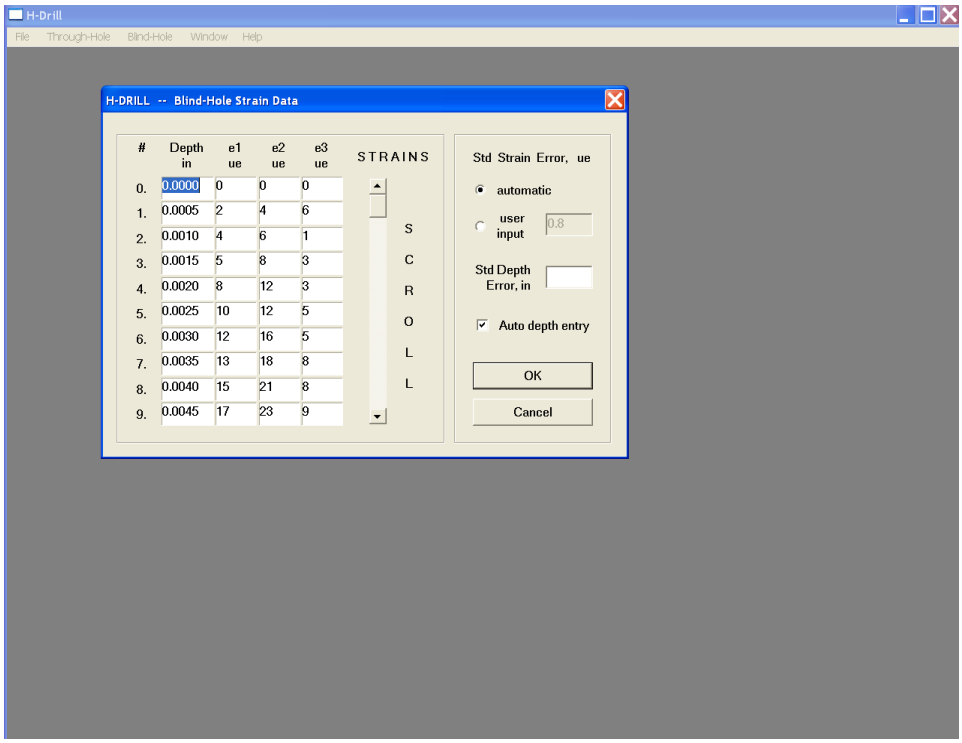

Figure 55 Blind-Hole Strain Data Window

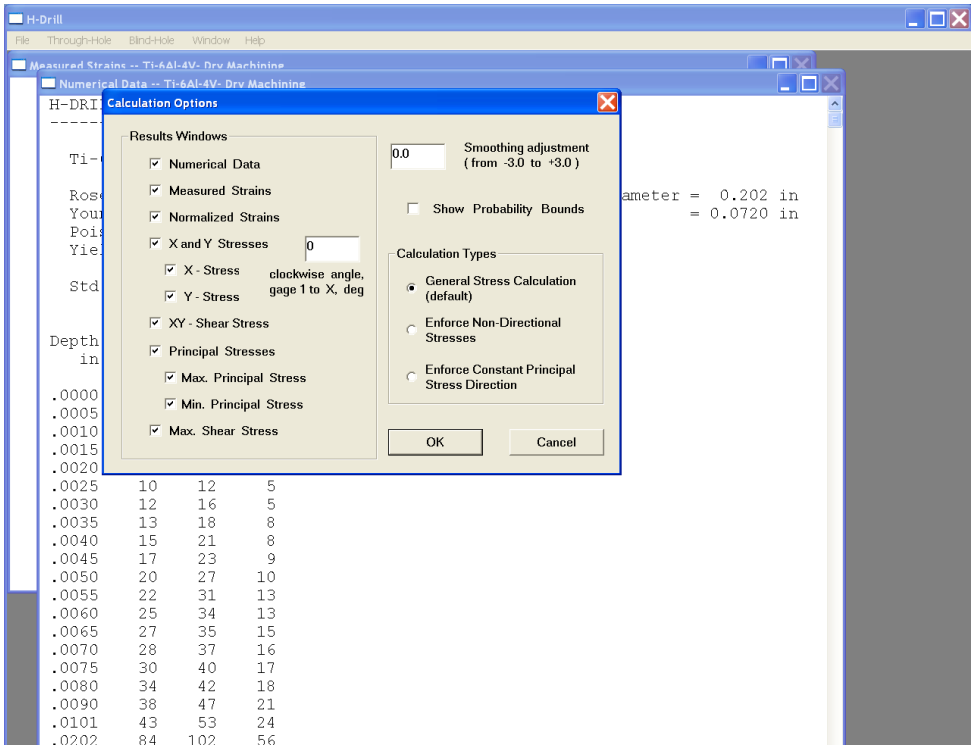

Figure 56 Calculation Option Window

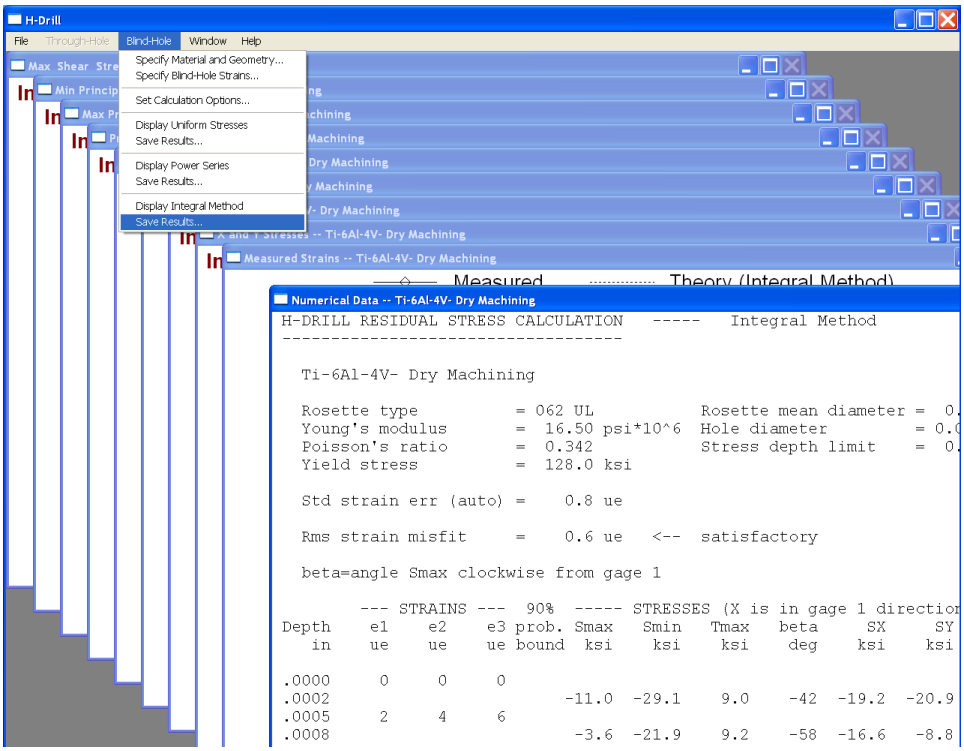

Figure 57 Results Window

APPENDIX C

EBSD ANALYSIS – INVERSE POLE FIGURE MAPS

As mentioned in Section 4.5.2, EBSD analysis was carried out to determine four different features of the microstructure. Since the β phase present in the microstructure was in the rage of nanometers, the resolution of the SEM used in this study was not able to consistently detect the β phase. Hence, the phase distribution data obtained from EBSD analysis is deemed irrelevant. Grain size distribution data obtained from the analysis is misleading as it represents the alpha colony size rather than the size of alpha lamella. Therefore, only the inverse pole figure maps and grain misorientation angle data are used in this study. The detailed analysis of grain misorientation angle data was presented in Section 4.5.3.

The inverse pole figure map represents the 3D orientation information in two dimensions. Each color in the map represents a unique orientation. Figure 58 – 65 represents the inverse pole maps or all eight machining experiments. The data is plotted with respect to the normal direction (ND) and cutting direction (CD) as represented in each image. No crystallographic texture was generated due to machining and hence the inverse pole figure data was not further analyzed.

Figure 58–61: Images from machining using uncoated tool.

Figure 62-65: Images from machining using PVD-coated tool.

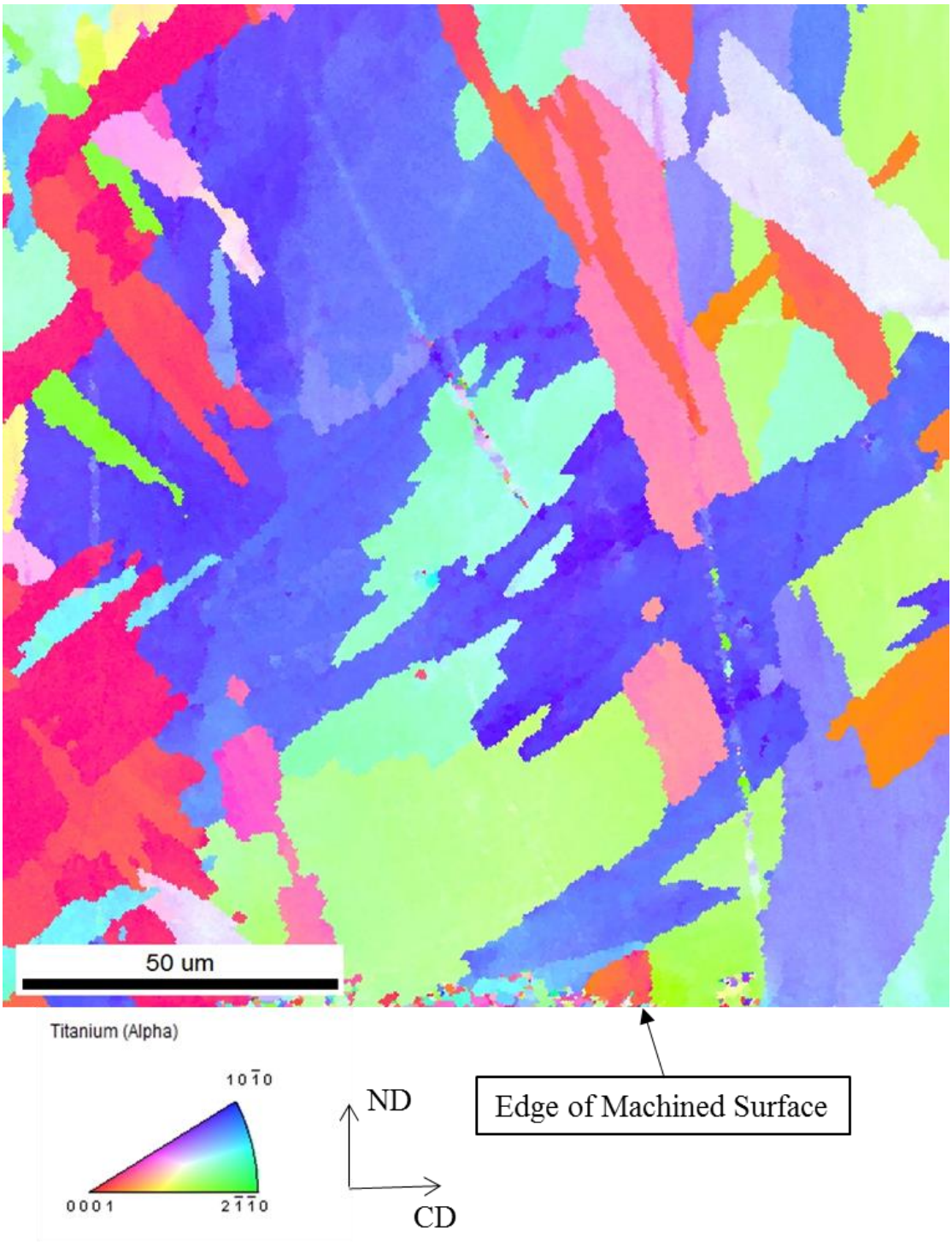

Figure 58 Inverse Pole Figure Map of Dry Machined Ti-6Al-4V Titanium Using Uncoated Tool

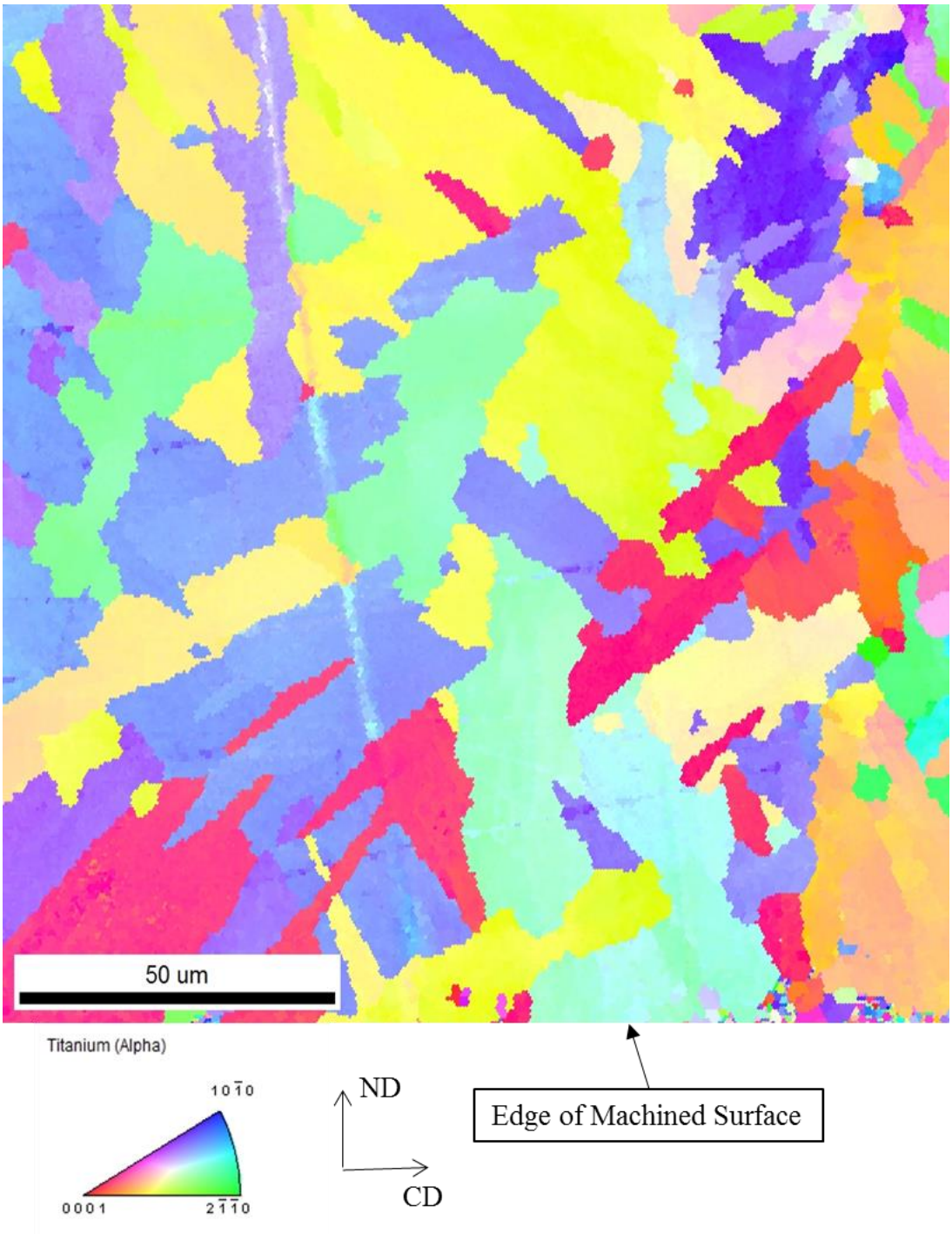

Figure 59 Inverse Pole Figure Map of Flood Machined Ti-6Al-4V Titanium Using Uncoated Tool

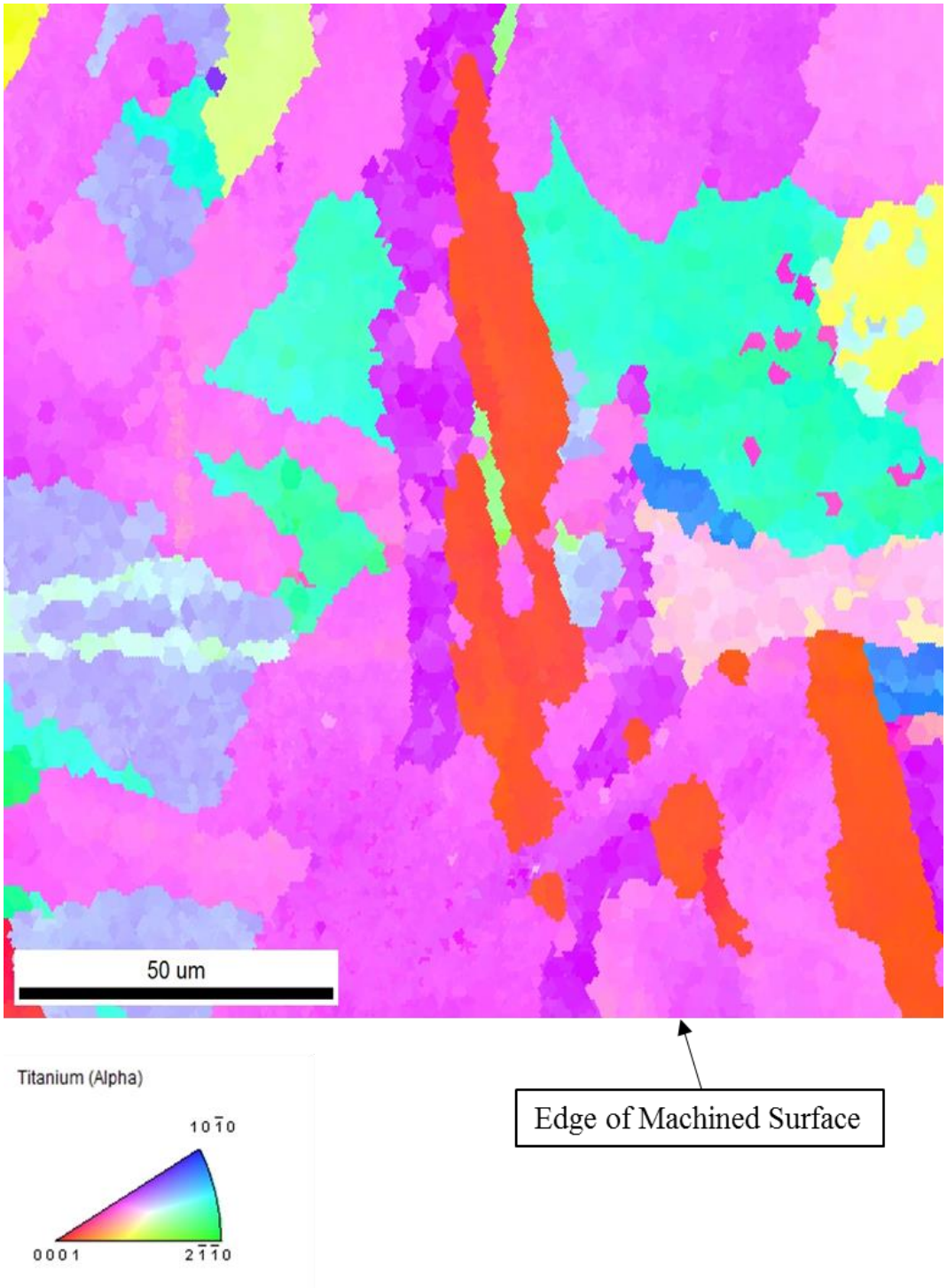

Figure 60 Inverse Pole Figure Map of TMQF (Syn. Fluid + Water +CA) Machined Ti-6Al-4V Titanium Using Uncoated Tool

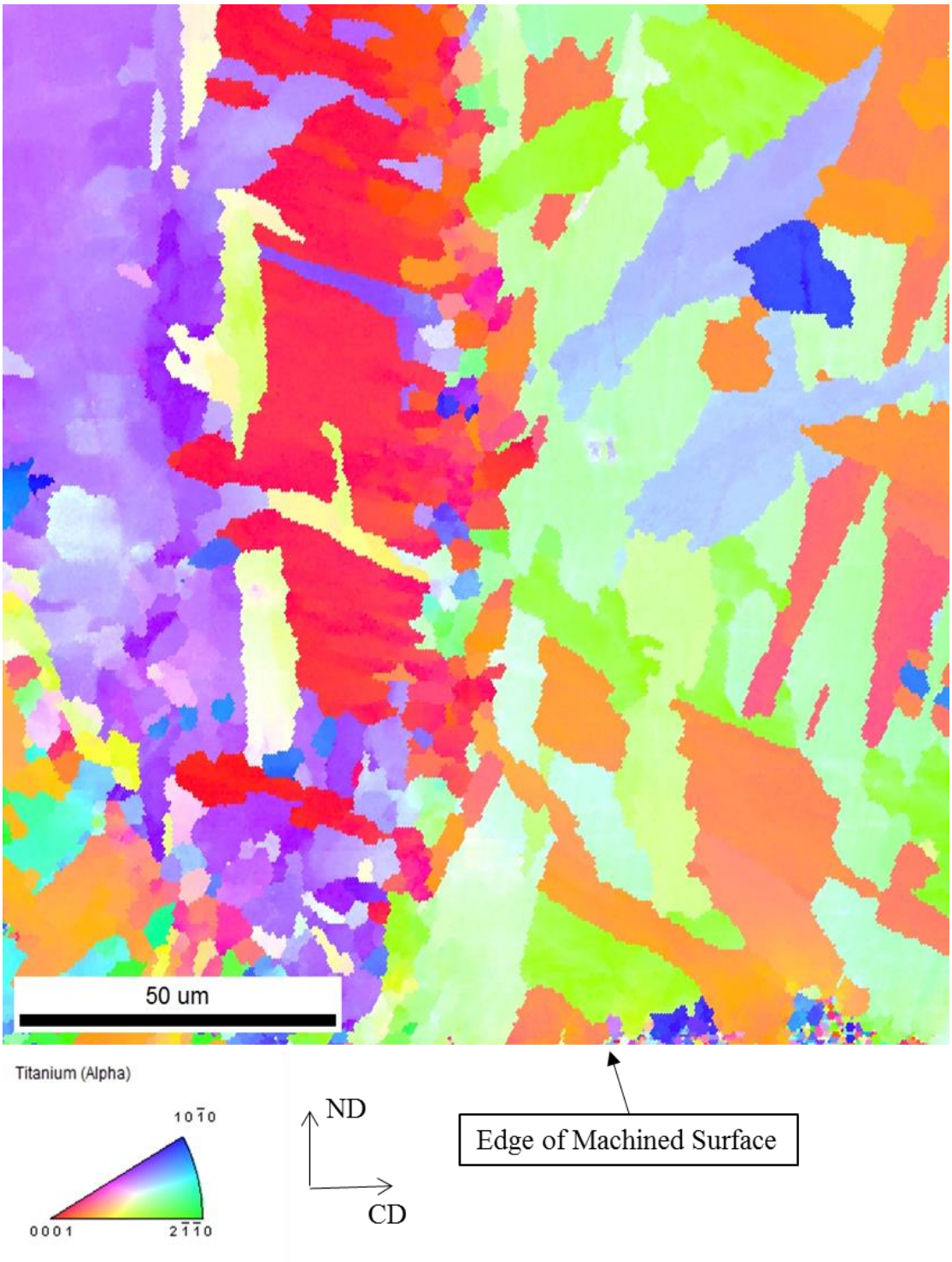

Figure 61 Inverse Pole Figure Map of TMQF (Veg. Oil+ CA) Machined Ti-6Al-4V Titanium Using Uncoated Tool

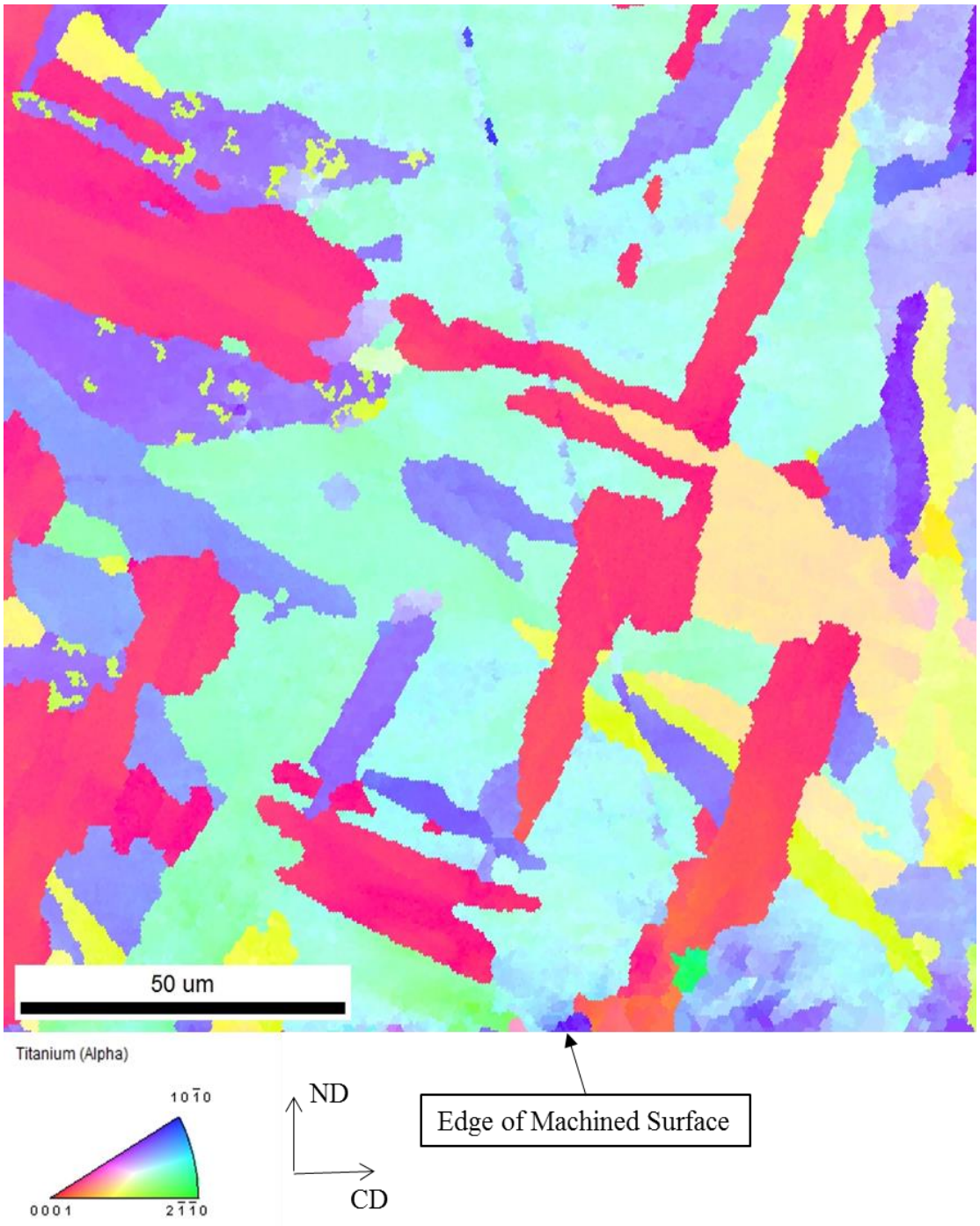

Figure 62 Inverse Pole Figure Map of Dry Machined Ti-6Al-4V Titanium Using PVD-Coated Tool

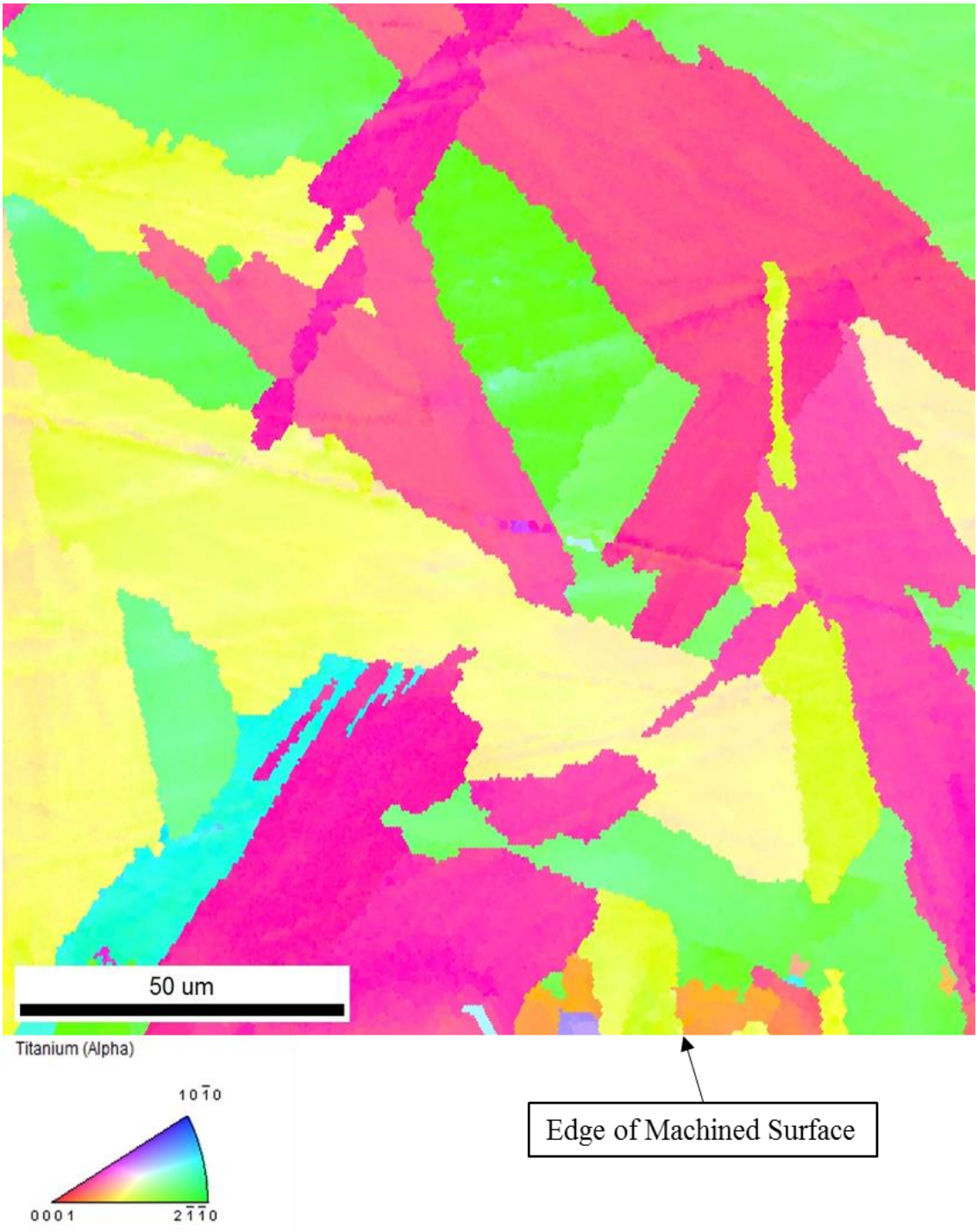

Figure 63 Inverse Pole Figure Map of Flood Machined Ti-6Al-4V Titanium Using PVD-Coated Tool

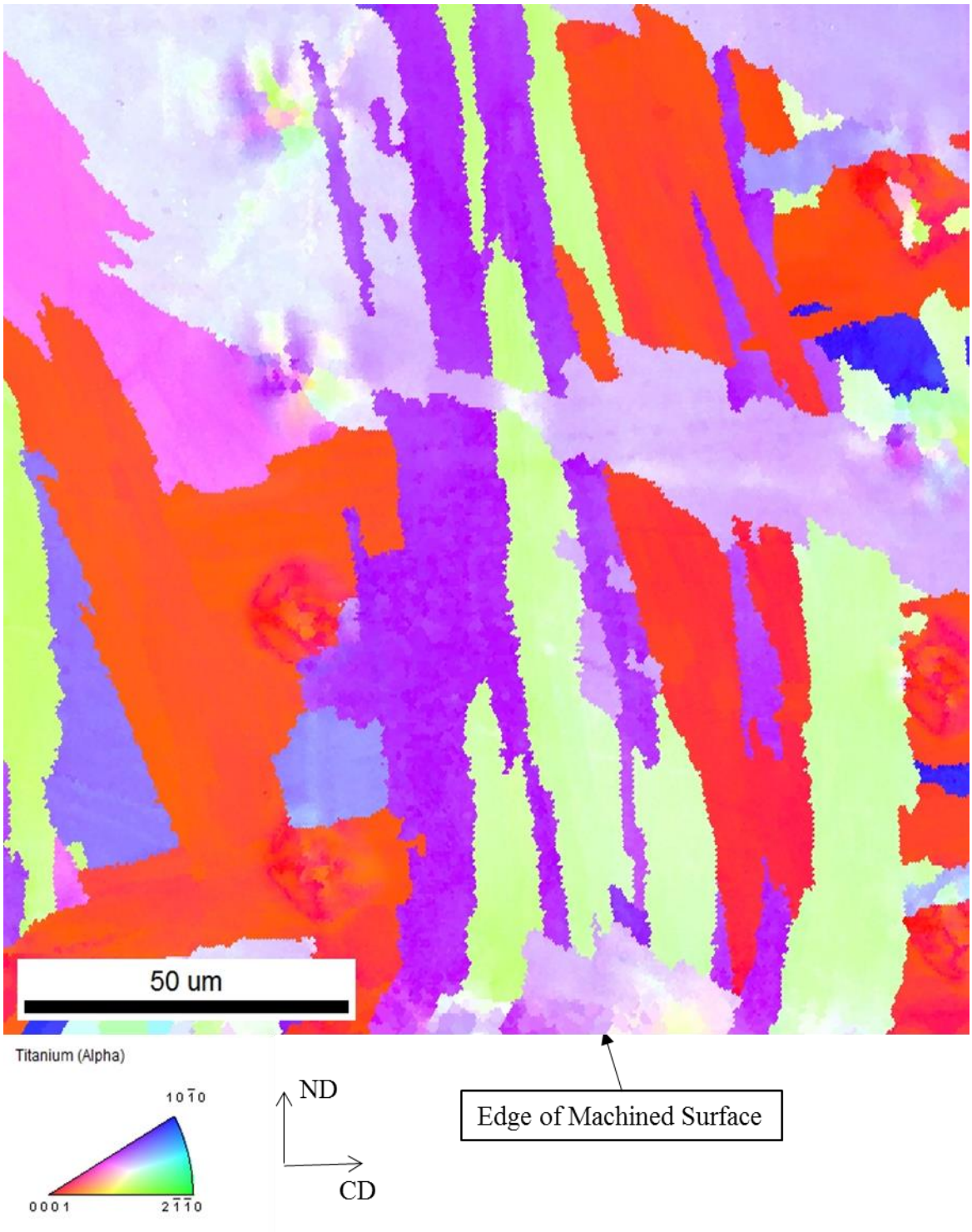

Figure 64 Inverse Pole Figure Map of TMQF (Syn. Fluid+ Water +CA) Machined Ti-6Al-4V Titanium Using-PVD Coated Tool

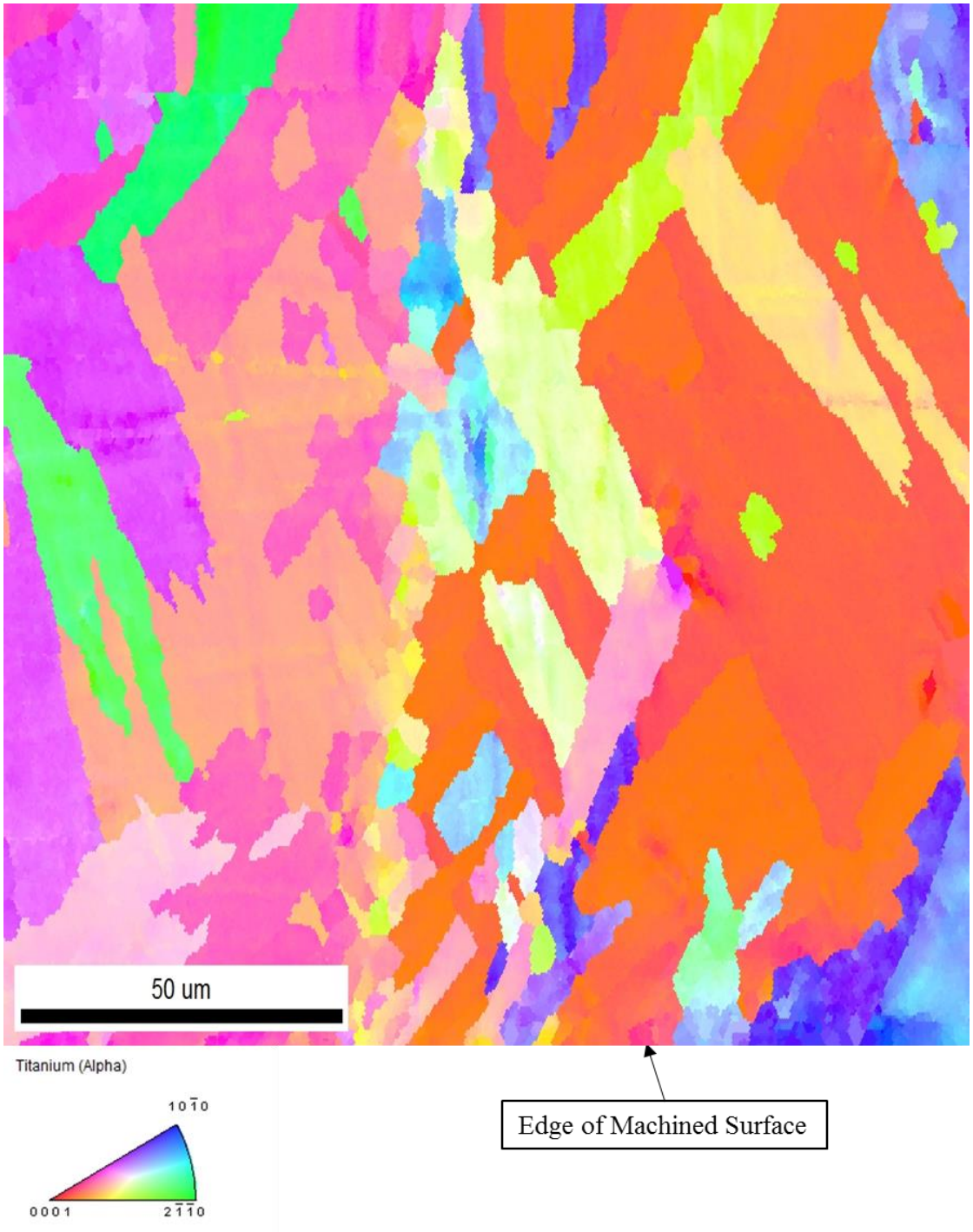

Figure 65 Inverse Pole Figure Map of TMQF (Veg. Oil+ CA) Machined Ti-6Al-4V Titanium Using PVD Coated Tool

REFERENCES

[1] M. C. Shaw, *Metal Cutting Principles*, 2nd ed. Oxford, UK: Oxford University Press, 2005.

[2] B. Griffiths, *Manufacturing Surface Technology : Surface Integrity & Functional Performance*, 1st ed. London, UK: Penton Press, 2001.

[3] S. Y. Liang and A. J. Shih, *Analysis of Machining and Machine Tools*. Boston, MA, US: Springer, 2016.

[4] C. N. Madu, *Handbook of Environmentally Conscious Manufacturing*. Boston, MA, US: Springer, 2001.

[5] Z. Wang, S. Nakashima, and M. Larson, "Energy efficient machining of titanium alloys by controlling cutting temperature and vibration," *Procedia CIRP*, vol. 17, pp. 523–528, Jan. 2014.

[6] I. Deiab, S. W. Raza, and S. Pervaiz, "Analysis of lubrication strategies for sustainable machining during turning of titanium Ti-6Al-4V alloy," *Procedia CIRP*, vol. 17, pp. 766–771, Jan. 2014.

[7] S. Debnath, M. M. Reddy, and Q. S. Yi, "Environmental friendly cutting fluids and cooling techniques in machining: A review," *J. Clean. Prod.*, vol. 83, pp. 33–47, Jul. 2014.

[8] K. Weinert, I. Inasaki, J. W. Sutherland, and T. Wakabayashi, "Dry machining and minimum quantity lubrication," *CIRP Ann. - Manuf. Technol.*, vol. 53, no. 1, pp. 511–537, Jan. 2004.

[9] C. S. Rakurty, P. I. Varela, and A. K. Balaji, "Effects of targeted minimum quantity fluid (MQF) application on surface integrity," *Procedia CIRP*, vol. 8, pp. 462–468, Jun. 2013.

[10] J. P. Byers, *Metalworking Fluids*, 2nd ed. Boca Raton, Fl, US: CRC/Taylor & Francis, 2006.

[11] R. Edwards, *Cutting Tools*, 1st ed. London, UK: The Insitute of Materials, 1993.

[12] R. Khettabi, L. Fatmi, J. Masounave, and V. Songmene, "On the micro and nanoparticle emission during machining of titanium and aluminum alloys," *CIRP J. Manuf. Sci. Technol.*, vol. 6, no. 3, pp. 175–180, Apr. 2013.

[13] J. P. Davim, *Nontraditional Machining Processes*, 1st ed. London, UK: Springer, 2013.

[14] H. A.-G. El-Hofy, *Advanced Machining Processes: Nontraditional and Hybrid Machining Processes*, 1st ed. New York, NY, US: McGraw-Hill Professional Publishing, 2005.

[15] M. P. Groover, *Fundamentals of Modern Manufacturing : Materials, Processes, and*

Systems, 5th ed. Hoboken, NJ, US: John Wiley & Sons, Inc, 2013.

[16] C. Cheng, D. Phipps, and R. M. Alkhaddar, "Treatment of spent metalworking fluids," *Water Res.*, vol. 39, no. 17, pp. 4051–4063, Oct. 2005.

[17] E. Brinksmeier, D. Meyer, A. G. Huesmann-Cordes, and C. Herrmann, "Metalworking fluids - Mechanisms and performance," *CIRP Ann. - Manuf. Technol.*, vol. 64, no. 2, pp. 605–628, Jun. 2015.

[18] Cimcool Fluid Technology Ltd., "CIMFREE VG-703ES Metalworking Fluid," Cincinnati, OH, US, 2011.

[19] Jeffrey D. Silliman, *Cutting and Grinding Fluids: Selection and Application*, 2nd ed. Dearborn, MI, US: SME, 1992.

[20] M. S. Najiha, M. M. Rahman, and A. R. Yusoff, "Environmental impacts and hazards associated with metal working fluids and recent advances in the sustainable systems: A review," *Renew. Sustain. Energy Rev.*, vol. 60, pp. 1008–1031, Jul. 2016.

[21] A. D. Jayal, "An experimental investigation of the effects of cutting fluid application on machining performance," Ph.D. dissertation, Dept. Mech. Eng., Univ. of Utah, Salt Lake City, UT 2007.

[22] P. Sreejith and B. K. Ngoi, "Dry machining: Machining of the future," *J. Mater. Process. Technol.*, vol. 101, no. 1, pp. 287–291, Apr. 2000.

[23] K. Okushima and Y. Kakino, "The residual stress produced by metal cutting," *Annals of the CIRP*., vol. 20, no. 1, pp. 13–14, Jan. 1971.

[24] A. K. Balaji, C. S. Rakurty, H. Montemayor, and V. Ghatikar, "A novel multiple cutting fluid dispensing system for sustainable manufacturing", presented at 2014 STLE Annual Meeting & Exhibition, Lake Buena Vista, FL, USA, May 18-22, 2014.

[25] B. Denkena and D. Biermann, "Cutting edge geometries," *CIRP Ann. - Manuf. Technol.*, vol. 63, no. 2, pp. 631–653, Jun. 2014.

[26] G. E. D'Errico, R. Chiara, and E. Guglielmi, "PVD coatings of cermet inserts for milling applications," *Surf. Coatings Technol.*, vol. 86–87, pp. 735–738, Dec. 1996.

[27] G. D'Errico, R. Calzavarini, and B. Vicenzi, "Influences of PVD coatings on cermet tool life in continuous and interrupted turning," *J. Mater. Process. Technol.*, vol. 78, pp. 53–58, Jun. 1998.

[28] A. D. Jayal and A. K. Balaji, "Effects of cutting fluid application on tool wear in machining: Interactions with tool-coatings and tool surface features," *Wear*, vol. 267, pp. 1723–1730, Sep. 2009.

[29] M. Narasimha, K. Sridhar, R. Reji Kumar, and A. Aemro Kassie, "Improving cutting tool life a review," *Int. J. Eng. Res. Dev.*, vol. 7, no. 1, pp. 2278–67, May 2013.

[30] B. G. Mellor, *Surface Coatings for Protection Against Wear*, 1st ed, Boca Raton, FL, US:

CRC Press LCC, 2006.

[31] M. Field and J. F. Kahles, “The surface integrity of machined and ground high strength steel,” *DMIC Rep. 210*, pp 54-77, Jun. 1964.

[32] M. Field, “Review of surface integrity of machined components” *Annals of the CIRP*. pp. 153–163, Jan. 1971.

[33] M. Field, J. F. Kahles, and J. T. Cammett, “A review of measuring methods for surface integrity,” *Ann. CIRP*, vol. 21, no. 2, pp. 219–238, Jan. 1972.

[34] J. P. Davim, *Surface Integrity in Machining*, 1st ed. London, UK: Springer, 2010.

[35] W. P. Koster, M. Field, J. F. Kahles, L. J. Fritz, and L. R. Gatto, “Surface Integrity of Machined Structural Components,” Metcut Reseach Associates, Cincnaati, OH, US, AFML-TR-70-11, 1970.

[36] *Surface Integrity*, ANSI Standard B211.1 -1986.

[37] R. M’Saoubi, J. C. Outeiro, H. Chandrasekaran, O. W. Dillon Jr., and I. S. Jawahir, “A review of surface integrity in machining and its impact on functional performance and life of machined products,” *Int. J. Sustain. Manuf.*, vol. 1, pp. 203–236, Jul. 2008.

[38] I. S. Jawahir, E. Brinksmeier, R. M’Saoubi, D. K. Aspinwall, J. C. Outeiro, D. Meyer, D. Umbrello, and A. D. Jayal, “Surface integrity in material removal processes: Recent advances,” *CIRP Ann. - Manuf. Technol.*, vol. 60, no. 2, pp. 603–626, Dec. 2011.

[39] A. Thakur and S. Gangopadhyay, “State-of-the-art in surface integrity in machining of nickel-based super alloys,” *Int. J. Mach. Tools Manuf.*, vol. 100, pp. 25–54, Jan. 2016.

[40] D. Ulutan and T. Ozel, “Machining-induced surface integrity in titanium and nickel alloys: A review,” *Int. J. Mach. Tools Manuf.*, vol. 51, no. 3, pp. 250–280, Mar. 2011.

[41] W. N. Thomas, “Effect of scratches and of various workshop finishes upon the fatigue strength of steel,” Ph.D. dissertation, Dept. Mech. Eng., Univ. of Oxford, Oxford, UK, 1923.

[42] Surface Texture (Surface Roughness, Waviness, and Lay), ASME B46.1-2009.

[43] D. Novovic, R. C. Dewes, D. K. Aspinwall, W. Voice, and P. Bowen, “The effect of machined topography and integrity on fatigue life,” *Int. J. Mach. Tools Manuf.*, vol. 44, pp. 125–134, Feb. 2004.

[44] J. O. Almen and P. Black, *Residual Stresses and Fatigue in Metals*, 1st ed. New York, NY, US: McGraw-Hill Book Inc., 1963.

[45] F. A. Kandil, J. D. Lord, A. T. Fry, and P. V Grant, “A review of residual stress measurement methods - A guide to technical selection,” NPL, Middlesex,UK, NPL Report MARC(A)04, Feb. 2001.

[46] K. Neailey, “Surface integrity of machined components: microstructural aspects,” *Metals and materials*, vol. 4, no. 2. pp. 93–96, Feb. 1988.

[47] A. J. Schwartz, M. Kumar, B. L. Adams, and D. P. Field, Eds., *Electron Backscatter Diffraction in Materials Science*. Boston, MA, US: Springer US, 2009.

[48] S. To, W. B. Lee, and C. F. Cheung, "Orientation changes of aluminium single crystals in ultra-precision diamond turning," *J. Mater. Process. Technol.*, vol. 140, no. 1–3 SPEC., pp. 346–351, Sep. 2003.

[49] A. Yamamoto, T. Yamada, S. Nakahigashi, L. Liu, M. Terasawa, and H. Tsubakino, "Effects of surface grinding on hardness distribution and residual stress in low carbon austenitic stainless steel SUS316L," *ISIJ Int.*, vol. 44, no. 10, pp. 1780–1782, Aug. 2004.

[50] R. M'Saoubi and L. Ryde, "Application of the EBSD technique for the characterisation of deformation zones in metal cutting," *Mater. Sci. Eng. A*, vol. 405, no. 1–2, pp. 339–349, Sep. 2005.

[51] S. Bissey-Breton, V. Vignal, F. Herbst, and J. B. Coudert, "Influence of machining on the microstructure, mechanical properties and corrosion behaviour of a low carbon martensitic stainless steel," *Procedia CIRP*, vol. 46, pp. 331–335, Apr. 2016.

[52] J. Zhou, V. Bushlya, R. L. Peng, Z. Chen, S. Johansson, and J. E. Stahl, "Analysis of subsurface microstructure and residual stresses in machined inconel 718 with PCBN and Al2O3-SiCw tools," *Procedia CIRP*, vol. 13, pp. 150–155, May 2014.

[53] C. Leyens and M. Peters, Eds., *Titanium and Titanium Alloys : Fundamentals and Applications*. Weinheim, FRG: Wiley-VCH Verlag GmbH & Co. KGaA, 2003.

[54] *Materials Properties Handbook: Titanium Alloys*. ASM International, 1993.

[55] C. Veiga, J. P. Davim, and A. J. R. Loureiro, "Review on machinability of titanium alloys: The process perspective," *Rev. Adv. Mater. Sci.*, vol. 34, no. 2, pp. 148–164, Jan. 2013.

[56] J. P. Davim, *Machining of Titanium Alloys*. Berlin/Heidelberg: Springer, 2014.

[57] E. O. Ezugwu, R. B. Da Silva, J. Bonney, and Á. R. Machado, "The Effect of argon-enriched environment in high-speed machining of titanium alloy," *J. of Tribology Trans.*, vol 38, no.1, pp 18-23, May 2014.

[58] A. Ginting and M. Nouari, "Surface integrity of dry machined titanium alloys," *Int. J. Mach. Tools Manuf.*, vol. 49, no. 3–4, pp. 325–332, Mar. 2009.

[59] F. Nabhani, "Machining of aerospace titanium alloys," *Robot. Comput. Integr. Manuf.*, vol. 17, pp. 99–106, Feb. 2001.

[60] A. R. Zareena and S. C. Veldhuis, "Tool wear mechanisms and tool life enhancement in ultra-precision machining of titanium," *J. Mater. Process. Technol.*, vol. 212, no. 3, pp. 560–570, Mar. 2012.

[61] R. A. Rahman Rashid, S. Palanisamy, S. Sun, and M. S. Dargusch, "Tool wear mechanisms involved in crater formation on uncoated carbide tool when machining Ti6Al4V alloy," vol. 83, no. 9–12, pp. 1457–1465, Apr. 2016.

[62] S. Palanisamy, S. D. McDonald, and M. S. Dargusch, “Effects of coolant pressure on chip formation while turning Ti6Al4V alloy,” *Int. J. Mach. Tools Manuf.*, vol. 49, pp. 739–743, Jul. 2009.

[63] M. H. Sadeghi, M. J. Haddad, T. Tawakoli, and M. Emami, “Minimal quantity lubrication-MQL in grinding of Ti–6Al–4V titanium alloy,” *Int. J. Adv. Manuf. Technol.*, vol. 44, no. 5–6, pp. 487–500, Sep. 2009.

[64] J. Fujiwara, T. Arimoto, and K. Tanaka, “High speed milling of titanium alloy”, *Adv. Mater. Res.*, vol. 325, pp. 387–392, Aug. 2011.

[65] G. Rotella, O. W. Dillon, D. Umbrello, L. Settineri, and I. S. Jawahir, “The effects of cooling conditions on surface integrity in machining of Ti6Al4V alloy,” *Int. J. Adv. Manuf. Technol.*, vol. 71, no. 1–4, pp. 47–55, Mar. 2014.

[66] M. V. Ribeiro, M. R. V Moreira, and J. R. Ferreira, “Optimization of titanium alloy (6Al-4V) machining,” *J. Mater. Process. Technol.*, vol. 143–144, no. 1, pp. 458–463, Dec. 2003.

[67] S. Ramesh, L. Karunamoorthy, and K. Palanikumar, “Surface roughness analysis in machining of titanium alloy,” *J. Mat. Manuf. Proc.,* vol 23, no. 2, pp. 174-181, Oct. 2007

[68] V. G. Sargade, S. R. Nipanikar, and S. M. Meshram, “Analysis of surface roughness and cutting force during turning of Ti6Al4V ELI in dry environment,” *J. of Ind. Eng. Comp.,* vol. 7, no. 2, pp. 257–266, Mar. 2016.

[69] J. Sun and Y. B. Guo, “A comprehensive experimental study on surface integrity by end milling Ti-6Al-4V,” *J. Mater. Process. Technol.*, vol. 209, no. 8, pp. 4036–4042, Apr. 2009.

[70] J. I. Hughes, A R. C. Sharman, and K. Ridgway, “The effect of cutting tool material and edge geometry on tool life and workpiece surface integrity,” *Proc. Inst. Mech. Eng. Part B Journal Eng. Manuf.*, vol. 220, pp. 93–107, Feb. 2006.

[71] J. D. P. Velasquez, A. Tidu, B. Bolle, P. Chevrier, and J. J. Fundenberger, “Subsurface and surface analysis of high speed machined Ti-6Al-4V alloy,” *Mater. Sci. Eng. A*, vol. 527, no. 10–11, pp. 2572–2578, Apr. 2010.

[72] C. H. Che-Haron and A. Jawaid, “The effect of machining on surface integrity of titanium alloy Ti-6% Al-4% V,” *J. Mater. Process. Technol.*, vol. 166, pp. 188–192, Aug. 2005.

[73] J. P. Colafemina, R. G. Jasinevicius, and J. G. Duduch, “Surface integrity of ultra-precision diamond turned Ti (commercially pure) and Ti alloy (Ti-6Al-4V),” *Proc. Inst. Mech. Eng. Part B J. Eng. Manuf.*, vol. 221, no. 6, pp. 999–1006, Jun. 2007.

[74] Y. M. Arisoy and T. Özel, “Machine learning based predictive modeling of machining-induced microhardness and grain size in Ti–6Al–4V Alloy,” *Mater. Manuf. Process.*, vol. 30, no. 4, pp. 425–433, Aug. 2015.

[75] *Standard test method for determining residual stresses by the hole-drilling strain-gauge method,* ASTM E 837-08, 2008.

[76] ASM handbook, “Properties and selection: non ferrous and special purpose materials,” *ASM*

Int., vol. 2, pp. 500–630, Oct. 1990.

[77] "2012 Kyocera Cutting Tools : Turning Catalog." Kyocera, kyota, JP, 2012.

[78] "Master Catalog Cutting Tools." Kennametal, Latrobe, PA, US, 2013.

[79] Cimcool Fluid Technology ltd., "CIMTECH 310 - Metalworking Fluid," Cincinatti, OH, 2011.

[80] V. R. Ghatikar, "Design of minimum quantity cutting fluid dispensing system for sustainable machining," M.S. thesis, Dept. Mech. Eng., Univ. of Utah, Salt Lake City, UT, US, 2010.

[81] P. J. Withers and H. K. D. H. Bhadeshia, "Residual stress part 1 – measurement techniques," *Mater. Sci. Technol.*, vol. 17, no. 4, pp. 355–365, Dec. 2000.

[82] Vishay Measurements Group, *Student Manual for Strain Gage Technology: A Brief Introduction and Guide to Selection, Installation, Instrumentation*. Vishay Measurements Group, Raleigh, NC, US,1992.

[83] R. D. Cook and W. C. Young, *Advanced Mechanics of Materials*, 2nd ed. London, UK: Pearson, 1985.

[84] G. S. Schajer, "H-Drill : Hole-drilling residual stress calculation program." Vancouver, Canada [Online]. Available: http://www.schajer.org/index.htm.

[85] T. K. Shoemaker, "Developing and applying a surface integrity framework to met`al cutting on 2024-T351 aluminum with wiper cutting tools," M.S. thesis, Dept. Mech. Eng., Univ. of Utah, Salt Lake City, UT, US, 2015.

[86] A. J. Wilkinson and T. B. Britton, "Strains, planes, and EBSD in materials science," *Mater. Today*, vol. 15, no. 9, pp. 366–376, Sep. 2012.

[87] J. Y. Wang, C. R. Liu, and K. K. Wang, "The effect of tool flank wear on the heat transfer, thermal damage and cutting mechanics in finish hard tuning," *CIRP Ann. - Manuf. Technol.*, vol. 48, pp. 53–58, Jan. 1999.

[88] A. Paranjpe, "Residual stresses in machined titanium (Ti-6Al-4V) alloys," M.S. thesis, Dept. Mech. Eng., Univ. of Utah, Salt Lake City, UT, US, 2014.

[89] L.V Colwell, M. J. Sinnott, J. C. Tobin, "The determination of residual stresses in hardened, ground steel" , *Trans. ASME*, vol. 77, pp. 1099-1105, Jan. 1990.

[90] Y. Kaynak, T. Lu, and I. S. Jawahir, "Cryogenic machining-induced surface integrity: A review and comparison with dry, MQL, and flood-cooled machining," *Mach. Sci. Technol.*, vol. 18, no. 2, pp. 149–198, May 2014.

[91] R. Ding, Z. X. Guo, and A. Wilson, "Microstructural evolution of a Ti–6Al–4V alloy during thermomechanical processing," *Mater. Sci. Eng. A*, vol. 327, no. 2, pp. 233–245, Apr. 2002.